

# **POWER QUALITY IMPROVEMENT IN GRID-TIED SOLAR PHOTOVOLTAIC SYSTEM**

Submitted by

**SANJAY UPRETI**

**(2K14/PhD/EE/05)**

**Department of Electrical Engineering**

*Submitted*

*In fulfilment of the requirements of the degree*

*of*

**DOCTOR OF PHILOSOPHY**

In

**Electrical Engineering**



Under the Supervision of:

**Prof. Narendra Kumar and Prof. Bhim Singh**

**DEPARTMENT OF ELECTRICAL ENGINEERING DELHI  
TECHNOLOGICAL UNIVERSITY**

**DELHI-110042, INDIA**

**AUGUST 2023**

## **CERTIFICATE**

It is certified that the thesis entitled “**Power Quality Improvement in Grid-Tied Solar Photovoltaic System,**” being submitted by **Mr. Sanjay Upreti** for award of the degree of **Doctor of Philosophy** in the Department of Electrical Engineering, Delhi Technological University, Delhi, is a record of the student work carried out by her under our supervision and guidance. The matter embodied in this thesis has not been submitted for the award of any other degree or diploma.

**Dated:**

**Dr. Narendra Kumar**  
**Department of Electrical**  
**Engineering**  
**Delhi Technological**  
**University, Shahbad**  
**Daulatpur, Main Bawana**  
**Road, Delhi, India, 110042**

**Dr. Bhim Singh**  
**Department of Electrical Engineering,**  
**Indian Institute of Technology (IIT),**  
**Delhi, Hauz Khas, New Delhi, Delhi,**  
**India, 110016**

## ACKNOWLEDGEMENT

The completion of my Ph.D. research work marks a significant milestone, but it also marks the beginning of a new journey in the world of research. While the past years were guided and supervised, I now have the freedom to explore the new avenues independently. I am immensely grateful to my supervisor, **Prof. Narendra Kumar**, whose guidance and unwavering support have been instrumental throughout this journey, from the initial coursework to the successful completion of my Ph.D. I owe a great debt of gratitude to **Prof. Bhim Singh**, whose constant supervision and mentorship have provided invaluable insights into the realm of research. His determination, dedication, and innovative approach have inspired me to complete this work. His attention to detail and encouragement have motivated me to excel and utilize my capabilities to the fullest. Working under his guidance has been a profound and enriching experience, shaping my research and personal growth. I will always cherish the valuable experiences and blessings received from both my supervisors, which will undoubtedly influence my future endeavors. Their support has been a true inspiration on this remarkable journey.

I wish to thank my SRC Members – **Prof. Uma Nangia** (Chairman, DRC, EED), **Prof. Bharat Bhushan** (Departmental expert, DTU), **Prof. Malti Bansal** (Expert outside the department, DTU), **Prof. Pramod Aggarwal** (IIT Roorkee, Expert outside DTU) for their constant motivation and whole-hearted support during my Ph.D. research work. I also wish to express my gratitude to Head of the Department, EED, DTU **Prof. Rachna Garg**, **Prof. Madhusudan Singh**, **Prof. Pragati Kumar** and other DRC members for their continued guidance and help during the entire Ph.D. research work. I also wish to thank **all the Faculty members and staff of Electrical Engineering Department, DTU** for their direct and indirect help during the tenure of my research work. I also wish to thank **Dr. Imran**

**Kadri, Dr. Shagufta Khan, Dr. Md. Tausif Ahmad, Dr. Ambrish Devanshu and Mr. Saket Gupta** from EED, DTU and **Mr. Shivam Kumar Yadav, EED, IIT Delhi** for extending all the help and support. Special thanks are due to **Mr. Shivam Kumar Yadav** for helping in the work.

I wish to thank **my family** for all the support extended during the course of this research work. Special thanks to my daughter **Shubhangi** for keeping his patience during the writing of the thesis and entire research work. I whole-heartedly thank my wife **Smt. Preeti Upreti** for her constant full support for the entire duration of my research work. Without her help I would not have been able to complete the research work.

I wish to thank my Father **late Sh. Mohan Chandra Upreti** for his constant motivation and guidance. It was his wish to see me complete the Ph.D. research work. I dedicate this thesis to him. I wish to thank my mother **Smt. Laxmi Upreti** for all the help, support and numerous prayers she has offered for me. Thanks are due to my elder brothers **Late Sh. Kishan Chandra Upreti & Late Sh. Lalit Kumar upreti** sisters **Smt. Nirmala Pant & Dr. Neeta Awasthy** and **brother in laws Sh. Mohan Chandra Pant & Dr. Lalit Mohan Awasthy** for all the help, support and patience shown and also being on my side when required the most. I would like to thank my parents in law **late Sh. Lalit Kumar Joshi** and **Smt. Indu Joshi**. I would like to thank them all for giving me the inner strength and wholehearted support. I also thank the honorable **Chairman and management of BPIT, Directors, Principal and Department of Electrical and Electronics Engineering of BPIT, Rohini, Delhi** for helping me during the course of my Ph.D. research work. Last I would like to thank the God Almighty for guiding me through-out and keeping me blessed.

**Date:**

**Sanjay Upreti**



## **ABSTRACT**

The integration of grid-tied solar photovoltaic (PV) systems has become a key strategy in transitioning towards a sustainable and renewable energy future. However, the intermittent nature of solar power generation possesses challenges to power quality, affecting the stability and reliability of the electrical grid. This thesis aims to address power quality issues in grid-tied solar PV systems by focusing on the enhancement of multilevel inverter technologies and advanced control methods.

The research begins with an extensive literature review, examining the current state-of-the-art techniques in power quality improvement for grid-tied solar PV systems. Multilevel inverters are identified as a promising solution to mitigate power quality challenges, and various topologies are explored, including five-level T-Type, three seven-level (PUC, PEC, and K-Type), nine-level CHB, eleven-level PEC, and thirteen-level ladder-type inverters.

To achieve accurate grid synchronization and harmonic reduction, advanced modulation techniques such as level shifted multi-carrier, nearest level, and selective harmonic elimination (SHE) are employed. The thesis investigates the performance of each multilevel inverter topology using these modulation techniques under various operating conditions.

Simulation models are developed in MATLAB/Simulink to evaluate the steady-state and dynamic performances of the proposed multilevel inverter-based grid-tied solar PV systems. The effectiveness of power quality improvement is analyzed, focusing on parameters like total harmonics distortion (THD), voltage regulation, and current harmonics reduction. The simulation results demonstrate the superiority of the proposed solutions in achieving grid-friendly power injection and reducing voltage fluctuations.

Moreover, a comparative analysis is conducted to highlight the strengths and weaknesses of each multilevel inverter topology and modulation technique concerning power quality enhancement. The findings reveal the most suitable combinations for specific applications and system requirements.

To validate the simulation results, real-time testing is performed using the OPAL-RT simulator. The test bench real-time validation experiments validate the simulation outcomes, providing confidence in the real-world applicability of the proposed multilevel inverter solutions.

The performance of the grid-tied solar PV systems is assessed in terms of their response to unpredictable variations in irradiance levels and change in temperature. The control mechanisms enable robust operation, ensuring consistent power quality improvement in challenging environmental conditions.

In conclusion, this thesis presents a comprehensive investigation into power quality improvement in grid-tied solar PV systems using multilevel inverters and advanced control techniques. The proposed solutions demonstrate significant enhancements in power quality metrics, making them valuable assets for the reliable integration of solar energy into the electrical grid. The research contributes to the development of more efficient and sustainable renewable energy systems, paving the way for a cleaner and greener energy future.

# TABLE OF CONTENTS

Certificate	i	
Acknowledgement	ii	
Abstract	iv	
Table of Contents	vi	
List of Figures	xi	
List of Table	xv	
List of Abbreviations	xvi	
<b>CHAPTER I</b>	<b>INTRODUCTION</b>	
1.1	Overview	1
1.2	State of Art	2
1.3	Grid-Tied Solar Photovoltaic Generating System	3
1.4	Multilevel Inverters Topologies	5
1.4.1	NPC Multilevel Inverter	6
1.4.2	Flying-Capacitor Multilevel Inverter	6
1.4.3	Cascaded H-Bridge Multilevel Inverter	6
1.4.4	Hybrid Multilevel Inverter	7
1.5	Multilevel Inverter Control Schemes	7
1.5.1	MMPT Algorithms	8
1.5.2	Multilevel Converters Control Structure	8
1.5.3	Modulation Techniques	9
1.5.3.1	Level shifted multicarrier pulse width modulation	9
1.5.3.2	Nearest level modulation	9
1.5.3.3	Selective harmonic elimination (SHE) modulation	9
1.6	OBJECTIVES AND SCOPE OF WORK	10
1.7	OUTLINE OF CHAPTERS	11
<b>CHAPTER II</b>	<b>LITERATURE REVIEW</b>	
2.1	Introduction	14
2.2	Review of MPPT Techniques for Solar PV Array Applications	15
2.3	Review of Multilevel Inverter Topologies for Solar PV Array Applications	17
2.4	Literature review of Modulation Techniques for Solar PV Applications	19
2.5	Literature review of Converter Control Methods for Solar PV Applications	22
2.6	Identified Research Gaps	24
2.7	Conclusions	25
<b>CHAPTER III</b>	<b>CONTROL AND REAL TIME EXECUTION OF FIVE LEVEL T-TYPE MULTI LEVEL CONVERTER FOR SOLAR PV GENERATION</b>	

## APPLICATIONS

3.1	Introduction	27
3.2	Circuit Configuration of T-Type Five Level Converter for Solar PV Generation Applications	28
3.3	Control Strategy of T-Type Five Level Converter for Solar PV Generation Applications	29
3.3.1	MPPT Control	31
3.3.2	Unit Template Inverter Control	31
3.3.3	New Multi-Carrier Modulation Scheme	32
3.4	MATLAB Modelling of T-Type Five Level Converter for Solar PV Generation Applications	34
3.5	Simulated Results of T-Type Five Level Converter for Solar PV Generation Applications	36
3.5.1	Steady State Analysis	36
3.5.2	Dynamic Response analysis	37
3.5.3	Harmonic Response analysis	39
3.6	Real Time Execution of T-Type Five Level Converter for Solar PV Generation Applications	42
3.6.1	Dynamic Response Analysis	42
3.6.2	Harmonic Response Analysis	42
3.7	Conclusions	43

## CHAPTER IV CONTROL AND REAL TIME EXECUTION OF PUC AND PEC TYPE SEVEN LEVEL CONVERTER FOR SOLAR PV GENERATION APPLICATIONS

4.1	Introduction	45
4.2	Circuit Configuration of PUC and PEC Type Seven Level Converter for Solar PV Generation Applications	46
4.2.1	PUC Converter	46
4.2.2	PEC Converter	48
4.3	Control Strategy Of PUC and PEC Type Seven Level Converter For Solar PV Generation Applications	51
4.3.1	Control Strategy of PUC Converter	51
4.3.1.1	DC-Link Voltage Control	51
4.3.1.2	Current Control	52
4.3.1.3	Multicarrier Modulation	53
4.3.2	Control Strategy of PEC Converter	55
4.3.2.1	DC-Link Voltage Control	55
4.3.2.2	Current Control	56
4.3.2.3	Multicarrier Modulation	56
4.4	MATLAB Modelling of PUC and PEC Type Seven Level Converter For Solar PV Generation Applications	58

4.4.1	PUC Converter	58
4.4.2	PEC Converter	60
4.5	Simulated Results of PUC and PEC Type Seven Level Converter for Solar PV Generation Applications	62
4.5.1	Steady-State and Dynamic Performance of PUC7 Converter	62
4.5.2	Harmonics Analysis of PUC7 Converter	63
4.5.2.1	Analysis with PD pattern	64
4.5.2.2	Analysis with POD pattern	64
4.5.2.3	Analysis with APOD pattern	65
4.5.3	Steady-State and Dynamic Performance of PEC7 Converter	66
4.5.4	Harmonics Analysis of PUC7 Converter	66
4.6	Real-Time Execution Of PUC and PEC Type Seven Level Converter For Solar PV Generation Applications	68
4.6.1	Performance of PUC7 Converter	68
4.6.2	Performance of PEC7 Converter	70
4.7	Conclusions	72

**CHAPTER V CONTROL AND REAL-TIME EXECUTION OF K-TYPE SYMMETRIC SEVEN LEVEL CONVERTER FOR SOLAR PV GENERATION APPLICATIONS**

5.1	Introduction	73
5.2	Circuit Configuration of K-Type Symmetric Seven Level Converter For Solar PV Generation Applications	73
5.3	Control Strategy of K-Type Symmetric Seven Level Converter For Solar PV Generation Applications	75
5.4	MATLAB Modelling of K-Type Symmetric Seven Level Converter For Solar PV Generation Applications	77
5.5	Simulated Results of K-Type Symmetric Seven Level Converter For Solar PV Generation Applications	78
5.6	Real-Time Execution of K-Type seven Level symmetric Converter For Solar PV Generation Applications	80
5.7	Conclusion	83

**CHAPTER VI CONTROL AND REAL-TIME EXECUTION OF CASCADED H BRIDGE NINE LEVEL CONVERTER FOR SOLAR PV GENERATION APPLICATIONS**

6.1	Introduction	84
6.2	Circuit Configuration of Cascaded H-Bridge Nine Level Converter For Solar PV Generation Applications	84
6.3	Control Strategy of Cascaded H-Bridge Nine Level Converter for Solar PV Generation Applications	86
6.3.1	Concept of Third Harmonic Injection	86

6.3.2	3rd Harmonic Injected Nearest Level Modulated Switching	87
6.3.3	Grid Tied Power Controller	88
6.4	MATLAB Model of Cascaded H-Bridge Nine Level Converter for Solar PV Generation Applications	89
6.5	Simulated Results of Cascaded H-Bridge Nine Level Converter for Solar PV Generation Applications	90
6.6	Harmonic Assessment of Cascaded H-Bridge Nine Level Converter for Solar PV Generation Applications	93
6.6.1	Analysis with Nearest Level Modulation (NLM)	93
6.6.2	Analysis with Multicarrier Modulation	94
6.7	Real-Time Execution of Cascaded H-Bridge Nine Level Converter For Solar PV Generation Applications	94
6.8	Conclusions	96

**CHAPTER VII CONTROL AND REAL-TIME EXECUTION OF PACKED E-CELL(PEC) ELEVEN LEVEL CONVERTER FOR SOLAR PV GENERATION APPLICATIONS**

7.1	Introduction	98
7.2	Circuit Configuration of Packed E-Cell (PEC) Eleven Level Converter for Solar PV Generation Applications	98
7.3	Control Strategy of Packed E-Cell (PEC) Eleven Level Converter for Solar PV Generation Applications	103
7.4	MATLAB Model of Packed E-Cell (PEC) Eleven Level Converter for Solar PV Generation Applications	105
7.5	Simulated Results of Packed E-Cell (PEC) Eleven Level Converter For Solar PV Generation Applications	107
7.6	Real-Time Execution of Packed E-Cell (PEC) Eleven Level Converter For Solar PV Generation Applications	109
7.7	Conclusions	110

**CHAPTER VIII CONTROL AND REAL-TIME EXECUTION OF LADDER TYPE THIRTEEN LEVEL CONVERTER FOR SOLAR PV GENERATION APPLICATIONS**

8.1	Introduction	111
8.2	Circuit Configuration of Ladder Type Thirteen Level Converter for Solar PV Generation Applications	111
8.3	Control Strategy of Ladder Type Thirteen Level Converter for Solar PV Generation Applications	115
8.4	MATLAB Model of Ladder Type Thirteen Level Converter for Solar PV Generation Applications	117
8.5	Simulated Results of Ladder Type Thirteen Level Converter For Solar PV Generation Applications	118

8.5.1	Operating performance Analysis	119
8.5.2	Harmonic Performance analysis	119
8.6	Real-Time Execution of Ladder Type Thirteen Level Converter For Solar PV Generation Applications	121
8.7	Conclusions	122
<b>CHAPTER IX</b>	<b>COMPARATIVE STUDY OF DIFFERENT MULTILEVEL CONVERTERS FOR SOLAR PV GENERATION APPLICATIONS</b>	
9.1	Introduction	123
9.2	Comparison of Five Level T-Type Converter with other Five Level Converters	124
9.3	Comparison of Seven Level PUC, PEC and K-Type Converters with other Seven Level Converters	124
9.4	Comparison of Nine Level CHB Converter with other Nine Level Converters	124
9.5	Comparison of Eleven Level PEC-Type Converter with other Eleven Level Converters	125
9.6	Comparison of Thirteen Level Ladder-Type with other Thirteen Level Converters	125
9.7	Conclusions	130
<b>CHAPTER IX</b>	<b>MAIN CONCLUSIONS AND FURTHER WORK</b>	
10.1	Introduction	131
10.2	Main Conclusions	131
10.3	Further Work	133
<b>REFERENCES</b>		134
<b>APPENDIX</b>		155
<b>LIST OF PUBLICATIONS</b>		157
<b>BIO DATA</b>		158

## LIST OF FIGURES

Fig.1.1.	Basic components of grid-tied solar photovoltaic system
Fig. 1.2.	Classification of multilevel inverter topologies
Fig. 3.1.	Five level T-Type SPV system
Fig. 3.2.	The control scheme of T-Type inverter
Fig. 3.3. (a-b)	(a) block diagram of modified triangular wave (b) Triangular and modified triangular signals
Fig. 3.4	New multi-carrier for five level output with reference signal
Fig. 3.5 (a-b)	MATLAB model of (a) power circuit (b) control scheme, of T-Type converter
Fig. 3.6.	DC link capacitors voltages balancing
Fig. 3.7.	Steady state response of five level T-Type converter based SPV
Fig. 3.8.	Dynamic response of SPV system during the fall of irradiance
Fig. 3.9.	Dynamic response of SPV system during the rise of irradiance
Fig. 3.10 (a-c)	Harmonic performance of converter voltage (a) with new multi-carrier (b) conventional SPWM and (c) grid current with new multi-carrier
Fig. 3.11 (a-b)	Dynamic performance of T-type SPV system (a) fall in irradiance (b) rise in irradiance in RT simulator
Fig. 3.12 (a-b)	Harmonic response in RT simulator (a) Converter voltage (b) Grid current THD
Fig.4.1	Seven level PUC SPV system
Fig.4.2.	Seven level PEC SPV system
Fig. 4.3	DC-Link voltage control for reference current generation
Fig. 4.4	Current control and switching pulse generation
Fig. 4.5	Modified triangular carrier generation
Fig. 4.6	Parabolic carrier signal generation
Fig. 4.7	DC link voltage control PEC7
Fig. 4.8	AC side current control of PEC7
Fig. 4.9	The carrier signal orientation of PD, APOD and POD Multi-carrier PWM



- Fig. 4.10 (a-b) MATLAB model of (a) power circuit (b) control scheme, of PUC7 converter
- Fig. 4.11 (a-b) MATLAB model of (a) power circuit (b) control scheme, of PEC converter
- Fig. 4.12 (a-c) Simulation results (a) steady-state (b) dynamic performance with fall in irradiance (c) dynamic performance with rise in irradiance.
- Fig. 4.13 (a-b) Harmonics analysis (a) converter voltage (b) grid current
- Fig. 4.14 (a)The steady state response, (b) dynamic response during the fall of irradiation of grid integrated PEC7
- Fig. 4.15 (a)The dynamic response at rise of irradiation , (b) dynamic response during the temperature rise of grid integrated PEC7
- Fig. 4.16 (a-b) The harmonic response of PEC7 (a) voltage THD (b) Current THD
- Fig. 4.17 (a-c) Real-time results-I (a) constant irradiance of  $1000 \text{ W/m}^2$  (b) Converter voltages (c)  $i_{ga}$ ,  $v_{ga}$  and  $V_{conpha}$  with rise in irradiation
- Fig. 4.18 (a-c) Real-time results-II (a)  $i_{ga}$ ,  $v_{ga}$ ,  $P_g$  and  $P_{pv}$  with rise in irradiation (b)  $i_{ga}$ ,  $v_{ga}$  and  $V_{conpha}$  with fall in irradiation (c)  $i_{ga}$ ,  $v_{ga}$ ,  $P_g$  and  $P_{pv}$  with fall in irradiation
- Fig. 4.19 Real-time results-III (a) Voltage THD (b) Current THD
- Fig. 4.20 Real-time simulated (a)The steady state response, (b) dynamic response during the fall of irradiation of grid integrated PEC7
- Fig. 4.21 Real-time simulated (a) The dynamic response at rise of irradiation , (b) dynamic response during the temperature rise of grid integrated PEC7
- Fig. 4.22 The real-time simulated harmonic response of PEC7 (a) voltage THD (b) Current THD
- Fig. 5.1 Improved seven-level K-type structure IK-7
- Fig. 5.2 (a) Output voltage profile (b) Positive peak level (c) zero level (d) Negative peak level of IK-7
- Fig. 5.3 Power and control scheme of solar-grid system of IK-7 multilevel inverter.
- Fig. 5.4 (a-b) MATLAB models of (a) power circuit (b) control circuit
- Fig. 5.5 (a-b) (a)The steady state response (b) dynamic response during irradiation fall of IK-7 multilevel inverter solar-grid system
- Fig. 5.6 (a-b) IK-7 multilevel inverter solar-grid system during (a) rise (b) zero irradiation

- Fig. 5.7 (a-b) IK7 converter (a) voltage profile and THD (b) The grid current and its THD
- Fig. 5.8 (a-b) OPAL-RT results, (a)The steady state response (b) dynamic response during irradiation fall of IK-7 multilevel inverter solar-grid system
- Fig. 5.9 (a-b) OPAL-RT results of IK-7 multilevel inverter solar-grid system during (a) rise (b) zero irradiation
- Fig. 5.10 (a-b) IK7 converter OPAL-RT results (a) voltage profile and THD (b) The grid current and its THD
- Fig. 6.1 Nine level CHB-PV system
- Fig. 6.2 (a)Algorithm for NLM Switching, (b) THI Modulating signal and converter output voltage
- Fig. 6.3 (a-b) Control circuit (a) Grid Power and (b) Switching Controller
- Fig. 6.4 (a-b) MATLAB models of (a) power circuit (b) control circuit
- Fig. 6.5 (a-c) Simulation results (a) steady-state (b) dynamic fall of solar (c) dynamic rise of solar
- Fig. 6.6 (a-b) Harmonics spectra of (a) converter voltage (b) grid current
- Fig. 6.7 (a-c) Real-time results-I (a) Constant irradiance of  $1000 \text{ W/m}^2$  (b) Converter Line Voltages (c) Modulating signals
- Fig. 6.8 (a-h) Dynamic results-I (a) Fall in solar power (b) Rise in solar power
- Fig. 6.9 (a-h) Dynamic results-II (a) Fall in grid current (b) Rise in grid current
- Fig. 6.10 (a-b) Harmonic analysis (a) Converter voltage (b) Grid Current
- Fig. 7.1 Eleven level PEC SPV system
- Fig. 7.2 Positive cycle operating path
- Fig. 7.3 Negative cycle operating path
- Fig. 7.4 Control structure of PEC11
- Fig. 7.5 (a-b) MATLAB models of (a) power circuit (b) control circuit
- Fig. 7.6 (a-b) Simulation results set I (a) Steady-state response of PEC11 (b) Dynamic response of PEC11 during the rise of irradiation
- Fig. 7.7 (a-b) Simulation results set II (a) Dynamic response of PEC11 during irradiation fall. (b) Grid current and converter voltage THD

- Fig. 7.8 (a-e) PEC11 response in Real-time simulator; (a) Steady state, (b) Rise in irradiation, (c), Fall in irradiation, (d) THD in real-time simulator, Voltage harmonic distortion and (e) Current harmonic distortion
- Fig. 8.1 Ladder type thirteen level solar PV System
- Fig. 8.2 Operating modes of six, five and four level
- Fig. 8.3 Operating modes of three, two, and one level
- Fig. 8.4 The Control Scheme (a) DC side control (b) AC side NLM-PR controller
- Fig. 8.5 MATLAB models of (a) power circuit (b) control circuit
- Fig. 8.6 Ladder type converter result (a) at constant irradiance (b) with insolation fall
- Fig. 8.7 Ladder type converter result with (a) insolation rise (b) insolation to zero
- Fig. 8.8 (a-b) RT simulator results (a) grid voltage, power(Active and reactive) and current (b) PV power, grid current, Converter voltage (Line and Phase) at steady state
- Fig. 8.9 (a-b) RT simulator result (a) Grid voltage, power(Active and reactive) and current (b)PV power, grid current, Converter voltage (Line and Phase) at irradiation fall
- Fig. 8.10 (a-b) RT simulator result (a) Grid voltage, power(Active and reactive) and current (b)PV power, grid current, Converter voltage (Line and Phase) at irradiation rise
- Fig. 8.11 (a-b) RT simulator result of (a) Voltage harmonic response (b) Grid current harmonic.

## LIST OF TABLES

Table 2.1	MPPT Techniques Reviewed
Table 2.2	Multilevel Inverter topologies reviewed
Table 2.3	Modulation techniques reviewed
Table 2.4	Inverter control methods reviewed
Table 2.5	Comparison of two level with multilevel inverter
Table 3.1	Switching states for T-Type SPV converter
Table 3.2	System Parameters
Table 3.3	Modulation index vs THD of converter voltage (%)
Table 3.4	Modulation Index vs fundamental voltage component(V)
Table 4.1	Switching states for phase A of PUC7
Table 4.2	Switching States For PV-PEC Converter
Table 4.3	Harmonic performance of seven-level PUC inverter output
Table 5.1	Switching Sequence of K-Type Converter
Table 6.1	Switch Logics of Cascade H-Bridge
Table 6.2	THI-NLM and Multicarrier PWM based Harmonic Comparison
Table 7.1	Switching states of PEC11
Table 7.2	System parameters of PEC11
Table 8.1	Switching modes of ladder converter
Table 9.1	Comparison of other converters with T-Type five level converter for solar
Table 9.2	Comparison of other converters with PUC and K-Type seven level
Table 9.3	Comparison of other converters with CHB nine level converter for solar
Table 9.4	Comparison of other converters with PEC eleven level converter for solar
Table 9.5	Comparison of other converters with PEC eleven level converter for solar

## LIST OF ABBREVIATIONS

AC	Alternating Current
DC	Direct Current
CHB	Cascaded H-Bridge
PUC	Packed U-Cell
PEC	Packed E-Cell
FFT	Fast Fourier Transform
HVDC	High Voltage Direct Current
IEEE	Institute of Electrical and Electronics Engineers
IGBT	Insulated Gate Bi-polar Transistor
MLC	Multi-Level Converter
MPPT	Maximum Power Point Tracking
NLM	Nearest Level Modulation
PF	Power Factor
PI	Proportional- Integral
PLL	Phase-Locked-Loop
LSPWM	Level Shifted carrier Pulse Width Modulation
PSPWM	Phase Shifted carrier Pulse Width Modulation
SPWM	Sinusoidal Pulse Width Modulation
PV	Photovoltaic
PWM	Pulse Width Modulation
P&O	Perturb and Observe
SHE-PWM	Selective Harmonic Elimination - Pulse Width Modulation
SPV	Solar Photo Voltaic
PD	Phase Disposition
POD	Phase Opposition Disposition
APOD	Alternate Phase Opposition Disposition

SRF	Synchronous Reference Frame
THD	Total Harmonic Distortion
VSC	Voltage Source Converter

# CHAPTER-I

## INTRODUCTION

### 1.1 OVERVIEW

In recent years, there has been a growing emphasis on harnessing renewable energy sources such as solar photovoltaics (PVs) generation and wind power to complement traditional fossil fuel-based electricity generation. The aim is to mitigate the detrimental impacts associated with the combustion of fossil fuels [1]. To ensure reliable and efficient extraction of power, it is anticipated that a majority of these eco-friendly power sources are to be connected to the electrical grid [2]. Power electronics converters assume a significant role in this scenario, acting as integrators that facilitate the seamless integration of distributed generation into the grid while maintaining high levels of efficiency and performance [3]-[5]. Given that the utility grid operates on alternating current (AC), inverters become indispensable components for grid-connected renewable energy sources [6]. The deployment of these inverters for reliable power transactions necessitates compliance with the harmonic limit standards set by the IEEE Std.-519 (2022) due to the discrete switching actions of inverters, which can result in harmonic distortions. Consequently, the literature reveals various modifications to inverter structures aimed at meeting these regulations [7]. Overcoming these challenges, multilevel inverters (MLIs) have emerged as a superior alternative to conventional two-level (2L) inverters in the field of grid integration. MLIs have not only found widespread use in grid-connected applications but also in motor drives, traction systems, flexible AC transmission systems (FACTS), high-voltage direct current (HVDC) systems, and numerous other domains [8].

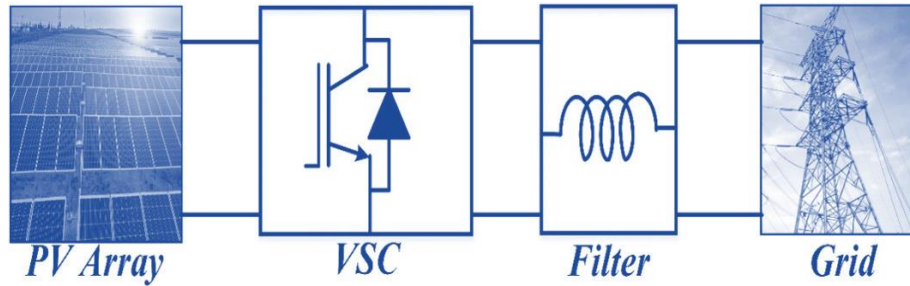


Fig. 1.1. Basic components of grid-tied solar photovoltaic system

## 1.2 STATE OF ART

The global energy landscape has witnessed a remarkable transformation in recent years, with a significant shift towards the utilization of renewable energy sources. Among these, solar photovoltaic (PV) systems have emerged as a key player in sustainable electricity generation. Grid-tied solar PV systems as shown in Fig. 1.1, which are connected to the utility grid, offer numerous advantages such as reduced carbon emissions, energy independence, and potential cost savings over the long term [9]-[11]. However, the integration of renewable energy sources into the grid introduces various challenges, particularly related to power quality.

As the adoption of grid-tied solar PV systems continues to grow, power quality issues have become a primary concern for power utilities, system operators, and end-users. The intermittent nature of solar power generation and varying solar irradiance can lead to voltage fluctuations, current harmonics, and grid instability. These power quality issues can adversely impact the performance of sensitive electronic devices, cause equipment malfunctions, and increase maintenance costs.

The successful implementation of advanced multilevel inverter-based grid-tied solar PV systems offer several significant contributions:



Enhanced Power Quality: The proposed systems mitigate power quality issues such as voltage fluctuations and harmonics, leading to a more stable and reliable grid operation.

Increased Renewable Energy Integration: Improving the power quality of grid-tied solar PV systems facilitates higher integration levels of renewable energy into the grid, reducing reliance on fossil fuels.

Cost Savings: By minimizing equipment malfunctions and reducing maintenance costs, the proposed solutions can potentially lead to economic benefits for both utilities and consumers.

### **1.3 GRID-TIED SOLAR PHOTOVOLTAIC GENERATING SYSTEM**

Solar photovoltaic (PV) power generation technology has emerged as a prominent renewable energy source in recent years, offering a sustainable and environmentally friendly solution to the increasing global energy demand. To efficiently integrate solar PV generation systems into the power grid, multilevel converters have gained significant attention due to their ability to address various challenges associated with conventional converters. This work explores the concept of multilevel converter-based grid-tied solar PV systems, their advantages, and their potential impact on the future of renewable energy.

Grid-tied solar PV systems are designed to operate in parallel with the utility grid, allowing the generated solar PV array energy to be used locally and excess power to be fed back into the grid. This two-way flow of electricity ensures energy stability and promotes the concept of net metering, wherein consumers receive credit for the surplus energy they contribute to the grid. However, integrating intermittent renewable sources like solar PV array into the grid presents technical challenges like voltage fluctuations, harmonic distortions, and grid synchronization issues.

A multilevel converter is a power electronic device that synthesizes a desired output voltage from several levels of lower voltage values. In comparison to traditional two-level converters, multilevel converters offer distinct advantages, including reduced harmonics distortion, lower switching losses, and higher voltage capabilities. These features make them ideal candidate for solar PV generation systems, as they enable higher power quality and efficient energy conversion.

Several multilevel converter topologies are used in grid-tied solar PV generation systems, with the most common being the neutral point clamped (NPC)[12]-[13], cascaded H-bridge (CHB)[14]-[15] and hybrid of conventional topologies, which offers more levels with reduced switch counts. T-Type, PUC (Packed U-Cell), K-Type, PEC (packed E-cell), ladder-type, X-type [16]-[21] are some hybrid configuration, which are used in multi-level converters. The NPC converter provides multiple voltage levels by clamping the neutral point of the DC link, while the CHB converter achieves multilevel operation by cascading H-bridge cells. Both topologies offer excellent scalability, making them adaptable to various system sizes and power requirements.

Following points show the importance of multilevel converter based PV systems.

- Improved Power Quality: Multilevel converters generate smoother output waveforms with reduced harmonics content, ensuring cleaner energy injection into the grid. This leads to fewer disturbances and higher power quality meeting the IEEE 519 standard [22].
- Higher Efficiency: Lower switching losses in multilevel converters contribute to higher overall efficiency, leading to better energy utilization and reduced operational costs.

- Grid Synchronization: Multilevel converters facilitate seamless synchronization with the grid, enabling quick and stable connection/disconnection without causing disturbances.
- Voltage Boosting: These converters allow for higher DC voltage levels, enabling longer strings of solar panels and reducing the current flowing through the system, which leads to lower resistive losses.

#### 1.4 MULTILEVEL INVERTERS TOPOLOGIES

A multilevel inverter (MLI) is a configuration comprising a collection of semiconductor devices and isolated voltage sources that are carefully controlled to generate a voltage waveform with multiple steps, allowing for adjustable and controllable amplitude, phase, and frequency. MLIs have gained widespread acceptance due to their remarkable features, including the ability to handle high voltages while minimizing device stress, reduced switching and conduction losses, and improved power quality with minimal harmonics distortion. Over time, numerous MLI topologies have been reported, broadly classified as shown in Fig. 1.2. Among the various options available, this new work will focus on a few recommended topologies that are considered both applicable and well-established as classic MLIs.

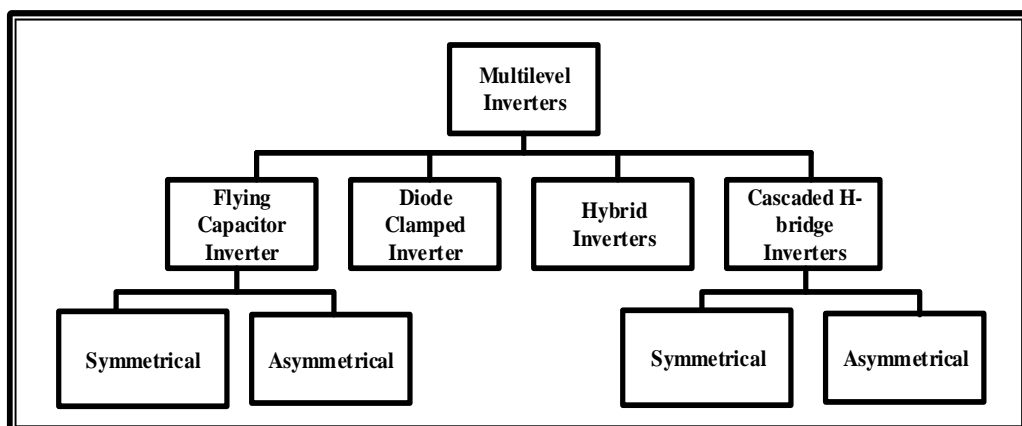


Fig. 1.2. Classification of multilevel inverter topologies

#### **1.4.1 NPC Multilevel Inverter**

The Neutral Point Clamped (NPC) converter is constructed by stacking two conventional two-level (2L) converters on top of each other and connecting them through series capacitors. To achieve higher power ratings and additional output voltage levels, the NPC topology can be expanded by incorporating extra power switches and clamping diodes. However, the number of required clamping diodes increases significantly as the number of output voltage levels rises. This, coupled with the growing complexity of controlling the unbalance in the DC-link capacitors, has posed challenges for industries in implementing the NPC topology for more than three voltage levels.

#### **1.4.2 Flying-Capacitor Multilevel Inverter**

The flying capacitor (FC) topology bears some resemblance to the NPC topology, although the primary distinction lies in the replacement of clamping diodes with flying capacitors. Similar to the NPC, the FC topology also requires only four gating pulses. However, the positions of complementary devices differ between the two topologies. In contrast to the NPC, the FC topology exhibits a modular structure that facilitates its seamless extension to higher voltage levels. This modularity provides an additional degree of freedom in converter control, utilizing numerous redundant states that are readily available.

#### **1.4.3 Cascaded H-Bridge Multilevel Inverter**

A cascaded H-bridge multilevel inverter is an advanced power electronic device used in high-power applications, particularly in grid-tied solar photovoltaic systems. It comprises of multiple H-bridge modules connected in series, producing a staircase-like output voltage waveform with several voltage levels. These inverters offer superior performance, reduced harmonic distortion, and improved power quality

compared to conventional inverters. The modular structure allows easy scalability and fault tolerance, enabling continuous operation even with the failure of individual modules. Cascaded H-bridge multilevel inverters play a vital role in optimizing solar energy harvesting, enhancing grid stability, and facilitating the integration of renewable energy into the electrical grid.

#### **1.4.4 Hybrid Multilevel Inverter**

Hybrid multilevel inverter topologies, such as T-Type, PUC (Partial Unit Cell), PEC (Partial Element Capacitor), K-Type, ladder type, X-type have shown great promise in improving the performance of solar PV array-grid operations. These topologies are capable of addressing various power quality issues commonly encountered in grid-tied solar PV generating systems.

Hybrid multilevel inverter topologies demonstrate remarkable performance in solar PV generation-grid operations. These advanced topologies effectively address power quality issues, such as harmonics distortion, voltage fluctuations, and power factor regulation, ensuring smooth integration of solar PV generating systems with the grid. By enhancing the efficiency and reliability of solar PV generation-grid operations, hybrid multilevel inverters contribute significantly to the sustainable growth of renewable energy adoption and the advancement of modern power systems. However, the specific choice of topology depends on the system's requirements, size, and the desired level of performance, and careful design and optimization are essential for achieving the best results.

### **1.5 MULTILEVEL INVERTER CONTROL SCHEMES**

Multilevel inverter control methods in solar PV generation-grid integrated systems play a crucial role in ensuring efficient energy conversion, grid synchronization, and power quality improvement. These control methods are designed to manage the

multilevel output voltage levels, regulate the grid connection, and optimize the solar power injection into the grid.

### **1.5.1 MPPT Algorithms**

As the widely recognized MPPT algorithms exhibit rapid convergence, this research work utilizes these algorithms. Among various known methods, the perturb and observe (P&O) and incremental conductance (INC) methods are selected for tracking the maximum power from the PV array. These techniques introduce small disturbances (perturbations) to track the maximum power point (MPP) and to determine the voltage at which, the PV array can deliver its maximum power. Each PV array is equipped with a dedicated MPPT algorithm and controller to effectively handle unpredictable variations in irradiance levels, ambient temperature, shading effects, and other relevant factors.

### **1.5.2 Multilevel Converters Control Structure**

The power extracted from the PV array is fed to the grid by a Voltage Source Converter (VSC) at unity power factor. The control of the VSC employs a decoupled current control based on Synchronous Reference Frame Phase-Locked Loop (SRF-PLL) and a voltage-oriented control with SRF-PLL for the grid synchronization. The SRF-PLL ensures accurate synchronization with the grid . The performance evaluation is conducted using MATLAB/Simulink software, analysing both steady-state and dynamic behaviours. Power quality improvement is assessed using the FFT tool in MATLAB, while the Total Harmonic Distortion (THD) of the output voltage and current waveforms at various levels is comprehensively compared. Furthermore, the results are validated through testing on the OPAL-RT simulator[23]-[25].

### **1.5.3 Modulation Techniques**

Multilevel inverter switching in solar PV-grid integrated systems play a crucial role in ensuring efficient energy conversion, grid synchronization, and power quality improvement. The modulation techniques are designed to manage the multilevel output voltage levels, regulate to the grid connection, and to optimize the solar PV array power injection into the grid. Here are some widely used modulation techniques used in multi-level converters.

#### **1.5.3.1 Level shifted multicarrier pulse width modulation**

Carrier-based PWM is a PWM technique commonly used in multilevel inverters[26]. It involves comparing a reference sinusoidal waveform with multiple triangular carrier waveforms to generate the appropriate switching signals. This technique results in a nearly sinusoidal output voltage with low harmonics distortion, making it suitable for solar-grid systems, where power quality is crucial.

#### **1.5.3.2 Nearest level modulation**

Nearest level modulation is a fundamental frequency switching technique used in multilevel inverters to control the switching of the power devices. It generates the nearest output voltage level to the desired reference voltage with round function[27]. In multilevel inverters, the output voltage can be synthesized by combining multiple voltage levels, and the nearest level modulation ensures that the inverter output closely matches the desired voltage reference.

#### **1.5.3.3 Selective harmonic elimination (SHE) modulation**

SHE control is a modulation technique used to eliminate specific harmonic components from the output voltage waveform [28]. By choosing appropriate switching angles, certain harmonics can be cancelled out, leading to a smoother and

cleaner output voltage. In solar PV-grid integrated systems, SHE control is used to mitigate harmonics distortion and to meet grid code requirements for power quality.

## **1.6 OBJECTIVES AND SCOPE OF WORK**

In this research work, the solar photovoltaic power generating systems formed by multi-level DC-AC conversion are investigated for the power quality improvement of injected power to the grid. Various topologies, control, PWM switching techniques are investigated to achieve the following research objectives.

- Classification and design of different solar multilevel converters are done for three-phase grid-tied applications. The power quality improvement is the main motive for different configurations.
- Design, Control and real-time test bench validation are carried out using MATLAB/Simulink and RT-LAB for different multilevel topologies.
- Different modulation techniques such as carrier PWM, nearest level PWM and SHE PWM are tested towards harmonics improvement of the solar multilevel converters.
- The analysis, design, modeling, control and implementation are carried for several PV array fed grid tied topologies such as T-Type-5 level, PUC-7 level, K-Type 7-level, PEC 11-level and Ladder-Type 13-level towards power quality improvement of solar photovoltaic power generating applications.
- System results of each topology are taken in constant and intermittent solar PV power profile for proper validation of power flow and system control in closed loop.



## 1.7 OUTLINE OF CHAPTERS

This thesis has following chapters as given here.

**Chapter I:** This chapter gives general scenario of solar PV array electricity status and future outlook. The requirement of multi-level inverter and solar irradiation to electricity generation process, is identified in detail. Multi-level inverter advantages in comparison to conventional two-level inverters are discussed. The pointwise research objectives and contribution are introduced with the orientation of the thesis.

**Chapter II:** The classification and evolution of multi-level converters topologies are given in detail. The literature survey of MPPT technologies, multi-level inverter topologies, modulation techniques and inverter control methods, are presented in this chapter along with identified research areas.

**Chapter III:** This chapter presents a new modified carrier modulation, which is first time investigated for five-level T-Type unit template based AC current control for solar photovoltaic applications. It is tested for harmonics performance with other carrier techniques. The power quality of solar PV array grid interfaced system is improved with minimum converter voltage THD. The simulated steady-state and dynamic performances are validated in real-time test bench.

**Chapter IV:** This chapter discusses the seven level PUC and PEC operation for solar PV generation with asymmetric voltage ratio. PUC converter has given seven level voltage output. In PUC, the power is fed in the grid with improved power quality and different modulation schemes i.e. triangular PWM, parabolic PWM and modified new triangular PWM. Switching states, modeling equations, closed-loop proportional control and generation of parabolic, modified triangular are thoroughly investigated in detail. PEC converter has generated seven voltage level output, which is fed to the grid with phase-opposition (PO), phase-opposition-disposition (POD) and alternate-phase-opposition-disposition (APOD) orientation of level shifted multi-carrier with the

objective to select the best modulation for PEC. Switching logic, modelling, solar grid PEC performance in steady state and varying solar irradiation are thoroughly presented in detail.

**Chapter V:** This chapter deals with the seven-level symmetric K type converter's testing and execution for steady-state and dynamic conditions. The power flow is regulated and controlled smoothly with K type arranged switches. Fifth and seven harmonics are curtailed with SHE modulation scheme. The power quality assessment is carried out with grid current within the IEEE-519 standard limits.

**Chapter VI:** This chapter presents the nine level CHB, modulated with integration of nearest level modulation with third harmonic control for solar PV power generation applications. Third harmonic injection has improved the fundamental component of the converter voltage and line voltage harmonics evaluation is made in detail. Effectiveness of the THI-NLM integrated control is validated by the obtained results in MATLAB simulator and verified in real-time test bench.

**Chapter VII:** This chapter deals with the implementation, design and modelling of eleven Level PEC for PV generating grid tied application. The converter is modified version of PUC by adding of two sources with bidirectional pair of switches. The complete control scheme with DC-link voltage of top and bottom PV arrays, resonant current controllers, and code of NLM is explained for PEC11. The MATLAB and real-time simulated results of DC and AC side of the PEC11 in steady and varying solar PV generation conditions are demonstrated by the appropriate findings.

**Chapter VIII:** This chapter presents the higher level converter of thirteen level for power quality improvement of solar power applications. It has a ladder structure with lesser switches for thirteen level output than CHB configuration. The converter performs excellently in steady state and dynamic conditions. The DC voltage control

by proportional-integral control and proportional resonant control for the AC side is discussed. Performance of ladder-type converter in terms of power quality and under varying environmental conditions is explained in detail.

**Chapter IX:** This chapter deals with a comparison of different topologies covered in the work. The topologies used in this thesis for every level is compared with other similar level inverters [28]-[52] in terms of number of switches, sources, diodes, capacitors per phase. A detailed comparison is carried for control, modulation technique, switching frequency and grid-tied application.

**Chapter X:** This chapter presents the summary of work contributed in the research work. Based on this research work, it is concluded that these solar PV generation multilevel converters with the adopted modulation techniques and controls are superior for solar photovoltaic power generation applications.

## **CHAPTER-II**

### **LITERATURE REVIEW**

#### **2.1 INTRODUCTION**

The best utilization of renewable resources is conversion of energy into electricity and its integration to the grid. This integration reduces the burden of traditional energy sources specifically coal, which is major contributor of CO<sub>2</sub> into the environment. However, electricity generated from renewable needs to be processed very carefully and it should meet the standards set by the regulator. Power electronics interface with the electric grid is an important research area and many related research work is presented by the researchers. The detailed review of literature for this thesis is done on multi-level power converter topologies, maximum power point tracking techniques, control of power converter, modulation techniques, power quality control. The multi-level inverters are reliable, efficient, economical interface solar PV array-grid interface for medium or high voltage system. This chapter has a detailed literature review of solar photovoltaic array system, multi-level converters, MPPT technique for solar panels, modulation techniques, power quality control of electrical power.

The grid tied solar photovoltaic system covers many aspects like MPPT techniques, converter topology, DC voltage source/sources and their voltage magnitudes ratio, modulation techniques, voltage and current control of AC and DC side. The selection of MPPT technique to extract maximum electrical power from solar panels, is very important and so the converter topology, PWM for switching, voltage and current controller. A detailed review of various level inverter topologies with symmetric & asymmetrical configurations are presented in the following subsections that cover

basic two level inverters to thirteen level for solar PV generation to grid power transfer.

## **2.2 REVIEW OF MPPT TECHNIQUES FOR SOLAR PV ARRAY APPLICATIONS**

The solar irradiation is an irregular phenomenon and varying nature of it affects the voltage output of solar panels. The I-V characteristic of solar panel clearly shows that it acts as constant current source for low voltage and constant voltage source for high voltage. It is very important to extract maximum power from the solar array to maximize the solar energy utilization. The maximum power extraction is a big challenge and researchers have developed various methods, referred as maximum power point tracking (MPPT). There are various methods available for MPPT such as perturb and observe (P&O) or hill climbing method, incremental conductance (IC), fractional short circuit current (FCC), fractional open circuit voltage (FOCV), ripple correlation control (RCC) are categorised in classical methods. Fuzzy logic (FC) controller, artificial neural network (ANN), sliding mode (SM) controller, Gauss-Newton approach based methods fall under the intelligent MPPT techniques. The particle swarm optimization (PSO), Grey wolf optimization (GWO), ant colony optimization (ACO), are some optimization techniques, which have high speed convergence. Besides these three categories there are some hybrid techniques, fuzzy particle swarm optimization (FPSO), GWO-P&O, PSO-P&O, which have the advantage of fast convergence and low oscillations. The intelligent algorithms are accurate techniques but response time of these methods is high. However, conventional methods are fast and robust so these methods have a widely employment in solar PV-power generation applications. Among the basic MPPT techniques, P&O and IC methods are most popular and applied in commercial and industrial applications. The P&O and IC methods track maximum power point

(MPP) by introducing small perturbations so that maximum power is extracted from solar PV array. Table 2.1 here shows the detailed review of MPPT techniques for solar PV applications.

Table 2.1 MPPT techniques reviewed

S.N.	Ref	Description
1	[29]	It proposes an enhanced adaptive perturb and observe (EA-P&O) maximum power point tracking (MPPT) algorithm for the photovoltaic system.
2	[30]	It proposes a MPPT technique, which is a hybrid between the adaptive perturb and observe and particle swarm optimization (PSO).
3	[31]	The proposal suggests altering the MPPT (Maximum Power Point Tracking) algorithm to incorporate a random selection of the sampling rate, fluctuating between fast and slow values.
4	[32]	It introduces an improved incremental conductance (IC) algorithm based on the mathematical residue theorem.
5	[33]	It proposes the P&O MPPT for constant power generation in PV systems.
6	[34]	Falcon optimization algorithm is introduced in this paper for the tracking of global maximum power point and implemented for the partial shading conditions.
7	[35]	In this paper, a novel approach is introduced, combining the Perturb and Observe (P&O) MPPT algorithm with Particle Swarm Optimization (PSO), which is enhanced with an improved search space.
8	[36]	Novel generic maximum power point (MPP) tracking technique, compatible with a wide range of transducers is presented in this work.
9	[37]	In this work, a Variable Step Size ANN-based MPPT technique is adopted. It is compared with the other MPPT techniques in terms of steady-state behavior, settling time of converter power, power point tracing speed, oscillations of MPP, and operating efficiency.
10	[38]	Global maximum power point tracking strategy is implemented in a efficient grid-tied PV inverter, which deploys one sensor each for voltage and current.
11	[39]	An advanced technique called Higher Order Sliding Mode Observer-based Integral Sliding Mode Control is applied for Maximum Power Point Tracking (MPPT) in a closed-loop DC microgrid. This approach guarantees a smooth and chatter-free output voltage.
12	[40]	This work introduces a novel algorithm designed to discover the global maximum power point by integrating two commonly used MPPT algorithms typically employed in uniform solar conditions.
13	[41]	A refined INC-MPPT technique is developed specifically for the boost converter, enabling enhanced energy extraction from solar PV modules.
14	[42]	A MPPT, which offers rapid convergence and small oscillations is derived from the golden section search, P&O, and INC methods to achieve faster convergence and smaller oscillation,

<b>15</b>	[43]	A Proton Exchange Membrane Fuel Cell (PEMFC) system is equipped with a predictive maximum power point tracking mechanism.
<b>16</b>	[44]	a three-point model driven peak power tracking is adopted in this work, which extract peak power in both normal and partial irradiation conditions.
<b>17</b>	[45]	The perturb and observation method is applied to the single input multiple output solar PV converter.
<b>18</b>	[46]	It investigates MPPT based on adaptive neuro-fuzzy inference system implementation to photovoltaic based battery charger.
<b>19</b>	[47]	It studies the fuzzy logic controller is adopted in MPPT for high voltage gain dc-dc converter control.
<b>20</b>	[48]	A new adaptive back-stepping neural network controller to extract peak power in real time, is discussed in this work.

### **2.3 REVIEW OF MULTILEVEL INVERTER TOPOLOGIES FOR SOLAR PV ARRAY APPLICATIONS**

Multilevel inverters have gained significant attention in recent years due to their ability to generate high-quality output voltages with reduced harmonic distortion. These power electronic devices synthesize a desired output voltage by combining multiple levels of DC voltages, offering numerous advantages over conventional two-level inverters.

There are several multilevel inverter topologies that have been developed and studied extensively. One popular topology is the Neutral Point Clamped (NPC) inverter, which utilizes capacitors to provide multiple voltage levels at the output. By using this topology, the voltage stress on the switches is reduced, leading to improved efficiency and lower switching losses. Another commonly used topology is the Flying Capacitor (FC) inverter, which employs capacitors connected between the DC sources to generate multiple output voltage levels. The FC inverter offers advantages such as lower component count, reduced switching losses, and improved voltage balancing compared to other topologies. The Cascaded H-Bridge (CHB) inverter is another popular choice, where multiple H-bridge modules are connected

in series to generate a stepped voltage waveform. The CHB inverter provides a high number of voltage levels and has excellent voltage waveform quality, making it suitable for high-power applications. Additionally, the asymmetric cascaded multilevel inverter is an emerging topology that utilizes different DC voltage sources to generate output voltage with fewer switches compared to the CHB inverter. The asymmetric multi-inverters offer improved efficiency and reduced complexity, making it a promising option for multilevel inverter applications.

Overall, multilevel inverter topologies have demonstrated significant advancements in power electronics, enabling high-voltage, high-power applications such as renewable energy systems, electric vehicles, and motor drives. Continued research and development in this area are expected to lead to further improvements in efficiency, reliability, and cost-effectiveness of multilevel inverters, expanding their applications in the future. Table 2.2 here shows the extensive review of multilevel topologies for various applications.

Table 2.2 Multilevel Inverter topologies reviewed

S.N.	Ref	Description
1	[49]	This article proposes a 9 level double boost common ground type flying capacitor multi-level inverter topology with no leakage current.
2	[50]	The paper introduces a current-based sliding mode control technique tailored for a filter-less multilevel inverter.
3	[51]	This paper investigate a new nine-level ANPC-based inverter, which needs a low number of switches compared to other symmetrical inverters.
4	[52]	This paper proposes a single DC source based double level-doubling network high-resolution multilevel inverter for the central inverter application.
5	[53]	It discusses the CHB inverter operation with trapezoidal PWM for equal power sharing in power cells.
6	[54]	It proposes the NPC topology for the reduction of leakage current
7	[55]	This work proposes a single-stage switched-capacitor topology for multilevel inverter to ,maintain the peak inverse voltage of all switches within the dc source voltage



8	[56]	This paper presents single phase PUC inverter with different modulation schemes.
9	[57]	This paper presents nine-level PEC (PEC9), which is formed by seven active switches and two dc capacitors and it makes use of a single dc link.
10	[58]	This paper presents a thirteen level inverter with boost factor 6 and improved performance with reduced voltage ripples.
11	[59]	This work discusses the the hybrid modular multilevel converter to improve the overall efficiency.
12	[60]	It proposes five level switched-capacitor multi-inverter with capability of output voltage boost and leakage current elimination.
13	[61]	A novel multilevel inverter topology for medium voltage is discussed which is formed by several conversion units.
14	[62]	This article proposes eleven level multi-level inverter consist of two hal-bridge, one full bridge and one switched capacitor for medium voltage applications.
15	[63]	This paper presents single source thirteen level inverter topology formed by a three-level T-type neutral point clamped (NPC), half-bridge, and three-level switched-capacitor converter.
16	[64]	This article presents switched-capacitor thirteen level multilevel inverter which offers voltage boost of six times.
17	[65]	This paper discusses the fifteen level inverter formed by the just eight switches and one DC source for renewable energy applications.
18	[66]	This article discusses a three triple voltage gain seven level inverter, which has the ability of DC link capacitors voltage control.
19	[67]	This article discusses the a new hybrid three phase multilevel inverter with transformer.
20	[68]	This work investigates the level-shifted PWM for THD reduction in a eleven level cascaded H-Bridge inverter.

## 2.4 REVIEW OF MODULATION TECHNIQUES FOR SOLAR PV GENERATION APPLICATIONS

Pulse Width Modulation (PWM): Pulse width modulation is the most commonly used modulation technique in multilevel inverters. It involves varying the width of the output pulses to control the average output voltage. In multilevel inverters, PWM techniques are implemented by comparing a high-frequency carrier waveform with a reference waveform. By comparing these two waveforms, the switching signals for the power electronic switches are generated. The most popular PWM techniques for multilevel inverters include sinusoidal PWM (SPWM), selective harmonic elimination PWM (SHEPWM), and space vector PWM (SVPWM).

Sinusoidal Pulse Width Modulation (SPWM): SPWM is a widely used modulation technique in multilevel inverters. It aims to synthesize an output voltage waveform that closely resembles a sinusoidal waveform. In SPWM, the reference waveform is a sinusoidal waveform, and the carrier waveform is a high-frequency triangular waveform. By comparing the instantaneous values of the carrier and reference waveforms, the switch control signals are generated. SPWM offers good harmonic performance and low switching losses but suffers from low modulation index capability.

Selective Harmonic Elimination Pulse Width Modulation (SHEPWM): SHEPWM is a modulation technique that aims to eliminate specific harmonics from the output voltage waveform. By selecting appropriate switching angles, SHEPWM can eliminate specific harmonic and improve the overall output waveform quality. This technique requires solving a set of nonlinear equations to determine the switching angles that achieve harmonic elimination. Although SHEPWM offers excellent harmonics performance, it is computationally intensive and requires a higher number of switching levels. Space Vector Modulation (SVM): SVM is an advanced modulation method applied in multilevel inverters. It is derived from the concept of the space-vector position and offers a good compromise between harmonics performance and complexity. In SVPWM, the reference voltage vector is decomposed into multiple voltage vectors in the space vector diagram. By selecting the appropriate voltage vectors and the switching times, the output voltage waveform can be synthesized. SVPWM provides a higher modulation index capability and improved harmonics performance compared to SPWM. Table 2.3 here shows the modulation techniques and review of the solar PV array generation topologies.

Table 2.3 Reviewed modulation techniques

S.N.	Ref	Description
1	[69]	A sine pulse width modulation (SPWM) is employed in this paper to drive switches, and switching pattern is mainly focused to balance the capacitors and to balance capacitor charging/discharging.
2	[70]	This paper discusses the generalized theory of phase-shifted carrier pulse width modulation for cascaded H-bridge converters and modular multilevel converters.
3	[71]	This article introduces a cascaded packed U-cell multilevel converter, which is operated at low-frequency switching, using the nearest level modulation technique.
4	[72]	This article presents a novel method that utilizes the Selective Harmonic Elimination-Pulse Width Modulation technique over a wide range of modulation indices. This approach enables the attainment of a high-quality output waveform in a cascaded H-bridge multilevel inverter.
5	[73]	This paper discusses the current state of the art in two-level Space Vector Modulation and extends it to 3-Level SVM. It includes a comparative analysis of the performance of 3L SVM with other Multi-Carrier Pulse Width Modulation techniques.
6	[74]	This article reviews the various modulation techniques and challenges associated with it.
7	[75]	A low frequency hybrid modulation of phase shift and selective harmonic PWM is proposed in this article.
8	[76]	This paper discusses the modulation ratio in details for the modular multi-level converters.
9	[77]	This paper proposes modulation technique to reduce insertion time of submodules.
10	[78]	This article discusses a simple and low-computational-cost modulation technique for multilevel cascaded H-bridge converters.
11	[79]	This article discusses the phase-shift and the step wave modulation techniques implementation to symmetrical cascaded H-bridge multilevel inverter.
12	[80]	This paper studies the challenges faced by low device switching frequency and improvement in the same.
13	[81]	It explores further development of pulsewidth modulation techniques for the current fed multi-level converters.
14	[82]	This paper proposes the injection of the third harmonic to mitigate the second harmonic current.
15	[83]	In this article fuzzy logic is proposed to implement the traditional modulation methods which uses the the logic gates.
16	[84]	A dual inverter with battery and capacitor as a power source with space vector modulation method is discussed in this article.
17	[85]	It reviews modulation techniques of fundamental switching frequency implemented in multilevel inverters.
18	[86]	It discusses the implementation of fuzzy logic based switching device.

<b>19</b>	[87]	This paper reviews various normal and modular multi-inverters with different modulation methods.
<b>20</b>	[88]	This article discusses the role of modulation techniques in power quality improvement and DC link utilization.

#### **2.4 REVIEW OF INVERTER CONTROL SCHEME FOR SOLAR PV POWER GENERATION APPLICATIONS**

Grid synchronization is a crucial aspect of multilevel inverter control when it comes to connecting them to the utility grid. Various control methods have been proposed to ensure accurate grid synchronization and power injection. One commonly used approach is the phase-locked loop (PLL), which tracks the grid voltage and generates a reference signal for synchronization. Different PLL variants, such as synchronous reference frame PLL and enhanced PLL, have been studied for multilevel inverters. Additionally, advanced control techniques like model predictive control and adaptive control have been explored to enhance grid synchronization accuracy and robustness. A review of these multilevel inverter grid synchronization control methods provides valuable insights into their performance, stability, and applicability in grid-connected applications as shown in Table 2.4.

Table 2.4 Reviewed Inverter control methods

<b>S.N.</b>	<b>Ref.</b>	<b>Description</b>
<b>1</b>	[89]	This article presents a model predictive control with discrete time control of grid integrated ANPC multilevel converter.
<b>2</b>	[90]	This article explores the application of a neutral-point-clamped multilevel converter in grid-connected solar Photovoltaic systems. It introduces a new voltage balancing converter to address voltage imbalances and enhance the performance of the multilevel converter in the PV systems.
<b>3</b>	[91]	The paper focuses on the control of a single-phase cascaded H-bridge multilevel inverter specifically designed for grid-connected photovoltaic systems.
<b>4</b>	[92]	This work uses model predictive control to control the thirteen level solar-grid integrated system.
<b>5</b>	[93]	This study introduces hysteresis control applied to the UXE-type inverter topology, incorporating a PI controller. The gains of the PI controller are determined through Particle Swarm Optimization (PSO) to enhance the performance of the inverter.

<b>6</b>	[94]	This paper discusses about unit template based AC current control using two methods: phase information from phase locked loop and voltage peak estimation method.
<b>7</b>	[95]	This paper presents a comparative study of discrete proportional integral and proportional resonant current control for single-phase uninterruptible power supply inverters.
<b>8</b>	[96]	In this paper, a fast and robust D-Q method for current control is introduced for the purpose of regulating the output power of single-phase grid-connected inverters.
<b>9</b>	[97]	This paper introduces a finite-control-set model predictive control technique specifically designed for grid-tied packed U-Cells multilevel inverters.
<b>10</b>	[98]	A comprehensive control scheme for multi-microgrid system is presented in this work, which compensates harmonics due to non-linearity in the loads.
<b>11</b>	[99]	The control scheme consist of proportional-integral, artificial neural network and fuzzy logic is presented in this work for a fifteen level multi-level converter.
<b>12</b>	[100]	This article implements closed loop current control and presents dynamic analysis in a solar panel companion inverter.
<b>13</b>	[101]	This work presents self-voltage balancing control for five level active neutral point clamped switched capacitor inverter.
<b>14</b>	[102]	This article presents the method of designing current controller for a grid-tied five-level packed U-cell inverter with LCL output filter.
<b>15</b>	[103]	This paper presents model predictive control as an alternative control strategy for H-bridge neutral-point-clamped converter for grid-integrated string solar PV systems.
<b>16</b>	[104]	In this paper, a robust and adaptive sliding-mode (SM) control approach is proposed for a grid-connected solar photovoltaic system that utilizes a cascaded two-level inverter.
<b>17</b>	[105]	The mixed staircase-pulse-width-modulation by using the sorting algorithm to decide cell's switching state is presented in this paper.
<b>18</b>	[106]	It discusses the control stucture based on multi-level energy buffer and voltage-modulator for micro-inverters.
<b>19</b>	[107]	This paper presents the control of two cascaded full bridge inverters with different DC-link voltages.
<b>20</b>	[108]	This article discusses the the active power transfer by the band stopmgeneralized integral control and enhanced phase-locked-loop for grid synchronization.

The comparison of the presented topologies from five level to thirteen level is done with similar level topologies: five level T-Type with other five level topologies discussed in [109]-[115], seven level PUC, K-Type and PEC with other seven level topologies discussed in [116]-[119], nine level CHB with the other similar level

topologies [120]-[123], eleven level PEC with other eleven level topologies presented in [124]-[130] and thirteen level ladder type with other similar level topologies presented in [131]-[135]. Multilevel inverters offer several advantages compared to traditional two-level inverters, primarily due to their ability to synthesize waveforms with higher voltage levels. Some advantages of having more levels in multilevel inverters are tabulated here,

Table 2.5 Comparison of two level with multilevel inverters

S.N.	Disadvantages of Two Level Inverters	Advantages of Multilevel Inverters
1	THD is high due to square waveshape of output voltage.	THD is low due to stepped waveshape of output voltage.
2	Low voltage handling capacity as high voltage cause more voltage stress	High voltage handling as high voltages are generated by stacking multiple voltage levels.
3	High $\frac{dV}{dt}$ and electromagnetic interference	Low $\frac{dV}{dt}$ and electromagnetic interference
4	Two level inverters are operated at high frequency which leads to high switching loss and poor efficiency.	Multilevel inverters operates at lower switching frequencies compared to two-level inverters.
5	Modularity and scalability is not possible.	Multilevel inverters can be designed in a modular fashion, allowing for easier scalability by adding more levels or modules.

## IDENTIFIED RESEARCH GAPS

Following research gaps have been identified from the outcome of the literature review.

- Design, control and real-time execution of five level T-type multilevel converter for solar PV array power generation applications.
- Design, control and real time execution of PUC and PEC type seven level converter for solar PV array power generation applications.
- Design, control and real-time execution of K-Type symmetric seven level converter for solar PV array power generation applications.

- Design, control and real-time execution of cascaded H-Bridge nine level converter for solar PV array power generation applications.
- Design, control and real-time execution of packed E-Cell (PEC) eleven level converter for solar PV array power generation applications
- Design, control and real-time execution of ladder type thirteen level converter for solar PV array power generation applications

## **2.5 CONCLUSIONS**

In this literature review, state-of-the-art on MPPT techniques are explored and multilevel inverter topologies, modulation techniques, and control methods are reviewed for various applications, particularly in the context of renewable energy systems. The findings indicate significant advancements and a growing body of research in these areas, demonstrating their importance in achieving efficient power conversion, improving grid integration, and optimizing energy generation.

Regarding MPPT techniques, it has been observed that conventional methods such as Perturb and Observe (P&O) and Incremental Conductance (INC) remain widely used due to their simplicity and effectiveness. However, more advanced techniques based on algorithms like artificial intelligence (AI), fuzzy logic, and neural networks have shown promising results in enhancing the efficiency and tracking accuracy of MPPT algorithms.

Numerous MLI topologies, such as Neutral-Point Clamped (NPC), Cascaded H-Bridge (CHB), and Flying Capacitor (FC) inverters, have been extensively investigated. The topologies emerging from the hybridization of traditional configurations are explored for solar PV-grid integrated applications. Each topology exhibits specific advantages and limitations in terms of complexity, cost, efficiency,

and harmonic performance. The choice of topology depends on the requirements of the application and the trade-offs between these factors.

Modulation techniques play a crucial role in multilevel inverters to synthesize high-quality output waveforms with reduced harmonics. Pulse width modulation (PWM) techniques, including carrier-based PWM (CBPWM), nearest level modulation, and selective harmonic elimination (SHE), have been extensively studied. Each technique offers advantages and challenges in terms of switching losses, harmonics distortion, and complexity.

Lastly, control methods for multilevel inverters have witnessed significant advancements. Traditional control approaches, such as proportional-integral (PI) and proportional-resonant (PR) control, have proven effective in ensuring stable and reliable operation. Further research is needed to explore the integration of these advanced control methods with multilevel inverters, considering the requirements of renewable energy systems, grid integration standards, and power quality regulations.

In conclusion, this literature review highlights the significant progress made in MPPT techniques, multilevel inverter topologies, modulation techniques, and control methods. However, several research gaps and future directions exist, including optimal topology selection, advanced control strategies, improved modulation techniques, fault detection and protection, scalability and expandability, reliability and durability, cost-effectiveness, and manufacturing. Addressing these gaps is to contribute to the development of more efficient, reliable, and cost-effective systems for renewable energy integration and grid fed operation. Future research efforts should focus on these areas to further advance the field and accelerate the adoption of these technologies in practical applications.



## **CHAPTER-III**

### **CONTROL AND DESIGN OF FIVE LEVEL T-TYPE MULTILEVEL CONVERTER FOR SOLAR PV GENERATION APPLICATIONS**

#### **3.1 INTRODUCTION**

In this chapter, the design, modelling and control of a modulation method with newly developed carrier signal is presented. This scheme is operated at low frequencies for the total-harmonics-distortion (THD) mitigation of three-phase five-level T-type multilevel inverter are carried out for solar PV grid-tied generation system. The proposed work is implemented without any DC-DC conversion state, which has reduced the overall cost and complexity. The control algorithm of this work consist of DC and AC side control. The DC-link voltage is maintained to the reference value equal to maximum power point voltage while AC side control consists of the comparison of grid current to the equivalent DC reference current. The outer loop of DC voltage control consists of MPPT controller for each PV array and P&O algorithm is implemented to track the reference voltage at maximum power point. The inner loop of current control for active power transfer, is attained by the unit template control method with the level shifted new low-frequency multicarrier pulse width modulation. The harmonic filter of low inductance is placed between the grid and the converter. The simulation of this system is done on MATLAB/SIMULINK and findings are validated in real-time simulator OPAL-RT. The solar PV generation system is operated in steady state and transient conditions and results are discussed in detail in this chapter. The operating performance is verified in accordance with the IEEE-519 standard. The system configuration,

applied control, results, modelling are discussed in various sections of this chapter.

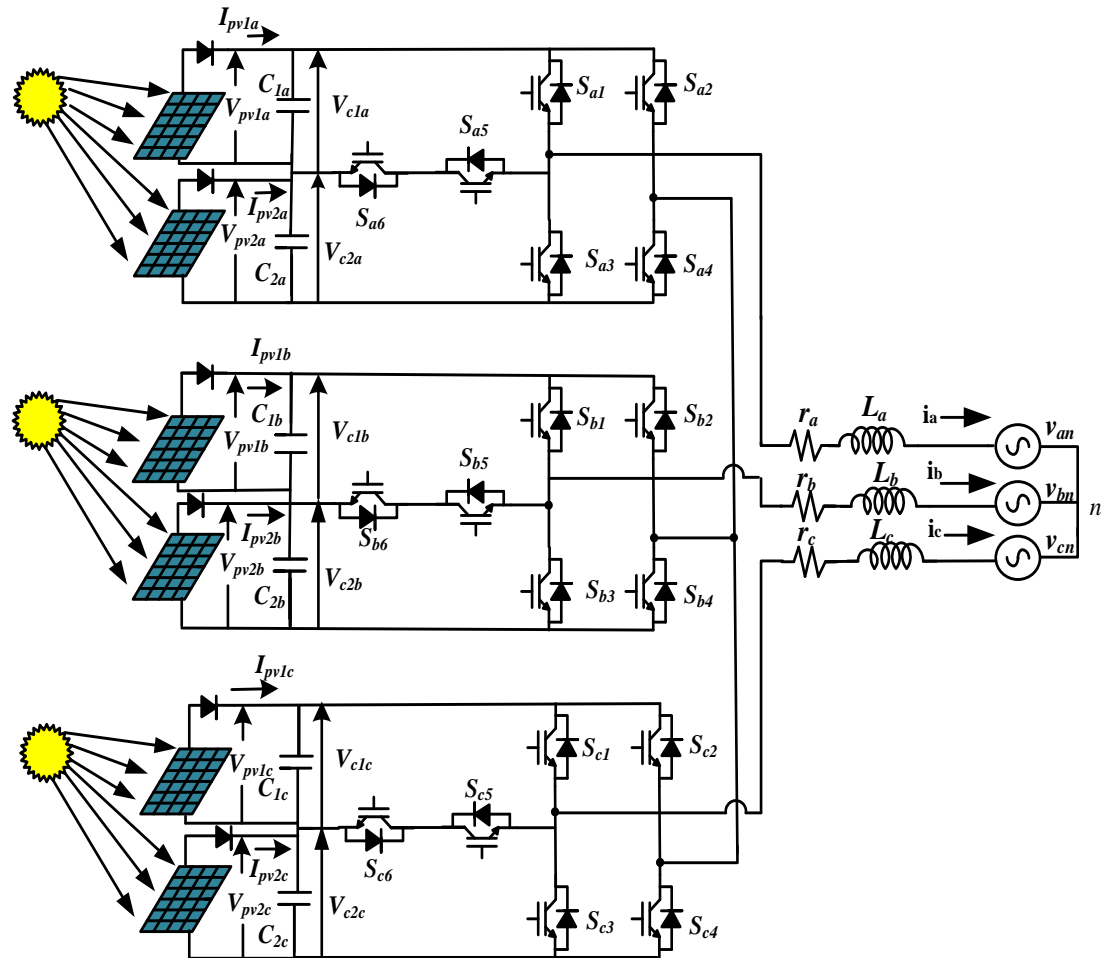


Fig. 3.1. Five level T-Type SPV system

### 3.2 SYSTEM CONFIGURATION OF FIVE LEVEL T-TYPE CONVERTER FOR SOLAR PV GENERATION SYSTEM

The five level T-type solar converter configuration is shown in Fig. 3.1, which comprises of total six solar arrays and each array generates 6.3 kW power at MPP.

This MLI topology has six number of switches in each phase where four switches  $S_1$ - $S_4$  form the H-Bridge power cell and  $S_5$ - $S_6$  act as a bidirectional directional switch. The stepped converter output voltage is fed to the harmonic filter, while two solar PV arrays in each phase power the inverter. The solar panel voltage  $V_{PV1}$  and  $V_{PV2}$  add up to generate the positive peak levels  $(V_{PV1} + V_{PV2})$  and negative peak

levels ( $-V_{PV1} - V_{PV2}$ ) while  $V_{PV1}$  &  $-V_{PV2}$  do generate first level first level in negative

Table 3.1 Switching states for T-Type SPV converter

S1	S2	S3	S4	S5	S6	Voltage level
On	Off	Off	On	Off	Off	$(V_{pv1} + V_{pv2})$
Off	Off	Off	On	On	Off	$V_{pv1}$
On	On	Off	Off	Off	Off	0
Off	On	Off	Off	Off	On	$-V_{pv1}$
Off	On	On	Off	Off	Off	$-(V_{pv1} + V_{pv2})$

and positive half cycle, respectively and zero level is generated by the bypass of all switches. The detailed switching sequence is tabulated in Table 3.1.

The KVL equation for the T-Type SPV converter is represented as,

$$V_{conx} - V_x = i_x r_x + L_x \frac{di_x}{dt} \quad (3.1)$$

Where x stands for phase 'a', 'b' and 'c',  $V_{con}$  and  $V_x$  are converter and grid voltage respectively, r and L are resistance and inductance of interfacing harmonic filter.

### 3.3 CONTROL STRATEGY OF T-TYPE FIVE LEVEL CONVERTER FOR SOLAR PV GENERATION APPLICATIONS

Fig. 3.2 depicts the adopted control scheme of T-Type SPV converter, which insures maximum solar power extraction from the six solar-arrays by the MPPT controllers employed in every array. The control scheme ensures power fed to the grid under all solar-irradiance conditions. The adopted control scheme is divided into three

subsections. The system specifications are shown in Table 3.2.

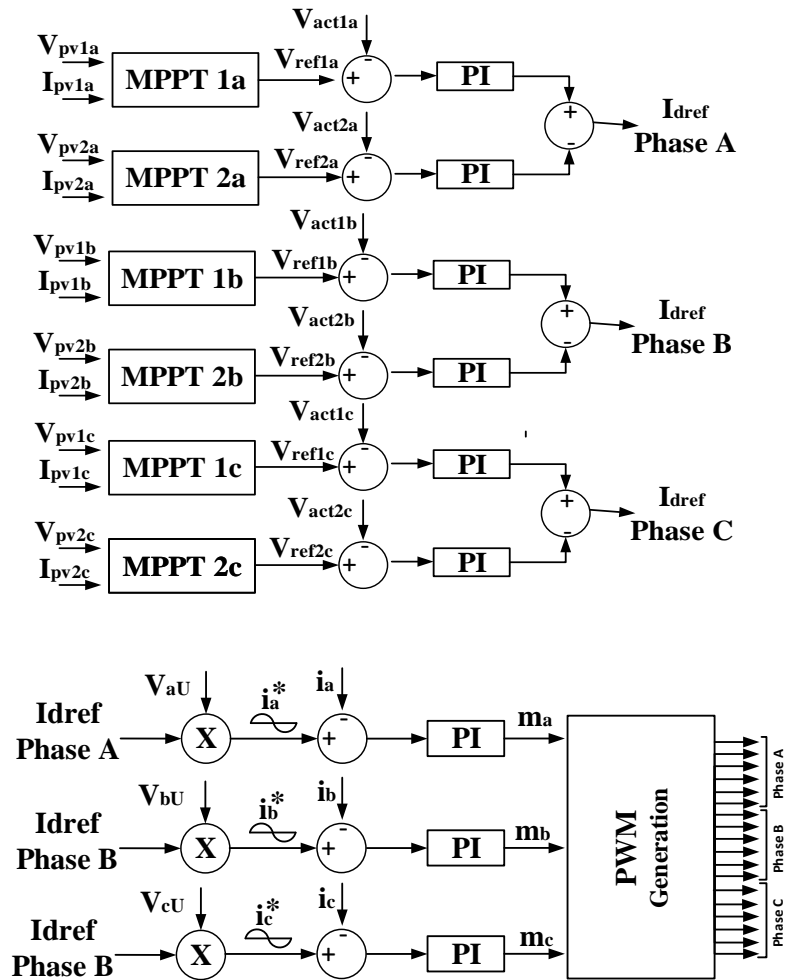


Fig. 3.2. The control scheme of T-Type inverter

Table 3.2 System Parameters

Symbol	Parameter	Value
$V_{pv}$	Voltage of solar panel at Maximum power point	197.88V
$I_{pv}$	Current of solar panel at maximum power point	31.88 Amps
$(P_{pv})_{phase}$	Power/phase of solar panel at maximum power point	12.616 kW
$P_{pv}$	Total Power of solar panels at maximum power point	37.850 kW
$P_{grid}$	Power fed to grid ( at 97% overall efficiency)	36.714 kW
$V_{gp}$	Peak grid phase voltage	338.8 V
$I_{gp}$	Peak grid Phase Current	72.24 A
$L$	Interfacing inductor	3.5 mH
$f_{sw}$ or $f_1$ or $1/T_s$	Switching frequency	500 Hz
$K_p, k_i$	Gain of Modulating signal PI Controllers	0.008, 0.001
$K_p, K_i$	Gain of DC link controllers	4.9, 0.48

### 3.3.1 MPPT Control

The widely adopted algorithm perturb & observation (P & O) is employed to track the reference voltage corresponding to the maximum power point (MPP). This algorithm works by varying the reference voltage perturbs and monitor the power change as observer. The execution of this algorithm takes place in steps of increasing reference voltage until MPP is reached. The MPP voltage determined from MPPT controller acts as a reference for DC-link capacitor voltages in each solar-array. The equations of this controlled voltage regulation are expressed as,

$$I_{d1x}(u) = I_{d1x}(u-1) + Kp(e_{c1x}(u) - e_{c1x}(u-1)) + K_i e_{c1x}(u) \quad (3.2)$$

$$I_{d2x}(u) = I_{d2x}(u-1) + Kp(e_{c2x}(u) - e_{c2x}(u-1)) + K_i e_{c2x}(u) \quad (3.3)$$

Where,

$$e_{c1x} = V_{ref1x} - V_{act1x}; e_{c2x} = V_{ref2x} - V_{act2x} \quad (3.4)$$

The total phase reference current is obtained by the addition of current of voltage balance controller.

$$i_{dref\_x} = i_{d1x} + i_{d2x} \quad (3.5)$$

This reference current regulates the active power into the grid by balancing the capacitor voltages in accordance with the solar-irradiance level.

### 3.3.2 Unit Template Inverter Control

The T-Type inverter synchronization with the grid is achieved by the unit template control method. The unit-template of grid phase-voltage are determined as,

$$V_{au} = \frac{v_{an}}{v_p}, V_{bu} = \frac{v_{bn}}{v_p}, V_{cu} = \frac{v_{cn}}{v_p} \quad (3.6)$$

These unit templates and reference DC current give grid reference currents as,

$$i_a^* = I_{dref,phaseA} * V_{aU}, i_b^* = I_{dref,phaseB} * V_{bU}, i_c^* = I_{dref,phaseC} * V_{cU} \quad (3.7)$$

These AC reference currents are used to generate the modulating  $M_{a-c}$ . The sinusoidal modulating signals act as reference signals with level shifted multi-carrier PWM. The modified triangular wave is used as a carrier to improve the power quality. The generation of new multi-carrier signal is discussed in next section.

### 3.3.3 New Multi-carrier Modulation Scheme

The level shifted multi-carrier sinusoidal pulse width modulation is a popular PWM method that compares the high frequency triangular carrier wave with reference sinusoidal and generates the switching pulses of inverter. Researchers have adopted many variations of level shifted carrier such as phase disposition (PD), phase opposition disposition (POD) for improvement of power quality. Many researchers have used carrier signal waveform other than triangular waveform. They have used parabolic shape for carrier, which has been generated by mixing of two signals. The new multi-carrier signal used in this work is a modified triangular wave, which is created by the integrating the two signals: pulse and triangular. Fig. 3.3(a) shows the schematic to generate the new multi-carrier signal. The triangular and modified triangular signals are shown in Fig. 3.3(b).

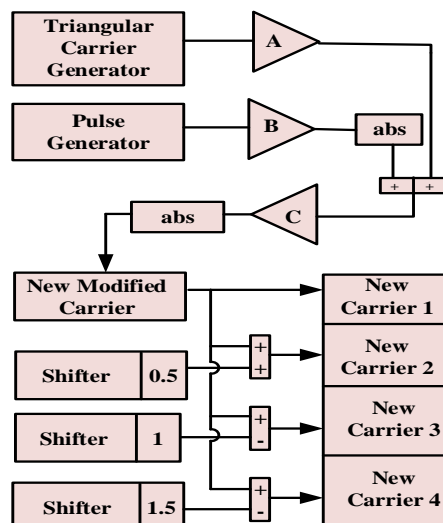
A triangular wave of five hundred Hertz and a pulse signal (2000 Hz) scaled by constants 'A' and 'B' respectively are added and resulting signal is scaled by the factor 'C'. The value of 'A', 'B' & 'C' decide the amplitude of modified while the frequencies of synthesized and triangular wave are same. The equation for the modified wave is formulated as,

$$W_{mod} = |(W_{tri}(f1) * A + |W_{pulse}(f2) * B|) * C| \quad (3.8)$$

New modified wave shape is achieved by integration of pulse function, however, the triangular wave frequency or modulation index doesn't change that is wave shape of triangular carrier is modified without changing its frequency. The frequency modulation index is given as.

$$m_f = \frac{\text{carrier frequency}}{\text{modulating signal frequency}} = \frac{f_1}{f_{\text{mod}}} \quad (3.9)$$

Fig. 3.4 validates of no change of time-period  $T_s$ , frequency of 500 Hz of modified carrier wave and modulating signal 500/50 that is equal to 10. This carrier signal created the four level shifted multi-carrier waves, which generate the five voltage steps at the multilevel inverter output. Fig. 3.4 shows four level shifted carriers that accommodate full reference sine wave signal for modulating index 10. This new multi-carrier scheme can be applied to the other higher levels also. The modified triangular wave is generated by the suitable selection of the frequencies  $f_1$  and  $f_2$ . The shape of the carrier depends on the pulse signal frequency  $f_2$  while change in the  $f_1$  causes the change in modulating signal. In this work, low frequency of 500 Hz is selected for carrier signal and 2000 Hz pulse signal is integrated in the triangular wave. This technique is applied to five level T-Type converter for achieving the enhanced power quality.



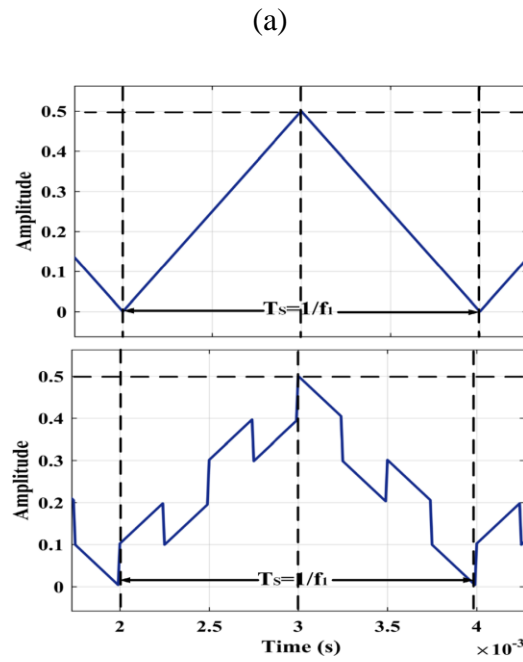


Fig. 3.3. (a) block diagram of modified triangular wave (b) Triangular and modified triangular signals

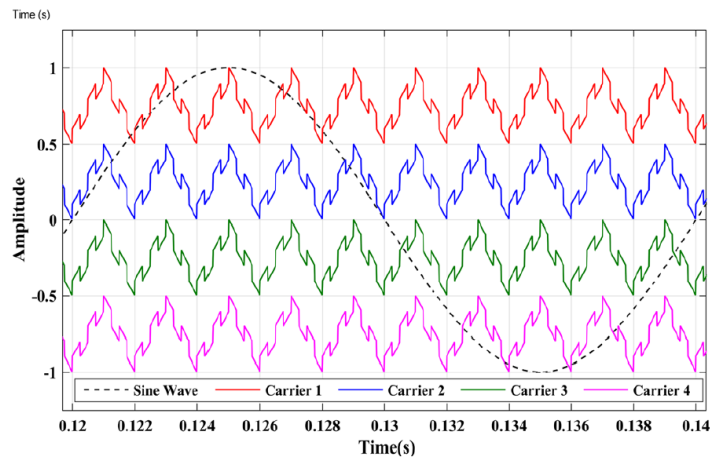


Fig. 3.4. New multi-carrier for five level output with reference signal

### 3.4 MATLAB MODELING OF T-TYPE FIVE LEVEL CONVERTER FOR SOLAR PV GENERATION APPLICATIONS

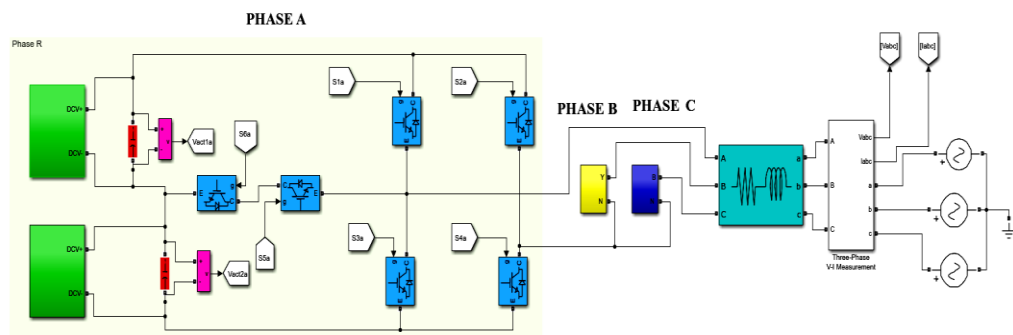
Fig. 3.5(a) shows the developed MATLAB model of power circuit the five level T-Type converter. Each phase consists of two solar arrays having two DC power terminals DC+ and DC-. The DC link capacitors are connected across the DC terminals of solar arrays and the voltage  $V_{act1a}$  &  $V_{act2a}$  are measured. The H-Bridge



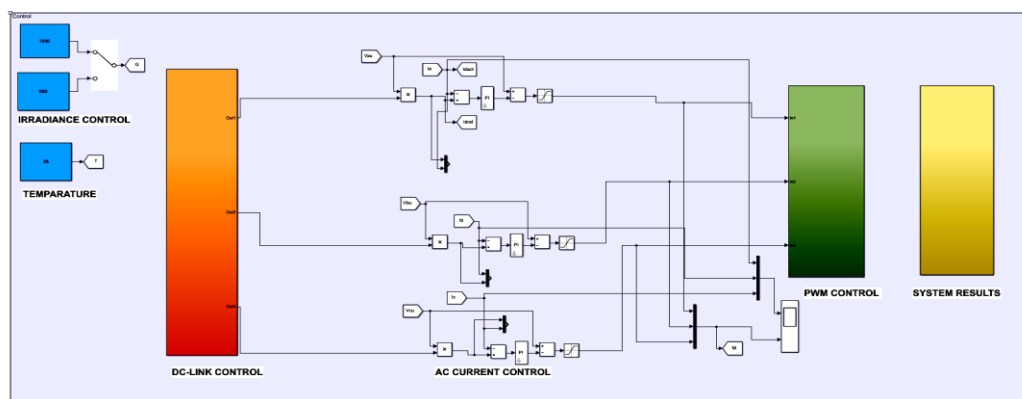
power cell is formed by the switches  $S_{1a}$ - $S_{4a}$ , while switches  $S_{5a}$  &  $S_{6a}$  are cascaded back to back to form a bidirectional path. Phases B and C are formed similar to Phase 'A'. Three phases of converter are connected in the star and are fed to R-L harmonic filter. The measurement of three phase voltages and currents is taken before feeding the power to the grid.

Fig. 3.5 (b) shows the control scheme implementation of this converter. The DC link voltage control consists of DC reference current generation by the balancing of capacitor voltages. The DC reference current is multiplied by the estimated unit voltage templates, which gives the modulating signals for PWM control. The system response at steady and transient state is recorded in the results block.

### Five Level T-Type Converter for Grid-Tied Solar Photovoltaic Applications



(a)



(b)

Fig. 3.5 MATLAB model of (a) power circuit (b) control scheme, of T-Type

converter

### 3.5 SIMULATED RESULTS OF T-TYPE FIVE LEVEL CONVERTER FOR SOLAR PV GENERATION APPLICATIONS

This T-Type solar power generation set-up is simulated in MATLAB and validated by the real time execution on OPAL-RT. The improved modulation strategy shows enhanced power quality for the T-Type converter based solar PV generation system. The results are discussed in three sections: steady state, dynamic state and harmonic performance.

#### 3.5.1 Steady State Analysis

Fig. 3.6 depicts the DC link capacitors voltage of phase A. The DC link capacitors voltage is tracked to the voltage corresponding to voltage at maximum power point by the proportional-integral (PI) controllers. The system performance at solar irradiation of  $1000\text{W}/\text{m}^2$  is depicted in Fig. 3.7. Total 37.8 kW electrical power is transferred, which is equally shared by all six solar-arrays of the three phases. A 36.8 kW power is transferred to the grid at unity power factor and 97% efficiency. The constant solar irradiation ensures constant grid current injection, and balanced grid voltages. The zero reactive power transfer ensures successful unity power factor operation.

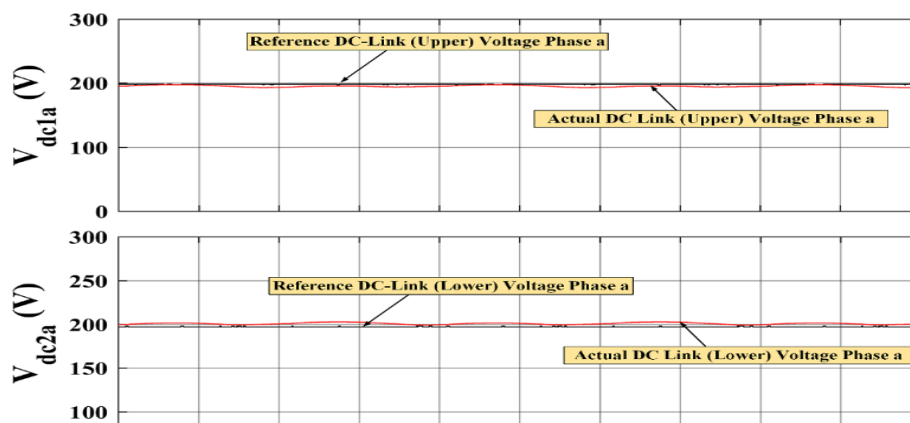


Fig. 3.6. DC link capacitors voltages balancing

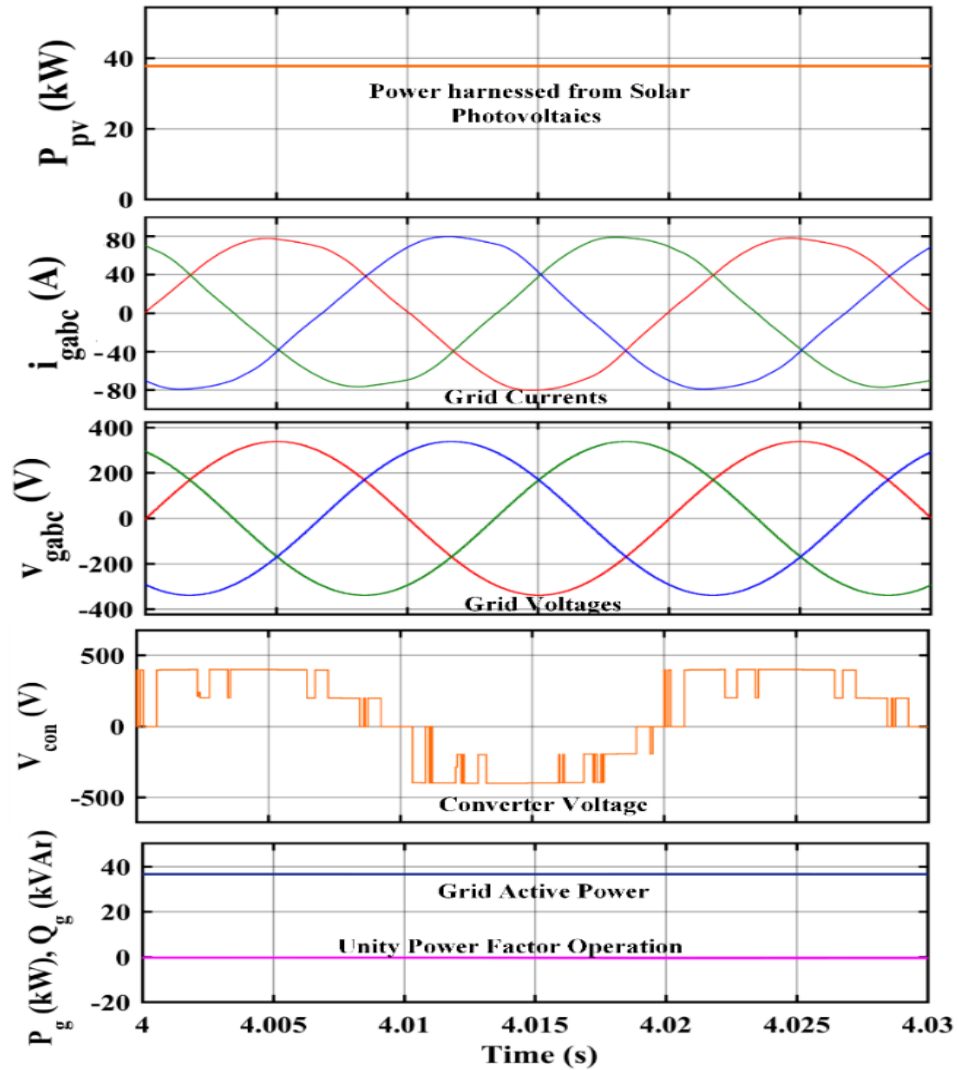


Fig. 3.7. Steady state response of five level T-Type converter based SPV generation system

### 3.5.2 Dynamic Response Analysis

Figs. 3.8-3.9 show the results of dynamic response of the solar photovoltaic system when there is a change in solar irradiation. Fig. 3.8 depicts that power generation fed to the grid becomes half when irradiance level decreases to half. The injected grid current, which directly depends on the solar-irradiance levels, stabilizes to half of the value corresponding to normal irradiance level. The converter five level voltage maintains its enhanced harmonic profile, which is closer to sinusoidal shape. Fig. 3.9 shows the system response when solar-irradiation is increased to normal level from

half, the power harnessed by the solar PV array is also increased to the normal level and power transfer to the grid become normal at unity power factor with grid current is increasing and stabilizing to normal value corresponding to normal irradiation levels. These results are taken by operating the solar PV generation system with closed-loop control and use of modulation with new multi-carrier. The system performance indicates the better power quality and good performance in varying irradiation situations.

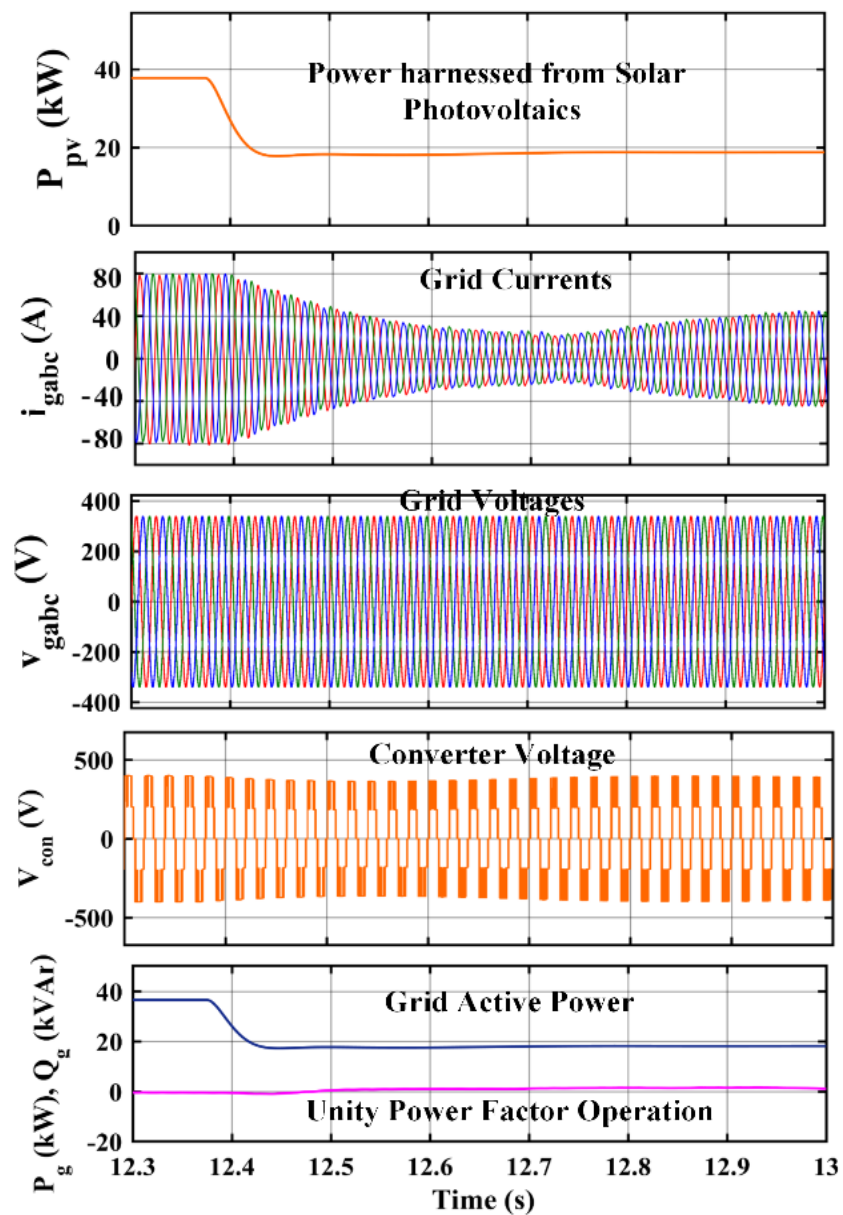


Fig. 3.8. Dynamic response of SPV system during the fall of irradiance

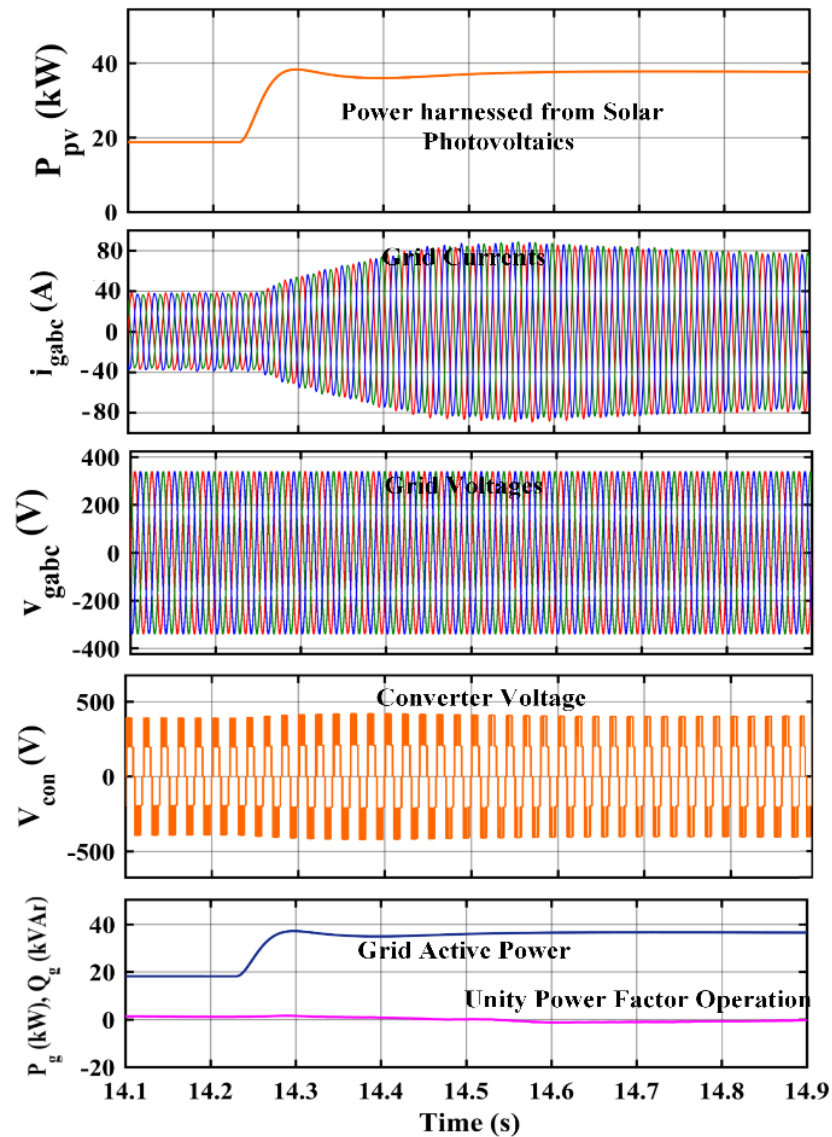
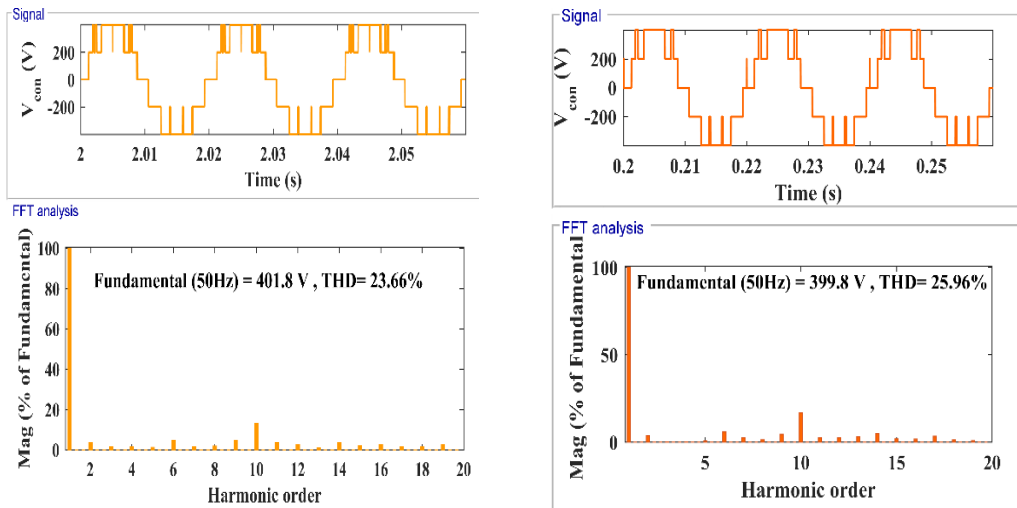


Fig. 3.9. Dynamic response of SPV system during the rise of irradiance

### 3.5.3 Harmonic Response Analysis

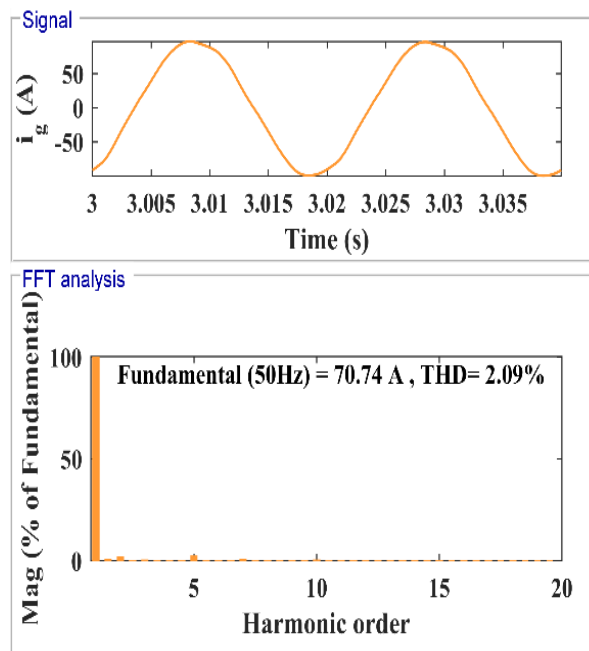
The comparative harmonic analysis is done for the new multi-carrier modulation scheme with the popular sinusoidal PWM. The comparison is carried for the THD with both methods. The voltage THD of converter at full modulation index is 25.96% for sinusoidal PWM at carrier frequency of 500 Hz. The voltage THD is improved to the 23.66% when PWM with new multi-carrier is employed, which ensures better harmonic performance. The improvement of THD is observed at the low frequency, which enhances performance further owing to lower switching loss.

Figs. 3.10 (a-b) show the converter voltage THDs for both new and basic PWM scheme, which shows that fundamental component of the converter voltage is also increased with new modulation. Moreover the THD of grid current is also observed



(a)

(b)



(c)

Fig. 3.10. Harmonic performance of converter voltage (a) with new multi-carrier (b) conventional SPWM and (c) grid current with new multi-carrier

TABLE 3.3 Modulation index vs THD of converter voltage (%)

Modulation Index	SPWM (PD)	SPWM (POD)	SPWM (APOD)	New Multicarrier PWM Scheme
0.5	52.14	47.82	54.62	46.38
0.6	44.22	41.11	48.9	40.49
0.7	41.40	40.40	44.34	39.24
0.8	38.32	38.37	36.34	35.28
0.9	33.29	32.66	30.39	28.85
1.0	25.96	29.82	27.12	23.66

TABLE 3.4 Modulation Index vs fundamental voltage component(V)

Modulation Index	SPWM (PD)	SPWM (POD)	SPWM (APOD)	New Multicarrier PWM Scheme
0.5	200.2	199.9	199.7	205.9
0.6	239.7	239.1	239.0	239.9
0.7	279.6	279.1	279.3	279.7
0.8	319.3	319.1	319.7	319.8
0.9	360.0	345.8	361.3	365.6
1.0	399.8	388.7	400.1	401.8

and the depicted in Fig. 3.10 (c), which shows the current THD is 2.09% under the IEEE 519 standard. Tables 3.3 and 3.4 shows the comparative assessment of the new multi-carrier modulation scheme with the level shifted PWM. The level shifted PWM in multiple orientations such as phase disposition (PD), phase opposition disposition (POD) and alternate phase opposition disposition (APOD) is used for comparison. The harmonic performance is observed at various modulation indexes,

which indicates the solar irradiation levels. The new multi-carrier scheme performance is better than traditional level shifted PWM and it gives high fundamental voltage component, which is shown in Table 3.4.

### **3.6 REAL TIME EXECUTION OF T-TYPE FIVE LEVEL CONVERTER FOR SOLAR PV GENERATION APPLICATIONS**

The solar photovoltaic system simulation results are validated by the real time execution on OPALRT. Digital time sampling control is used to validate the PI controllers with modulating scheme. The real time simulation is performed at the sampling rate of  $5e^{-5}$  sec.

#### **3.6.1 Dynamic Response Analysis**

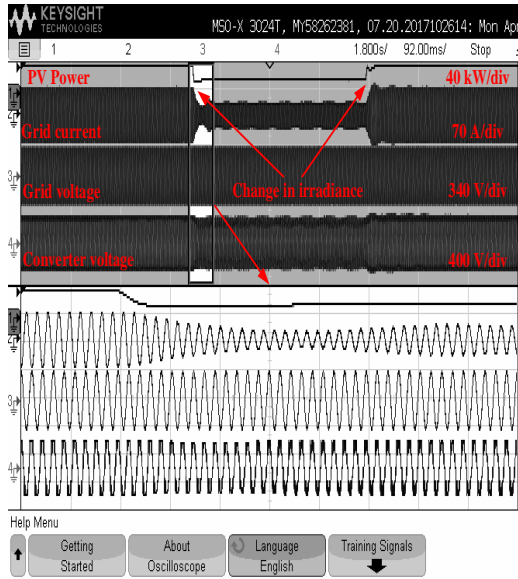
Fig. 3.11 (a) shows the system performance when solar irradiance fall by half and effect of grid power decrease is depicted by the zoomed view. The current injection to the power-grid decreases with the decrease in the solar insolation.

Fig. 3.11 (b) shows the performance of T-Type system when the solar irradiation increases to normal value of  $1000 \text{ W/m}^2$ . The power fed increases in proportion to the solar irradiation increase. The five level converter voltage maintains its waveform and magnitude during varying irradiation.

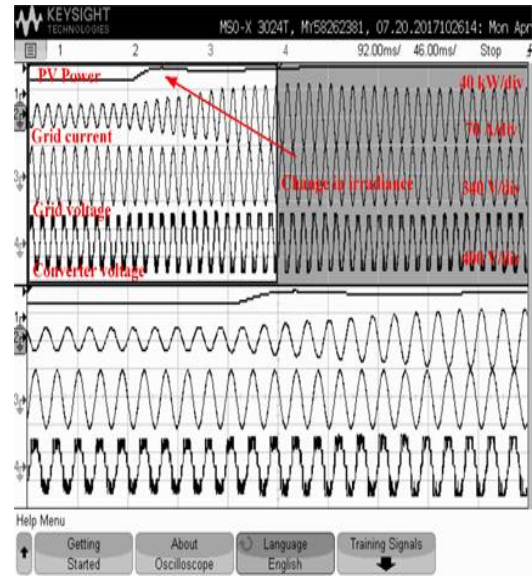
#### **3.6.2 Harmonic Response Analysis**

Fig 3.12 (a-b) shows the harmonic performance with real-time simulator, which validates the performance of system in MATLAB Simulink. The converter voltage performance is validated in real-time with a value 23.19%, which is better than with triangular carrier PWM. The grid current THD is 2.07% fairly better than permissible limit of 5%. This shows the validation of successful operation of five T-Type converter based solar photovoltaic generation system.



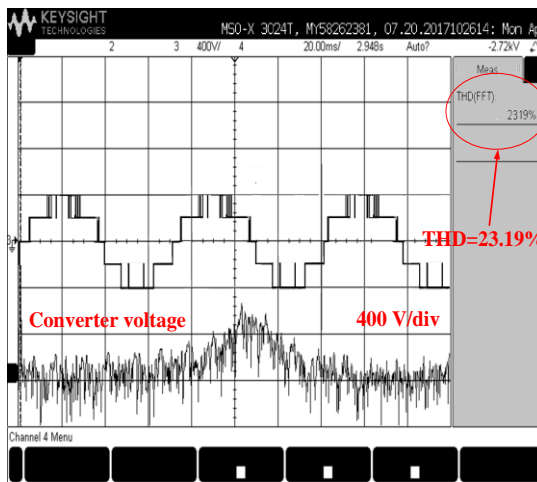


(a)

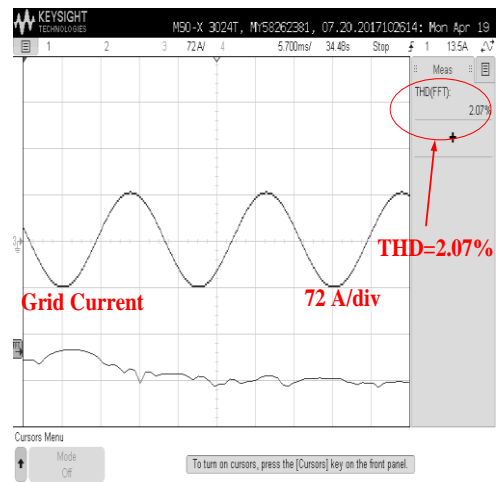


(b)

Fig. 3.11 Dynamic performance of T-type SPV system (a) fall in irradiance (b) rise in irradiance in RT simulator



(a)



(b)

Fig. 3.12 Harmonic response in RT simulator (a) Converter voltage THD (b) Grid current THD

### 3.7 CONCLUSIONS

The use of new multi-carrier modulation has improved the harmonic performance of the five level T-type multilevel converter. This new multi-carrier is generated from two different signals of different frequencies to provides a new modified wave shape. The frequency modulation index of new PWM scheme remains same and

fundamental voltage component of converter is improved. The new carrier signal at lower than widely used frequencies is presented to switch the converter in the feedback control mode. The dynamic response is verified in real-time digital simulator. This work provide the new scope of power quality improvement of solar PV generation system by application of the new modulation method. The low frequency switching has improved the inverter efficiency owing to low frequency switching. Harmonic performance is tested with THD of converter phase voltage is 23.19% and current THD of 2.07%. The harmonic performance of grid current is within the 5% limit of the IEEE-519 standard.

## **CHAPTER-IV**

### **CONTROL AND REAL TIME EXECUTION OF PUC AND PEC TYPE SEVEN LEVEL CONVERTER FOR SOLAR PV GENERATION APPLICATIONS**

#### **4.1 INTRODUCTION**

In this chapter, a seven level packed U-cell (PUC) in three phase configuration is investigated for the harmonics distortion mitigation or power quality improvement. three power quality investigation of a seven level three phase packed U-cell (PUC) is presented. The system is compared for total harmonic distortion (THD) with various multicarrier PWM schemes. The seven level PUC is formed by two solar photovoltaic (PV) panels of different voltage in each phase and operated in grid-tied mode to transfer the transformed solar power to the utility grid. The harmonic performance of converter output voltage determines the quality of power transfer to the grid and modulation technique plays important rule in that. The level shifted pulse width modulation method is most popular for inverter switching control among various methods because of the simple adaptation. The pulse width modulation method for PUC7 converter based solar power generation system used a new modified triangular shape carrier signal. The new scheme also increases the fundamental voltage component of converter. The comparative analysis of modulation techniques shows the better performance with new modified carrier based PWM. The solar PV generation system is implemented with the closed loop control and an inclusion of modified switching scheme. The power transfer to the grid takes place smoothly as the proportional-controller (PR) performs excellently. System is modelled in MATLAB and operated in varying irradiance parameters. The outcome of response in SIMULINK confirms the minimization of THD by using the new multi-carrier PWM. The system response in steady and dynamic state is

validated in the real-time simulator under varying solar irradiation conditions. This chapter is divided into sections to discuss the system configuration with the explanation of converter switching logic for creating all voltage levels, control scheme implementation for DC & AC side, modulation technique, performance in result section and conclusion.

## 4.2 CIRCUIT CONFIGURATION OF PUC AND PEC TYPE SEVEN LEVEL CONVERTER FOR SOLAR PV GENERATION APPLICATIONS

The seven level symmetrical and asymmetrical converters are formed in by PUC and PEC configuration, respectively. The performance of both inverters is analyzed by implementation of different control and modulation techniques.

### 4.2.1 PUC Converter

Fig. 4.1 shows the three phase solar PV generation system based on seven level three phase PUC multi-level inverter. This inverter topology generates seven voltage levels by using the six unidirectional switches and two solar panels of different voltages in each phase. The solar powered inverter is tied to the grid through a harmonic filter. All solar arrays are equipped with MPPT controller to ensure

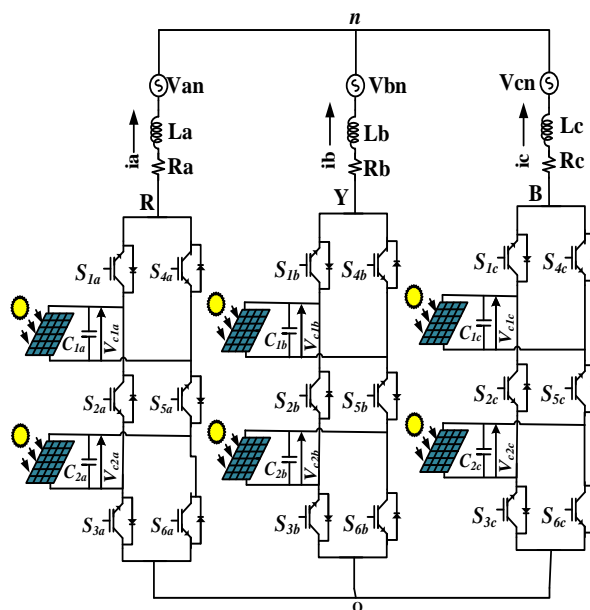


Fig.4.1. Seven level PUC SPV generation system

the maximum power extraction. Table 4.1 shows the switching logic for every voltage level PUC inverter output. Moreover, the upper solar PV voltages  $V_{PV1}$  and lower solar PV voltage  $V_{PV2}$  are added to generate the peak voltage level  $V_{PV1} + V_{PV2}$  of inverter, which is higher than the voltages of individual solar arrays. The voltage of upper and lower solar module are 300V and 150V, respectively which is in ratio of 2:1. The voltages of six levels other than zero voltage level, are  $+V_{PV2}$  (+150V),  $+V_{PV1}$ (+300V),  $+V_{PV1}+V_{PV2}$  (+450V) in positive half cycle and  $-V_{PV2}$  (-150V),  $-V_{PV1}$ (-300V),  $-V_{PV1}-V_{PV2}$  (-450V) in negative half cycle. The peak voltage levels of  $\pm(V_{pv1} + V_{pv2})$  is more than the higher source voltage  $V_{pv1}$ . Switching sequence logic is given by these equations,

$$v_{RO} = v_{pv1}(S_{1a} - S_{2a}) + v_{pv2}(S_{3a} - S_{2a}) \quad (4.1)$$

$$v_{YO} = v_{pv1}(S_{1b} - S_{2b}) + v_{pv2}(S_{3b} - S_{2b}) \quad (4.2)$$

$$v_{BO} = v_{pv1}(S_{1c} - S_{2c}) + v_{pv2}(S_{3c} - S_{2c}) \quad (4.3)$$

$$v_{abc} = Ri_{abc} + L \frac{di_{abc}}{dt} + v_{gabc} \quad (4.4)$$

Equation (4.4) gives a natural 'abc' reference voltage loop equation. The notations R and L are the resistance and inductance of the harmonic filter placed between the converter and the grid.

The inverter switching sequence for generating all the voltage levels is shown in Table 4.1. The power balance equation at the DC-Link of each phase is given by the equation (4.5) as,

$$C \frac{dv_{dci}}{dt} = ip_{vi} - i_i \quad (4.5)$$

Subscript  $i=1-6$  represents the six solar modules.

Table 4.1: Switching states for phase A of PUC7

$S_{1a}$	$S_{2a}$	$S_{3a}$	$S_{4a}$	$S_{5a}$	$S_{6a}$	$V_{out}(V)$
1	0	1	0	1	0	$V_{pv1} + V_{pv2}$
1	0	0	0	1	1	$V_{pv1}$
0	0	1	1	1	0	$V_{pv2}$
0	0	0	1	1	1	0
1	1	1	0	0	0	0
1	1	0	0	0	1	$-V_{pv2}$
0	1	1	1	0	0	$-V_{pv1}$
0	1	0	1	0	1	$-(V_{pv1} + V_{pv2})$

Following are the system parameters of PUC Converter.

#### PV ARRAY I

$V_{pv1}=301.2$  V,  $I_{pv1}=33.5$  A,  $N_{s1}=10$ ,  $N_{p1}=5$ ,  $V_{MPP}=30.12$ V,  $I_{MPP}=6.7$  A,  $P_{pv1}=10.10$  kW

#### PV Array II

$V_{pv2}=150.6$  V,  $I_{pv1}=33.5$  A,  $N_{s2}=5$ ,  $N_{p1}=5$ ,  $V_{MPP}=30.12$ V,  $I_{MPP}=6.7$  A,  $P_{pv1}=5.04$  kW.

#### Grid and Control Parameters

$R=0.005$   $\Omega$ ,  $L=2.5$  mH,  $V_g=415$  V,  $C=70000$   $\mu$ F,  $T_s=10$   $\mu$ S,  $f_s=1000$  Hz,  $PI_{dc}$ :  $k_{pdc}=20.2$ ,  $k_{idc}=3.25$ ,  $PR_{ac}$ :  $k_{pm}=0.009$ ,  $k_{im}=0.00001$ .

### 4.2.2 PEC Converter

Fig. 4.2 illustrates a seven-level PEC-based topology ideally suited for a three-phase system. This configuration is a modification of the PUC design, wherein the lower U-cell is transformed into an E-cell by introducing a bi-directional switch,  $G_{7a}$ - $G_{8a}$ , within phase 'a'. Alongside, there are six other switches,  $S_{1a}$ - $S_{6a}$ , identical to those in the original PUC setup. The staircase voltage levels of positive and negative cycles in phase 'a' are generated. The positive Half cycle is expressed as,

$$V_{an} = V_{Ua} \text{ (} G_{1a}, G_{5a} \text{ and } G_{6a} \text{ are ON)} \quad (4.6)$$

$$V_{an} = V_{Ua} - V_{Ba2} \text{ (} G_{1a}, G_{5a}, G_{7a} \text{ and } G_{8a} \text{ are ON)} \quad (4.7)$$

$$V_{an} = V_{Ua} - V_{Ba1} - V_{Ba2} \text{ (} G_{1a}, G_{5a}, \text{ and } G_{3a} \text{ are ON)} \quad (4.8)$$

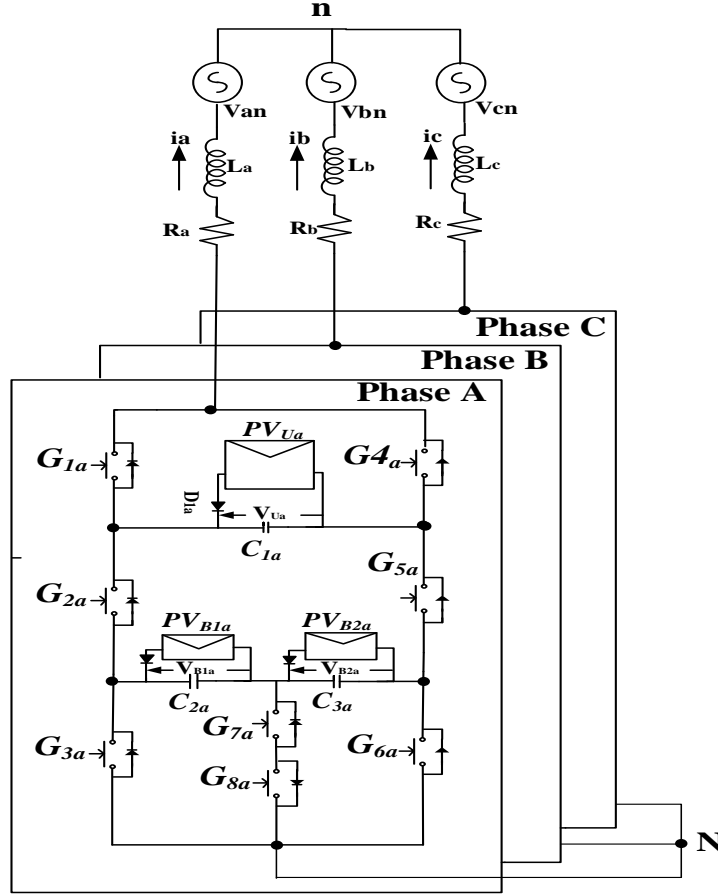


Fig.4.2. Seven level PEC SPV generation system

$$V_{an} = 0 \text{ (} G_{1a}, G_{2a}, \text{ and } G_{3a} \text{ are ON)} \quad (4.9)$$

Similarly negative half cycle equations are given as,

$$V_{an} = -V_{Ua1} \text{ (} G_{2a}, G_{3a} \text{ and } G_{4a} \text{ are ON)} \quad (4.10)$$

$$V_{an} = -V_{Ua1} + V_{Ba1} \text{ (} G_{2a}, G_{4a}, G_{7a} \text{ and } G_{8a} \text{ are ON)} \quad (4.11)$$

$$V_{an} = -V_{Ua1} + V_{Ba1} + V_{Ba2} \text{ (} G_{2a}, G_{4a}, G_{6a} \text{ and } G_{8a} \text{ are ON)} \quad (4.12)$$

$$V_{an} = 0 \text{ (} G_{1a}, G_{5a}, \text{ and } G_{6a} \text{ are ON)} \quad (4.13)$$

Table 4.2 provides a comprehensive overview of the detailed switching states of the inverter switches. The peak converter step is set at 369V, achieved by linking the upper solar array,  $PV_{Ua1}$ , as described in equation (4.6). The second peak voltage level is attained by connecting  $PV_{Ba2}$  in series with  $PV_{Ua1}$ , resulting in a net converter voltage of 246V ( $369V - 123V$ ), as expressed in equation (4.7). The first voltage level is accomplished by connecting both bottom solar arrays,  $PVB1a$  and  $PVB2a$ , in series and in opposition with  $PV_{Ua1}$ , leading to a net converter voltage of 123V ( $369V - 123V - 123V$ ). To achieve the zero level, all the arrays are bypassed, as indicated in (4.9). Similarly, the negative half cycle of the converter's stepped output is generated in switching states as shown in equations (4.10) to (4.13).

Table 4.2 Switching States For PV-PEC Converter

$G_{1a}$	$G_{2a}$	$G_{3a}$	$G_{4a}$	$G_{5a}$	$G_{6a}$	$G_{7a}$	$G_{8a}$	$V_{out}(V)$
1	0	0	0	1	1	0	0	$+V_{Ua}$
1	0	0	0	1	0	1	1	$+V_{Ua} - V_{Ba2}$
1	0	1	0	1	0	0	0	$+V_{Ua} - V_{Ba1} - V_{Ba2}$
0	0	0	1	1	1	0	0	0
1	1	1	0	0	0	0	0	0
0	1	1	1	0	0	0	0	$-V_{Ua}$
0	1	0	1	0	0	1	1	$-V_{Ua} + V_{Ba1}$
0	1	0	1	0	1	0	0	$-V_{Ua} + V_{Ba1} + V_{Ba2}$

System parameters of PEC converter

$V_{pv}=360$  V,  $V_2 = 154$ ,  $V_3 = 52$  V,  $I_{pv}=23$  A,  $P_{pv}=8.3$  kW,  $C_1 = C_2 = C_3= 1000$   $\mu$ F,  $L_1= L_2 = 4$  mH,  $f_{sw}= 500$  Hz, Grid Voltage,  $v_s = 230$  V.

Controller gains:

$K_{p1} = 0.1$ ,  $K_{i1}=0.002$ ,  $K_{p2}=1$ ,  $K_{i2}=0.004$ ,  $K_{p3}=0.1$  and  $K_{i3}= 0.009$ ,  $K_{p4} = 1$ ,  $K_{i4} = 2$  and  $K_{p5} =0.1$  and  $K_{i5}= 0.09$ .



### 4.3 CONTROL STRATEGY OF PUC AND PEC TYPE SEVEN LEVEL CONVERTER FOR SOLAR PV GENERATION APPLICATIONS

This section explains the control structure for the PUC and PEC based solar PV generation system. Two different control methods are presented to regulate the power flow from DC to AC grid. The PUC converter utilizes PI controller based DC-link balancing and PR controller based tracking of actual grid currents to the reference magnitudes. The PEC converter is controlled with d-q theory based three phase controller. The control is described in detail in the subsections here.

#### 4.3.1 Control Strategy of PUC Converter

The control structure is divided into three sections: DC-link voltage control, current control, and multicarrier modulation technique. The complete control scheme is explained following subsections.

##### 4.3.1.1 DC-Link voltage control

Fig. 4.3 shows the regulation of capacitor voltage and active reference current generation  $I_{dref1}$ ,  $I_{dref2}$ . The reference voltages at maximum power point of three solar arrays connected to the upper power-cell of converter are added and averaged. Similarly average DC-Link capacitor voltages of upper power cell are obtained and compared with reference voltage, error voltage equation is given as,

$$e_U = (V_{ref1})_{AV} - (V_{act1})_{AV} \quad (4.6)$$

A PI controller is employed to minimize the error  $e_u$ , which balances the DC-link voltages of upper SPV arrays and its equation is given as,

$$I_{dref1}(k+1) = I_{dref1}(k) + k_{pu} \{e_u(k+1) - e_u(k)\} + k_{iu} e_u(k+1) \quad (4.7)$$

Error voltage equation for lower SPV arrays is given as,

$$e_L = (V_{ref2})_{AV} - (V_{act2})_{AV} \quad (4.8)$$

Similarly, PI controller is employed to minimize the error  $e_L$ , which balances the DC-link voltages of upper SPV arrays, and its equation is given as,

$$I_{dref2}(k+1) = I_{dref2}(k) + k_{pL}\{e_L(k+1) - e_L(k)\} + k_{iL}e_L(k+1) \quad (4.9)$$

Fig. 4.3 shows that the total active component is given as,

$$I_{dTref} = I_{dref1} + I_{dref2} \quad (4.10)$$

#### 4.3.1.2 Converter current control

Proportional resonant controller is used in this solar photovoltaic system, which produces a high gain at resonance frequencies. The expression of the controller is given by the equation (4.11) as,

$$G_{sPR} = K_{px} + K_{ix}f_1(s) \quad (4.11)$$

Where,

$$f_1(s) = \frac{2\omega_c s}{s^2 + 2\omega_c s + \omega_c^2} \quad (4.12)$$

Where  $\omega_c$  is the frequency band around the resonant frequency of  $\omega_o$ . At  $\omega_o$ , controller has a fixed gain, which generates a small steady-state error. It performs at the high precision and accuracy in comparison to PI controllers. The applied current control method is shown in Fig. 4.4, where reference direct current is converted to three-phase reference current by the inverse Park transformation dq0 to abc. Transformed reference grid currents are compared with sensed grid currents, and the equation gives an error signal as,

$$e_{Ix} = I_{dref} - i_x \quad (4.13)$$

Subscript x=a, b, c represent the three phases of grid current.

Three proportional resonant controllers, one each for each phase are employed for the minimization of error and gives the modulating signal for pulse generation for switching the inverter, its equation is given as

$$m_x(k+1) = m_x(k) + k_{px} \{e_{Ix}(k+1) - e_{Ix}(k)\} + k_{ix} f_1(s) e_{Ix}(k+1) \quad (4.14)$$

#### 4.3.1.3 Multicarrier modulation

In this work, modified-triangular level-shifted multicarrier modulation techniques are implemented for a switching-pulse generation. Modified-triangular and parabolic

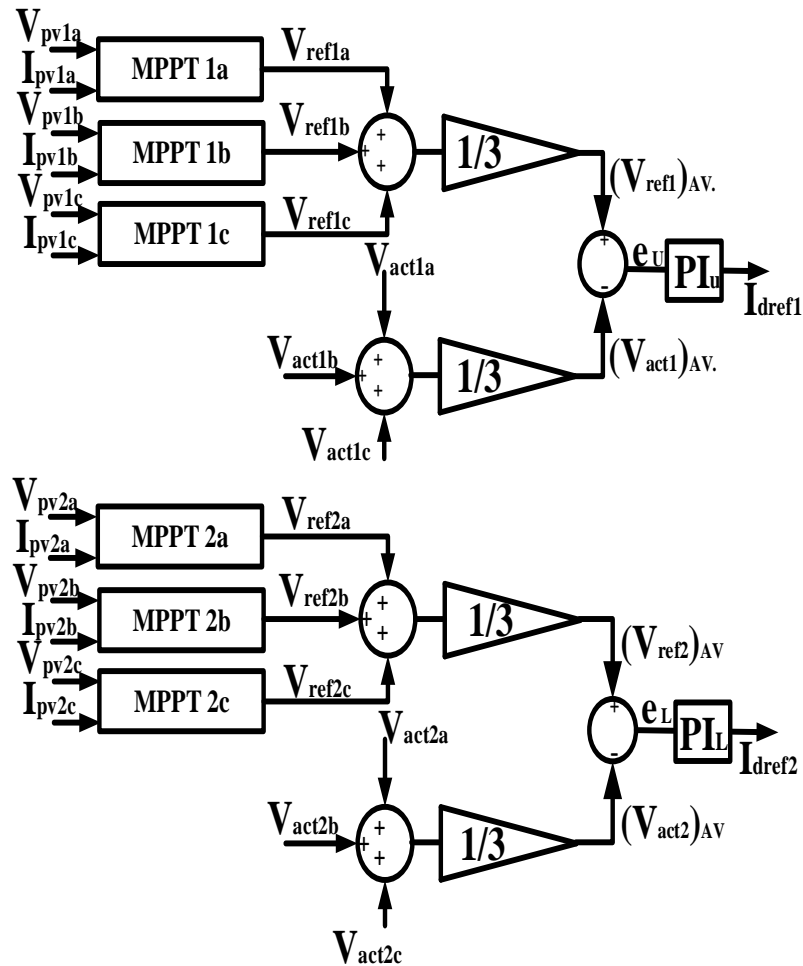


Fig. 4.3. DC-Link voltage control for reference current generation

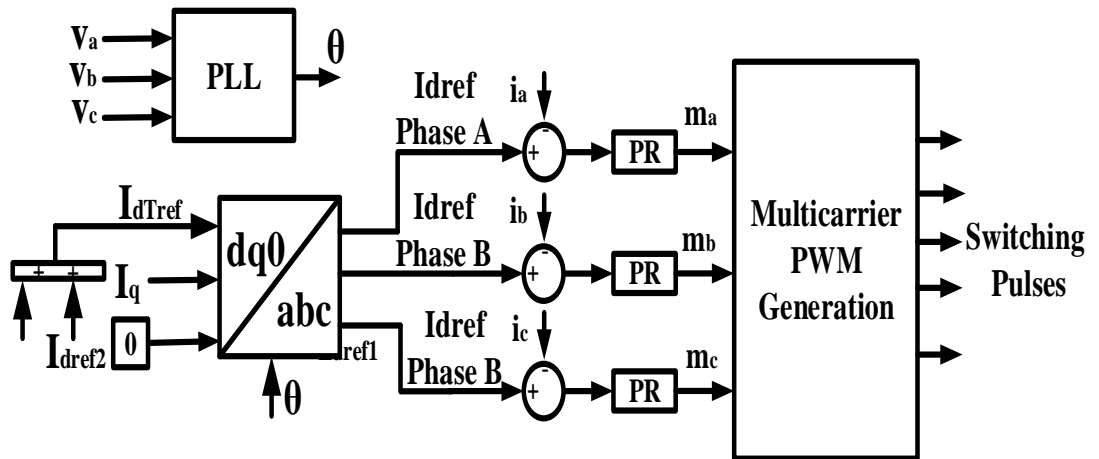


Fig. 4.4. Current control and switching pulse generation

shape multicarrier signals are used in PD, POD, and APOD patterns. The generation of the modified triangular wave is shown in Fig. 4.5. The triangular wave  $s_1$  is a repeating triangular wave of amplitude 0.0875 and frequency of 1 kHz,  $s_2$  is a rectangular pulse of amplitude 0.0225 frequency 4 kHz.  $s_3$  is obtained by summation of  $s_1$  and  $s_2$  and amplifying it by three times. The frequency of carrier wave  $s_3$  is the same as that of  $s_1$ .

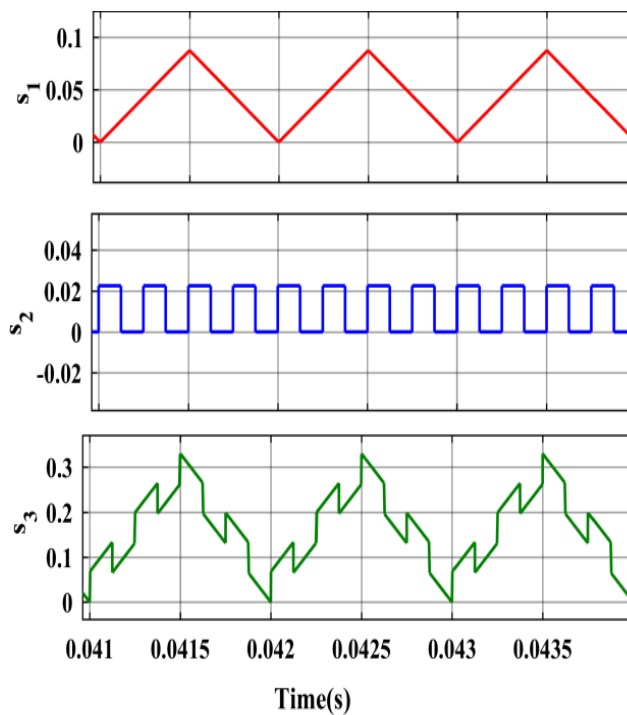


Fig. 4.5. Modified triangular carrier generation

The frequency modulation index signal of  $s_3$  is given as,

$$F_m = \frac{f_c}{f_m} \quad (4.15)$$

Where  $f_c$  and  $f_m$  are carrier and reference Sine wave frequency.

As shown in Fig. 4.6, the parabolic carrier is generated by subtracting the pulse signal  $p_1$  of the amplitude of 0.5 and frequency 1kHz from signal  $p_3$  ( $|\text{abs}|$  of sinusoidal signal  $p_2$  of frequency 500 Hz and amplitude of 0.5),  $|\text{abs}|$  of the subtracted signal is multiplied by 0.66 to get the parabolic carrier  $p_4$ .

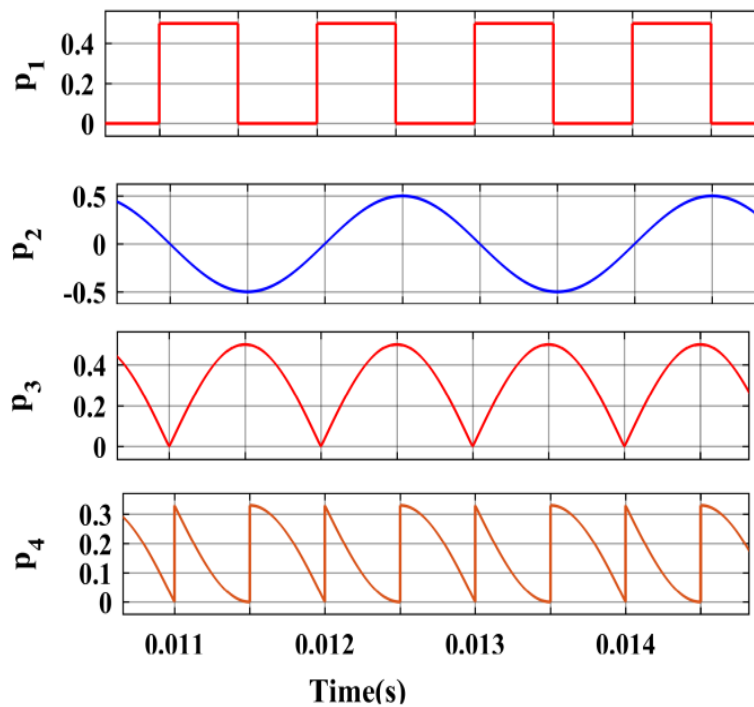


Fig. 4.6. Parabolic carrier signal generation

### 4.3.2 Control Strategy of PEC Converter

The control strategy comprises of three key components: DC-link voltage control, grid current control, and multi-carrier PWM for generating the switching pulses for the inverter.

#### 4.3.2.1 DC-Link voltage control

Fig. 4.7 illustrates the setup, where the DC-link voltage is compared with the reference voltage obtained from the MPPT controller. To minimize the error signal, PI controllers are employed. Additionally, the reference DC current is derived by

summing up all the reference currents from each of the solar panels. The orthogonal components of DC reference current  $i_{dref}$  and  $i_{qref}$  are represented as,

$$i_{dref}^{(k)} = i_{dref}^{(k-1)} + K_{pdc} e_{dc} + K_{idc} e_{dc} \quad (4.16)$$

$$i_{qref}^{(k)} = i_{qref}^{(k-1)} + K_{pdc} e_{dc} + K_{idc} e_{dc} \quad (4.17)$$

#### 4.3.2.2 Converter current control

The direct-quadrature (D-Q) control of the AC side is depicted in Fig. 4.8. In this control scheme, the grid voltages  $v_{abc}$  and currents  $i_{abc}$  are transformed into direct ( $v_d$ ) and quadrature ( $v_q$ ) components, as well as direct ( $i_d$ ) and quadrature ( $i_q$ ) currents. These components,  $i_d$  and  $i_q$ , are compared to reference values  $i_{dref}$  and zero, respectively, resulting in modulating reference signals  $m_{abc}$ .

These modulating reference signals,  $m_{abc}$ , are then compared with high-frequency multi-carriers, generating the switching sequence for the PEC7 inverter. This process ensures efficient and precise control of the AC side of the system, allowing for smooth and optimized operation. The mathematical model of the current control is represented as,

$$u_d = \left( k_p + \frac{k_i}{s} \right) (i_{dref} - i_d) - \omega L i_q + v_d \quad (4.18)$$

$$u_q = \left( k_p + \frac{k_i}{s} \right) (i_{qref} - i_q) + \omega L i_d + v_q \quad (4.19)$$

Here  $u_d$  and  $u_q$  are the direct and quadrature axis components of the converter output voltage.

#### 4.3.2.3 Multicarrier modulation

The inverter's PWM switching is produced by comparing the reference signal with high-frequency level-shifted multi-carrier signals. To achieve the seven levels, six triangular carrier signals with identical amplitude and frequency are employed. Three different types of level-shifted modulation techniques are utilized: phase disposition (PD), phase opposition disposition (POD), and alternate phase opposition

disposition (APOD). These modulation techniques are visually represented in Fig. 4.9, demonstrating the methods employed to generate the desired PWM patterns and achieve efficient control over the inverter's output. The PD multicarrier modulation as shown in Fig. 4.9 all six multi-carrier signals are vertically shifted top most carrier signal varies between 0.67 to 1.0, second signal between 0.33-0.67 and third signal oscillates in between 0.0- 0.33 for positive half cycle. Frequency of all the signals is kept at 1 kHz. Similarly other three carriers are vertically shifted equally between 0 to -1.

In the APOD modulation, alternate carrier signals are phase-shifted by  $180^{\circ}$ , as illustrated in the middle section of Fig. 4.9. The number of carriers and their frequency remain the same as that of the PD modulation. This arrangement ensures efficient utilization of carrier signals while achieving the desired phase opposition disposition to regulate the inverter's switching and control the output effectively. In the POD modulation, depicted in the bottom section of Fig. 4.9, the three carrier signals on the positive side are in phase and evenly spaced vertically between 0 and 1. Meanwhile, the three carrier signals on the negative side are in phase with each other but are phase-shifted by 180 degrees with respect to the signals on the positive half.

The comparators compare all the multi-carrier signals with the sinusoidal reference, and they respond when the value of the carrier is lower than that of the sinusoidal reference. This comparison allows for precise control and regulation of the inverter's switching patterns, ensuring smooth and accurate generation of the desired sinusoidal output waveform.

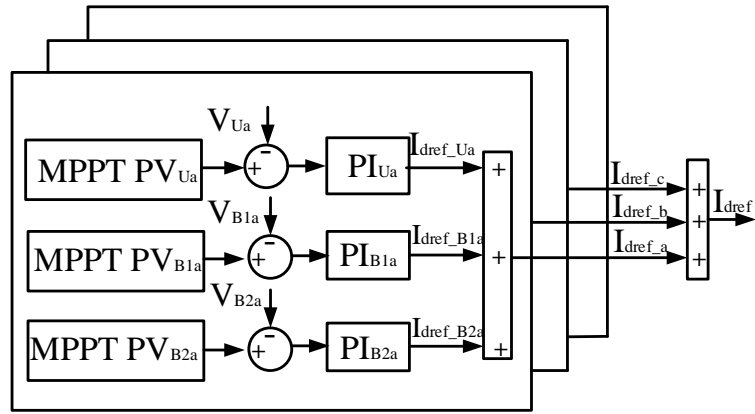


Fig. 4.7. DC link voltage control PEC7

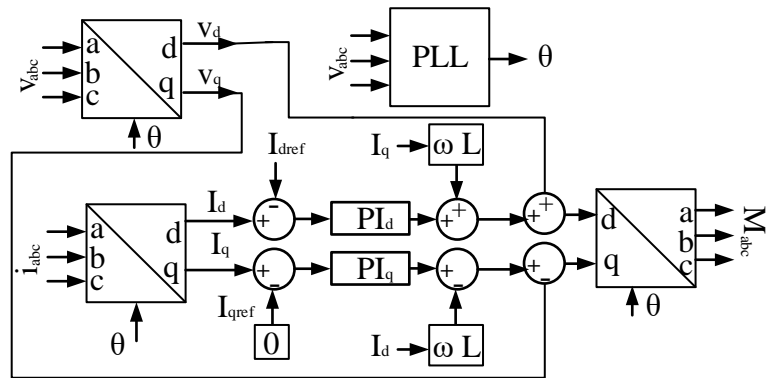


Fig. 4.8. AC side current control of PEC7

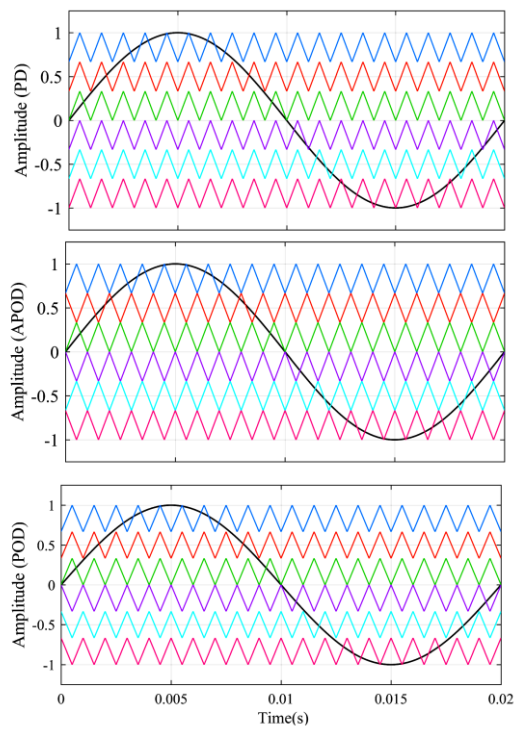


Fig. 4.9. The carrier signal orientation of PD, APOD and POD Multi-carrier PWM



#### 4.4 MATLAB MODEL OF PUC AND PEC TYPE SEVEN LEVEL CONVERTER FOR SOLAR PV GENERATION APPLICATIONS

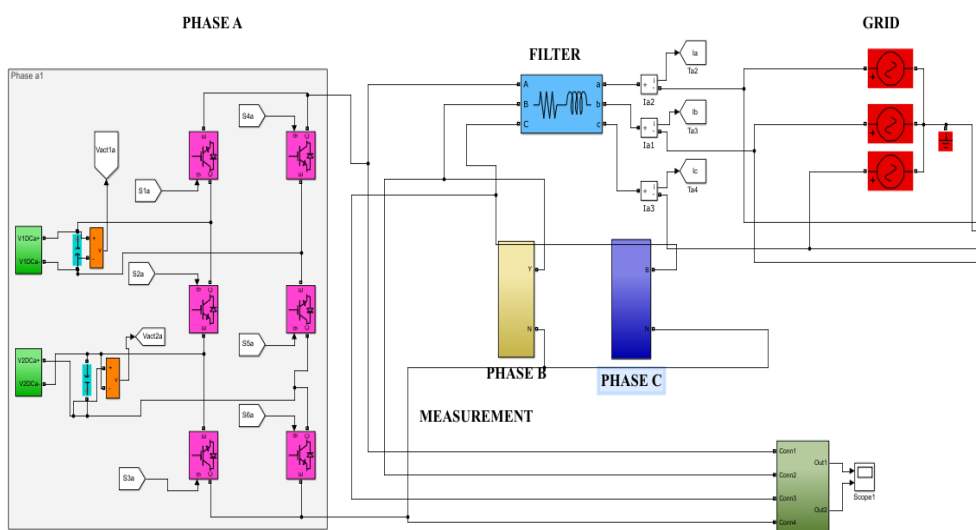
The PUC and PEC converters are modelled in MATLAB according to their power circuit configuration and control scheme. Simulation is carried for various environmental conditions and results of the same are discussed. The power and control circuits are shown here.

##### 4.4.1 PUC Converter

Fig. 4.10 (a) shows the MATLAB model of power circuit the seven level PUC converter. Each phase consists of two solar arrays having two DC power terminals. The DC link capacitors are connected across the DC terminals of solar arrays and the voltage  $V_{act1a}$  &  $V_{act2a}$  are measured. The power circuit is formed by the switches  $S_{1a}$ - $S_{6a}$ . Phase 'B' & 'C' are formed similar to Phase 'A'. Three phase of converter are connected in the star and are fed to R-L harmonic filter. The measurement of three phase voltages and currents are taken before feeding the power to the grid.

Fig. 4.10 (b) shows the control scheme implementation of this converter. The DC link control consists of DC reference current generation by the balancing of capacitor voltages. The DC reference current is converted to equivalent reference AC current by Park's transformation. The grid current is tracked to reference AC current by proportional resonant controller. The system response at steady and transient state is recorded in the results block.

Seven Level PUC Converter for Grid-Tied Solar Photovoltaic Applications



(a)

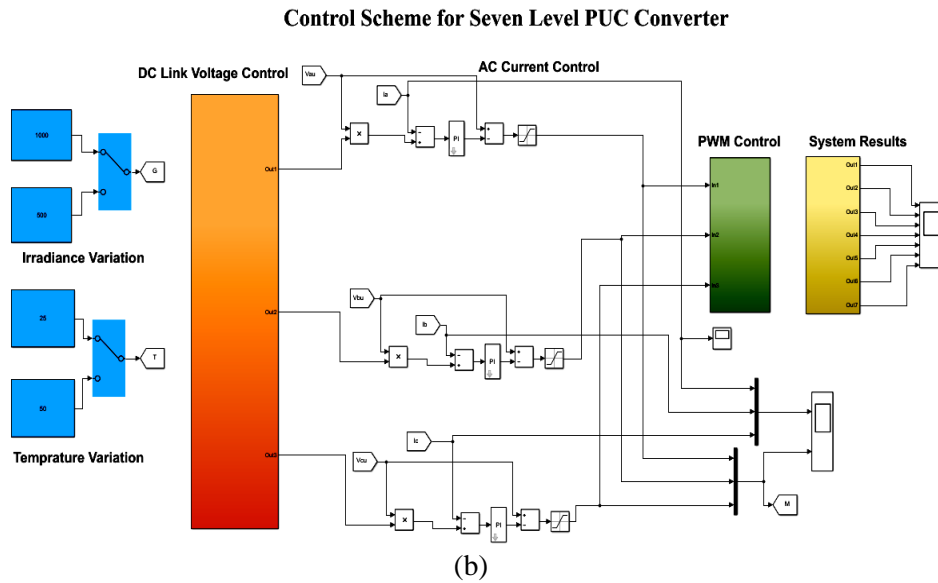
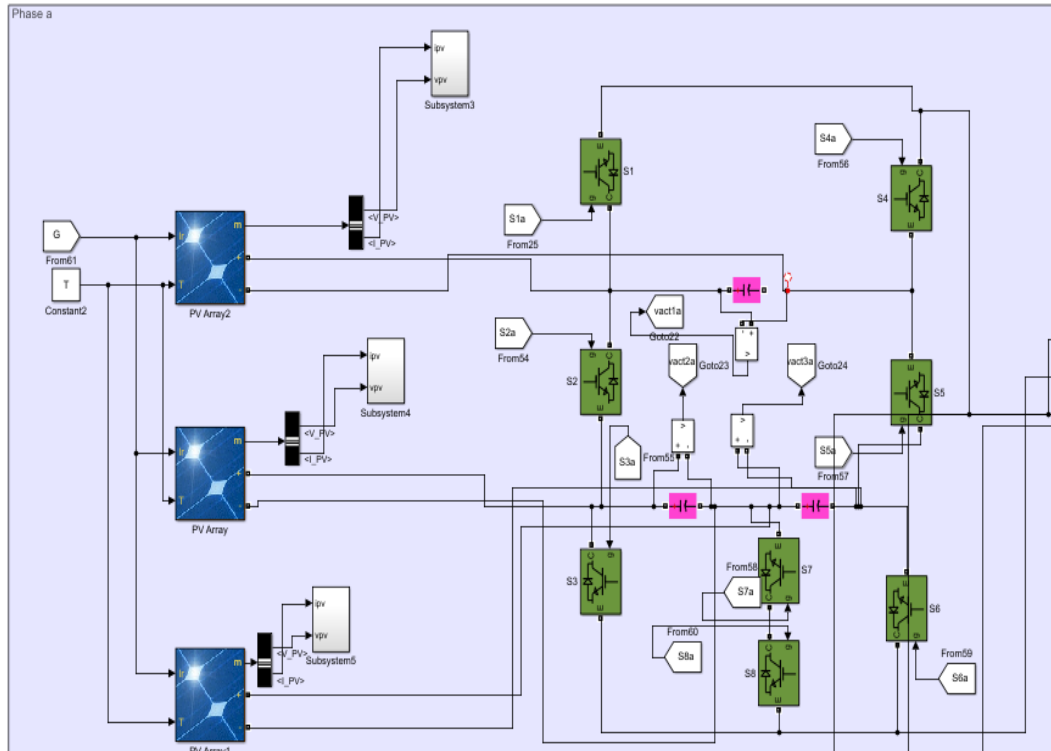


Fig. 4.10 MATLAB model (a) power circuit (b) control scheme PUC7 converter

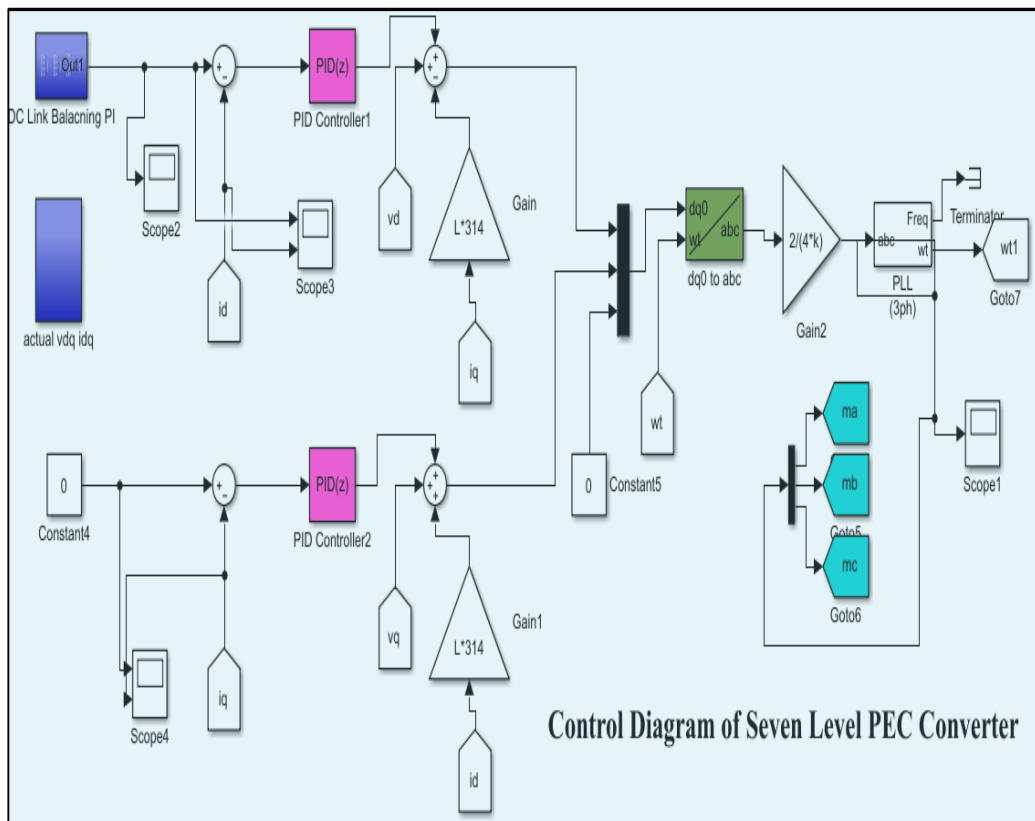
#### 4.4.2 PEC Converter

Fig. 4.11(a) shows the MATLAB model of power circuit the seven level PEC converter. Each phase consists of three solar arrays having two DC power terminals. The DC link capacitors are connected across the DC terminals of solar arrays and the voltage  $V_{Ua}$ ,  $V_{B1a}$  and  $V_{B2a}$  are measured. The power circuit is formed by the switches  $G_{1a}$ - $G_{8a}$ . Phase 'B' & 'C' are formed similar to Phase 'A'. Three phase of converter are connected in the star and are fed to R-L harmonic filter. The measurement of three phase voltage and current is taken before feeding the power to the grid.

Fig. 4.11(b) shows the control scheme implementation of this converter. The DC link control consists of DC reference current generation by the balancing of capacitor voltages. The grid currents are converted to equivalent DC current, which is tracked to the reference current of DC side. The modulating signals are generated after adjusting the harmonic filter voltage drop.



(a)



(b)

Fig. 4.11 MATLAB model of (a) power circuit (b) control scheme, of PEC converter

## **4.5 SIMULATED RESULTS OF PUC AND PEC TYPE SEVEN LEVEL CONVERTER FOR SOLAR PV GENERATION APPLICATIONS**

The presented system is implemented in the MATLAB/Simulink, and harmonics assessment is done for the triangular, parabolic, and modified triangular level-shifted modulating carrier in PD, POD, and APOD patterns. The system is analysed for the THD and fundamental component of converter voltage. A detailed comparative harmonic performance is shown in Table 4.3. The system performance is assessed for a steady-state and dynamic solar environment.

### **4.5.1 Steady-State and Dynamic Performance of PUC7 Converter**

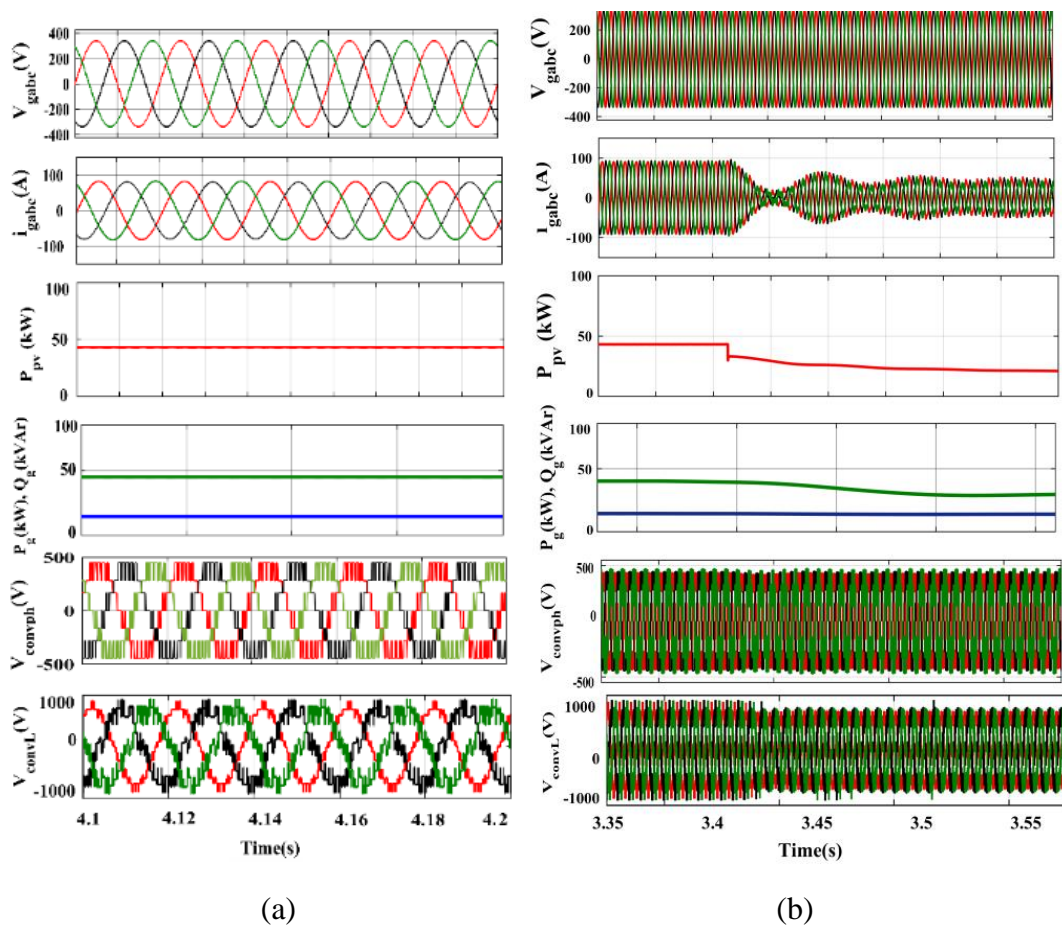
System performance at the solar irradiance of  $1000 \text{ W/m}^2$  is shown in Fig. 4.12(a). Each phase has two solar PV panels of  $10.10 \text{ kW}$  and  $5.04 \text{ kW}$ . The MPPT controller of each PV panel ensures extraction of maximum power i.e.  $15.14 \text{ kW}$  per phase. The three-phase solar PV array grid-tied system operates at total solar power ( $P_{pv}$ ) of  $45.40 \text{ kW}$ . The power transferred to the grid  $P_g$  (kW) is  $44.00 \text{ kW}$  with an efficiency of  $97\%$ . The injected grid current is constant for fixed  $1000 \text{ W/m}^2$  irradiation the while grid voltages remain balanced. The target of power transfer at unity power factor is achieved, and reactive power  $Q_g$ (kVAr) remains zero. The PUC inverter generates seven-levels phase voltage ( $V_{conph}$ ) and 13-levels line voltage ( $V_{conL}$ ).

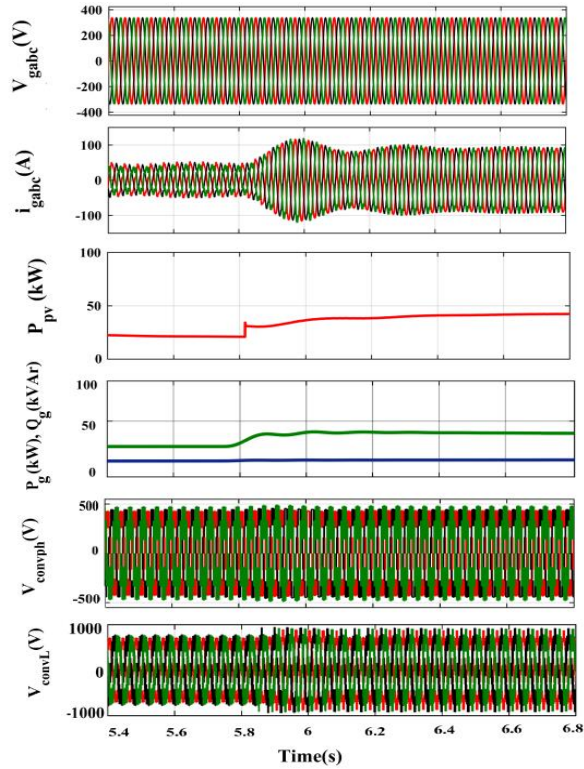
Figs. 4.12(b)-(c) show the dynamic results of solar PUC inverter during the rise and fall solar irradiation. The solar irradiation level projected on PV panels, determines the grid currents ( $i_{gabc}$ ), and seven-level PUC converter voltages ( $V_{convL}$  and  $V_{convph}$ ) are achieved with low harmonics profile. When solar irradiation decreases to  $500 \text{ W/m}^2$  from  $1000 \text{ W/m}^2$ , then power fed to the grid also decreases to  $22 \text{ kW}$ , which is half of  $44 \text{ kW}$  at  $1000 \text{ W/m}^2$ . The grid current also falls to half of the rated current. Similarly, during irradiation, a rise to  $1000 \text{ W/m}^2$  from  $500 \text{ W/m}^2$  power of solar PV ( $P_{pv}$ ) increases to  $45.40 \text{ kW}$ , and the grid power also increases to  $44.00 \text{ kW}$  with

perfect dynamic balance. The converter output voltage is shown in the dynamic conditions. These results are obtained at the closed-loop control, and new carrier PWM has improved the power quality and performance in varying solar conditions.

#### 4.5.2 Harmonic Analysis of PUC7 Converter

Table 4.3 shows the comparative harmonic performance of the seven-level PUC with different multicarrier schemes. The results are taken for different modulation indexes, which vary with solar irradiation. The following subsections represent the superiority of the adopted new modified multicarrier modulation. The notations to have simplified discussion are marked as A for SPWM, B for parabolic PWM, and C for modified triangular PWM.





(c)

Fig. 4.12. Simulation results (a) steady-state (b) dynamic performance with fall in irradiance (c) dynamic performance with rise in irradiance.

#### 4.5.2.1 Analysis with PD Pattern

For  $M_a=1$ , C shows the best harmonics performance with a THD of 16.47%, while A and B have more THD of 17.90 % and 18.87%, respectively. Similarly, C shows better harmonic performance for lower modulation indexes with lower THD i.e. 22.91%, 30.08%, and 40.74% for  $M_a=0.8, 0.6$  and  $0.4$ , respectively.

Coming to the fundamental component  $V_f$  of seven-level converter voltage, C shows the best performance with  $V_f = 456.9V$  and value of  $V_f = 451.7 V$  and  $456.2 V$  for A and B, respectively. Hence, the presented new modified scheme improves the system's power quality with a phase disposition pattern.

#### 4.5.2.2 Analysis with POD pattern

Technique C shows THD of 14.91% at  $M_a=1.0$  with POD pattern, and THD of techniques A and B are 16.05% and 18.87 respectively for  $M_a=1$ . Performance of C remains better than techniques A and B for lower modulation indexes. The

fundamental voltage component  $V_f$  is 457.7V, which is better than that of A (451.4V) and B (456.2V).

Table 4.3: Harmonic performance of seven-level PUC inverter output

Modulation Scheme	Carrier Arrangement	$M_a=1.0$		$M_a=0.8$		$M_a=0.6$		$M_a=0.4$	
		THD(%)	$V_f(V)$	THD(%)	$V_f(V)$	THD(%)	$V_f(V)$	THD(%)	$V_f(V)$
Sinusoidal	PD	17.90	451.7	24.22	361.6	33.35	271.1	44.33	180.6
triangular	POD	16.05	451.4	22.81	361.4	32.99	269.9	43.69	180.0
PWM	APOD	18.47	452.0	22.23	361.3	33.14	271.1	44.00	180.6
Parabolic	PD	18.87	456.2	25.62	371.2	36.13	268.8	48.76	187.8
PWM	POD	18.87	456.2	25.62	371.2	36.13	268.8	48.76	187.8
	APOD	18.87	456.2	25.62	371.2	36.13	268.8	48.76	187.8
Modified	PD	16.47	456.9	22.91	360.5	30.08	278.7	40.74	178.7
Triangular	POD	14.91	457.7	22.10	362.7	29.41	279.0	40.44	178.4
PWM	APOD	16.67	460.2	21.32	361.3	29.72	278.9	40.75	178.8

#### 4.5.2.3 Analysis with APOD pattern

Harmonic performance of C with APOD pattern is best with THD of 16.67% for  $M_a=1$ , whereas A and B show THD of 18.47% and 18.87% respectively for the same  $M_a=1.0$ . Again technique C performs better lower modulation indexes i.e.  $M_a = 0.8, 0.6, \text{ and } 0.4$ . Converter output voltage performance is also the best with  $V_f=460.2V$  compared to  $V_f= 452.0V$  and  $456.2V$  for A and B.

The best performing technique C with POD pattern is implemented in closed-loop control. Simulation results in Fig. 4.13(a) show the converter voltage has a THD of 14.91%. Fig. 4.13(b) shows the grid current, which has THD of 1.35% with technique C, which meets IEEE 519 standard.

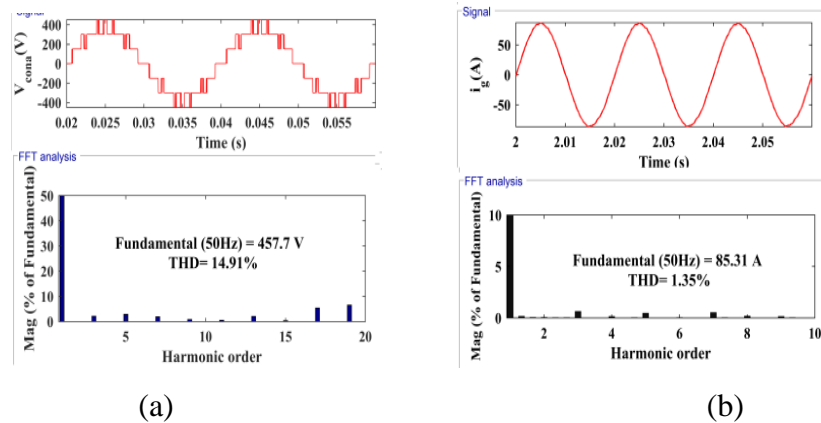


Fig.4.13. Harmonics analysis (a) converter voltage (b) grid current

### 4.5.3 Steady-State and Dynamic Performance of PEC7 Converter

Figs. 4.14 – 4.16 shows the response of grid integrated solar system PEC7. The solar PV generating system is operated at solar irradiation of  $1000 \text{ W/m}^2$  with the objective active power injection to the grid and response at the steady state is shown in Fig. 4.14. The total extracted solar power  $P_{PV}$  is 82.9 kW and grid power  $P_g$  is 81.3 kW at unity power factor and at the efficiency of 98%. The grid voltage  $V_g$  and current  $i_g$  are shown in the diagram. The dynamic response of the PEC7 when solar irradiation falls to 50% of  $1000 \text{ W/m}^2$  the solar power  $P_{PV}$  falls to half 41.5 kW and grid power also follows the solar power and reduces to half 40.6 kW at unity power factor. The converter voltage  $V_{conv}$  is maintained and grid current reduces to 50%. The dynamics of the system during the fall of irradiation are shown in Fig. 4.15. The rise of solar irradiation to normal at  $1000 \text{ W/m}^2$  and the response of system is shown in Fig. 4.15. The solar power  $P_{PV}$  resumes to 82.9 kW and grid power follows to settle at 81.3 kW, reactive power remains zero. The converter voltage maintains its shape while grid current  $i_g$  rises by 100%.

### 4.5.4 Harmonics Analysis of PEC7

The harmonic analysis of the PEC7 converter is done for three types of the modulations methods: PD, POD and APOD and results are tabulated in Table 4.2. The PD modulation technique is selected for the analysis as it has given best



harmonic response. Fig. 4.16 displays the harmonic response of the PEC7 with PD multi-carrier PWM, Fig. 4.16 (a) depicts the voltage harmonic response, the phase voltage component at 50Hz is 369 V and THD is 16.85%. Fig. 4.16(b) shows the current harmonics, which stand at the 2.35% that meets the grid standards.

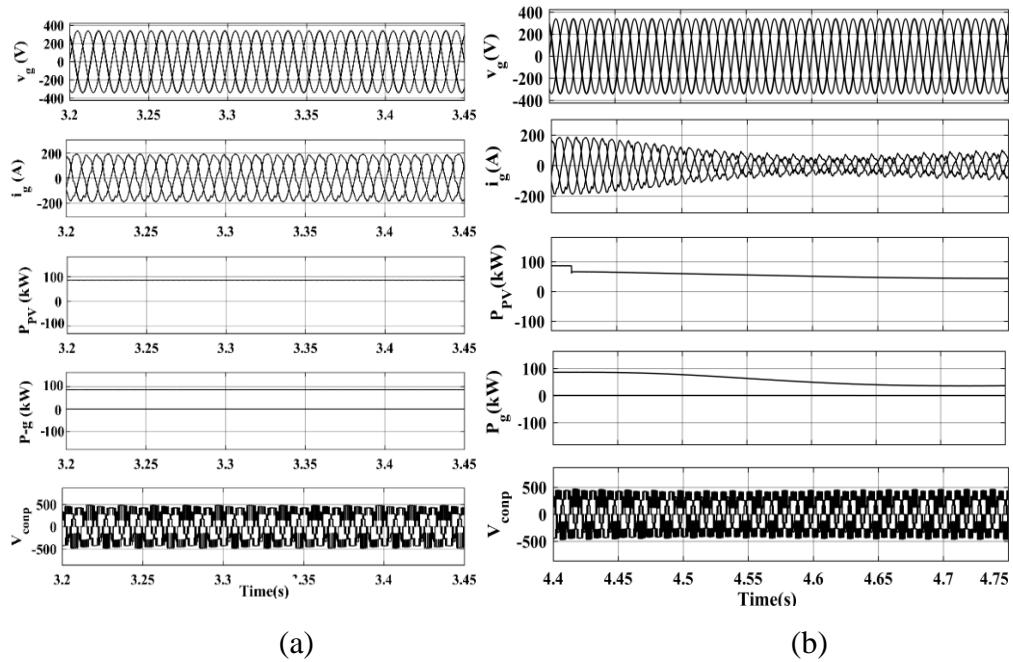


Fig. 4.14. (a) Steady state response, (b) dynamic response during the fall of irradiation of grid integrated PEC7

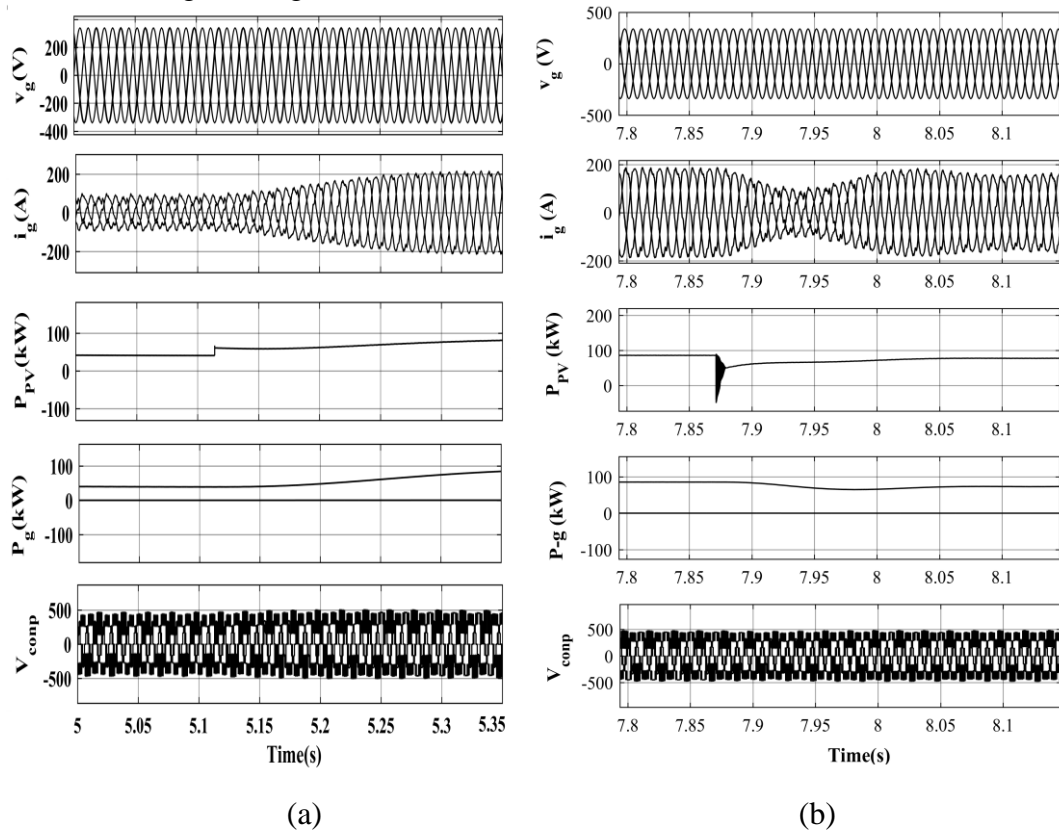


Fig. 4.15 (a) Dynamic response at rise of irradiation , (b) dynamic response during the temperature rise of grid integrated PEC7

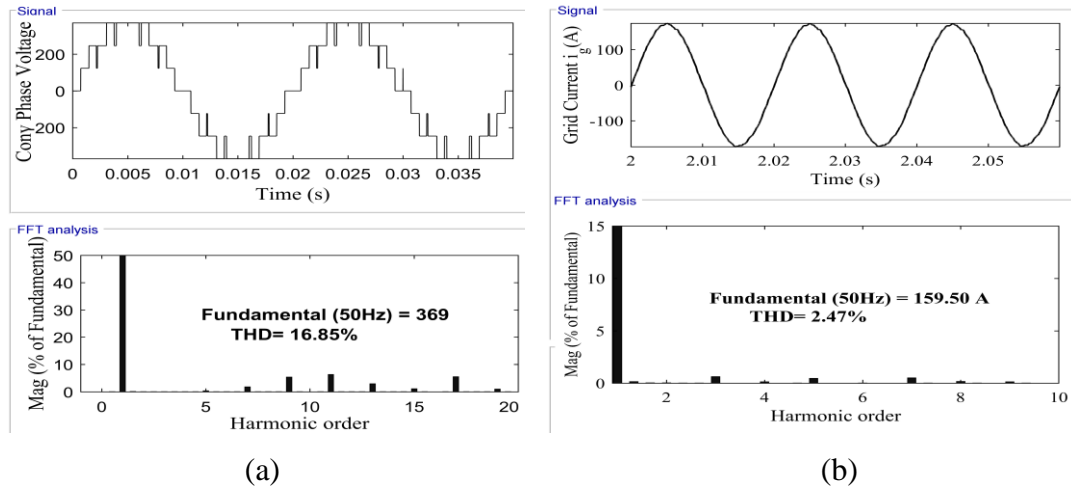


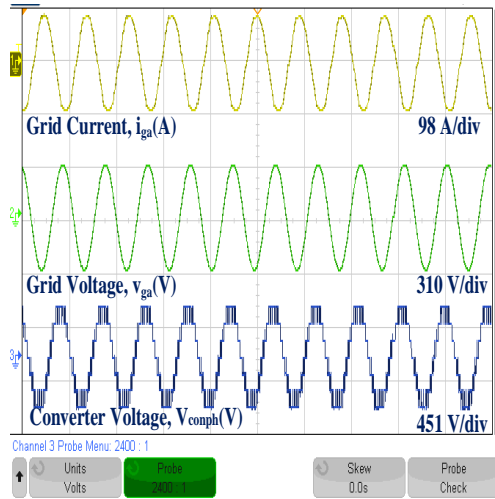
Fig. 4.16 Harmonic response of PEC7 (a) harmonic spectrum of voltage (b) harmonic spectrum of Current

#### 4.6 REAL-TIME EXECUTION OF PUC AND PEC TYPE SEVEN LEVEL CONVERTER FOR SOLAR PV GENERATION APPLICATIONS

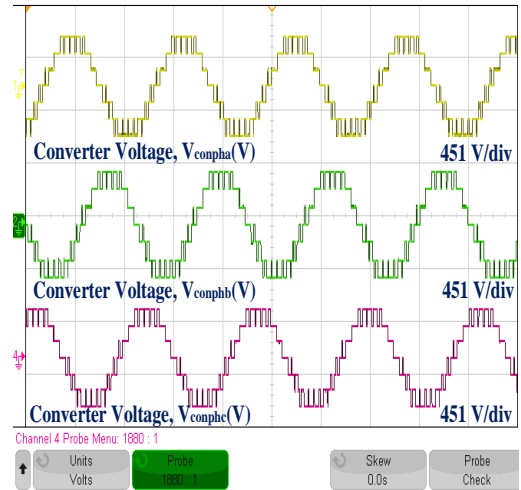
The OPAL-RT simulator validates the system performance in a real-time environment. It divides plant and controller into master and console blocks to communicate through real-time dynamic processors. This solar generating system is executed in real time and performance is assessed with RT test bench.

##### 4.6.1 Performance of PUC7 Converter

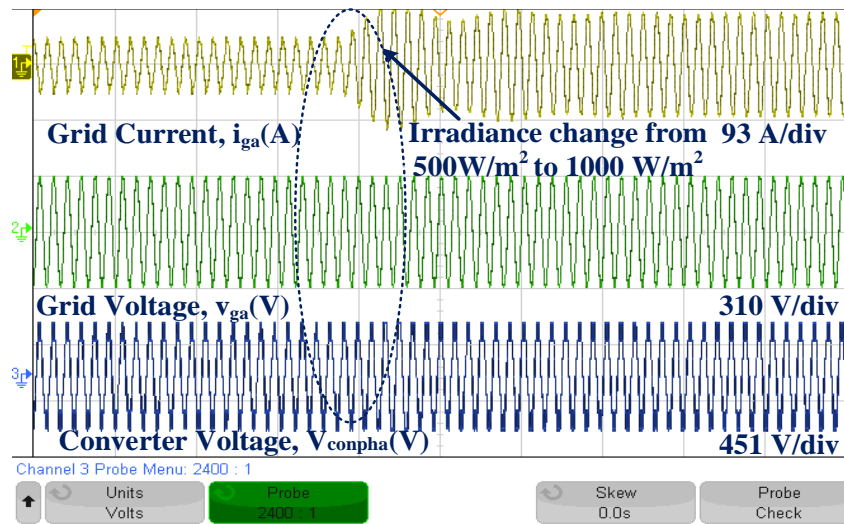
Figs. 4.17 (a-b) show the results obtained from the real-time digital simulator in a steady-state. The parameters  $i_{ga}$ ,  $v_{ga}$ ,  $V_{conpha}$  are constant for irradiance of  $1000 \text{ W/m}^2$  in Fig. 4.17 (a). Converter phase voltages of three phases are shown in Fig. 4.17(b). The dynamical parameters  $i_{ga}$ ,  $v_{ga}$  and  $V_{conpha}$  for irradiance rise are shown in Fig. 4.17(c). The grid powers  $P_g$  and  $P_{pv}$  and  $i_{ga}$  and  $v_{ga}$  are shown in Fig. 4.18(a), which shows that power increases with irradiation. Figs. 4.19 (b-c) show the results with fall in irradiance for  $i_{ga}$ ,  $v_{ga}$ ,  $V_{conpha}$ ,  $P_g$  and  $P_{pv}$ . Both grid and PV power fall with the fall in irradiance. Figs. 4.19 (a-b) show the voltage and current harmonic performance which validates the simulated results in the MATLAB.



(a)

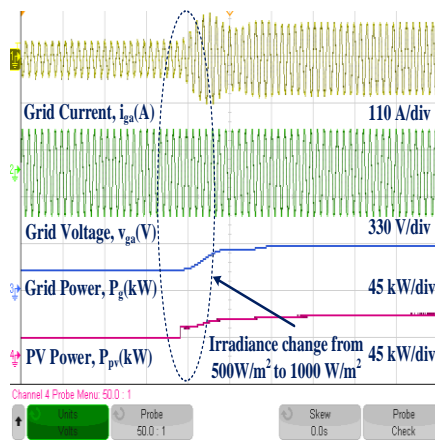


(b)

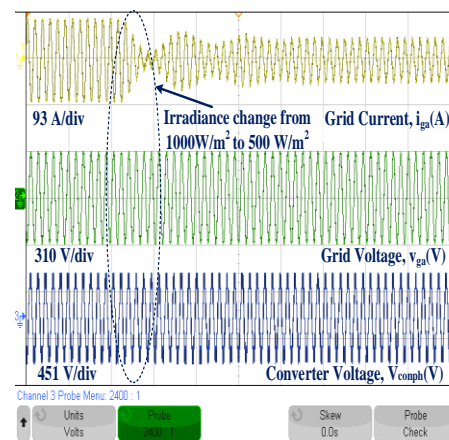


(c)

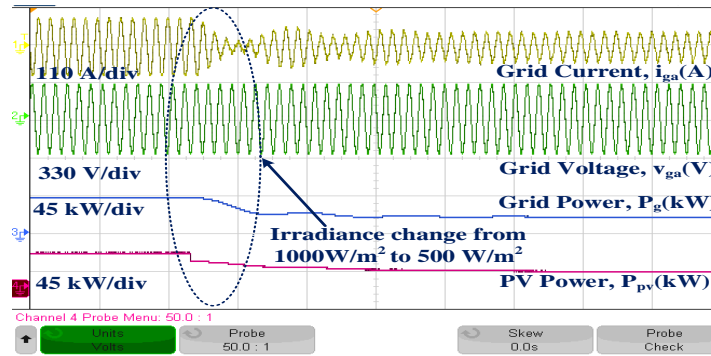
Fig. 4.17 Real-time results-I (a) constant irradiance of 1000 W/m<sup>2</sup> (b) Converter voltages (c)  $i_{ga}$ ,  $v_{ga}$  and  $V_{conpha}$  with rise in irradiation



(a)

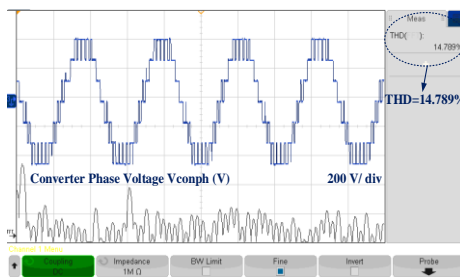


(b)

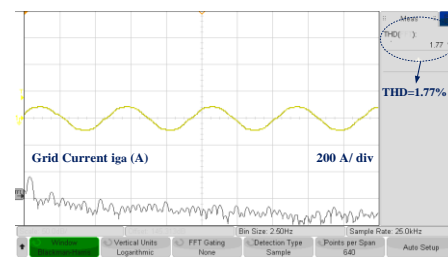


(c)

Fig.4.18. Real-time results-II (a)  $i_{ga}$ ,  $v_{ga}$ ,  $P_g$  and  $P_{pv}$  with rise in irradiation (b)  $i_{ga}$ ,  $v_{ga}$  and  $V_{conpha}$  with fall in irradiation (c)  $i_{ga}$ ,  $v_{ga}$ ,  $P_g$  and  $P_{pv}$  with fall in irradiation



(a)



(b)

Fig. 4.19. Real-time results-III (a) Voltage THD (b) Current THD

#### 4.6.2 Performance of PEC7 Converter

The solar photovoltaic generation system with PEC7 converter’s MATLAB simulated responses are validated by the real time simulator OPAL-RT. Fig. 4.20(a) depicts the steady state response at the solar insolation of  $1000W/m^2$ . The obtained response in real-time simulator validates the response shown by the MATLAB simulation. The dynamic response when solar irradiation changes to  $500W/m^2$  from  $1000W/m^2$  is shown in the Fig. 4.20(b). The solar PV power also reduces to half when irradiation decreases to the  $500W/m^2$ . Fig. 4.21 (a) shows the dynamic response when solar irradiation increase back to normal  $1000W/m^2$  from  $500W/m^2$ , which validates the MATLAB simulated results during the irradiation rise. Fig. 4.21 (b) shows the solar system response when temperature rises to  $50^{\circ}C$  from  $25^{\circ}C$ .

The harmonic response is shown in Fig. 4.22 (a)-(b), which shows the voltage THD of 16.736% and current THD of 2.376%, these values are very close to simulated values.

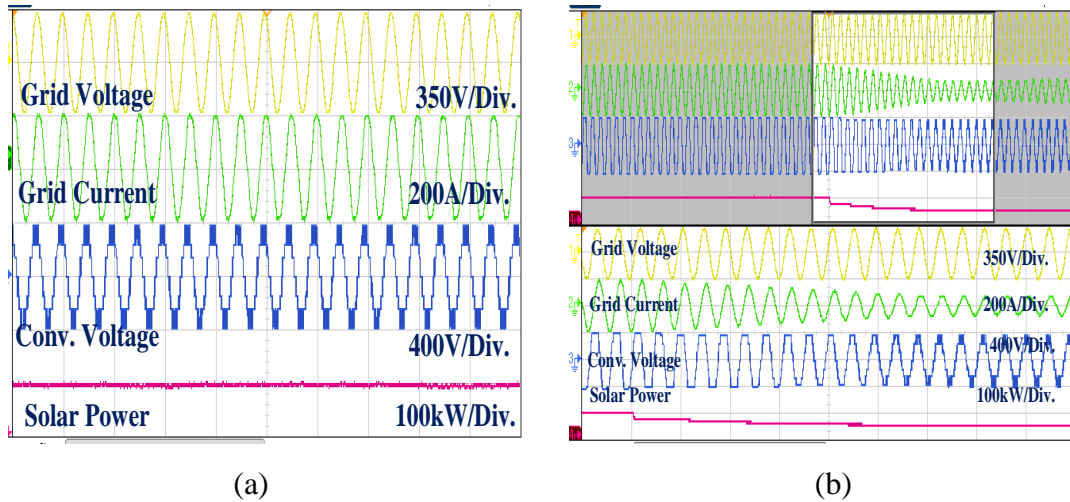


Fig. 4.20. Real-time simulated (a) steady state response, (b) dynamic response during the fall of irradiation of grid integrated PEC7

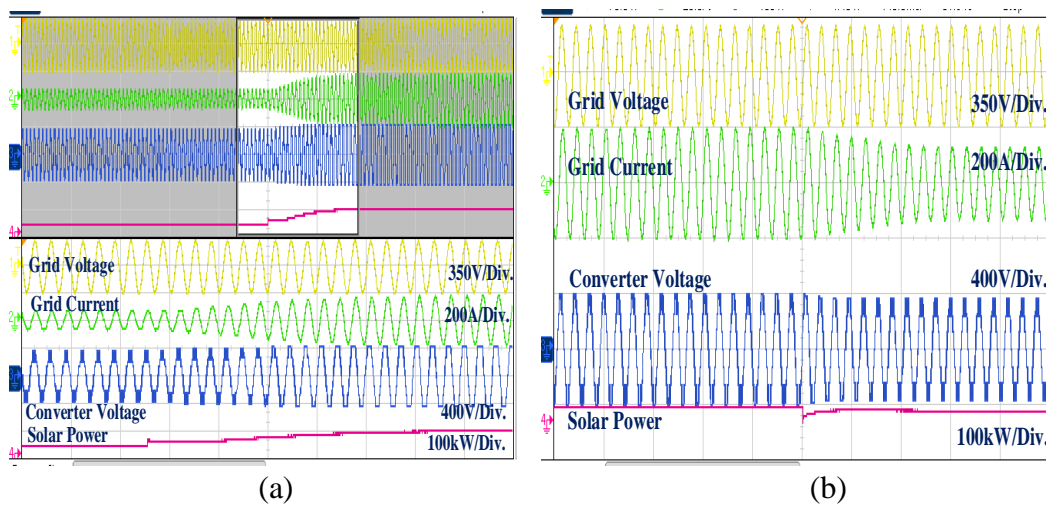


Fig. 4.21. Real-time simulated (a) Dynamic response at rise of irradiation , (b) dynamic response during the temperature rise of grid integrated PEC7

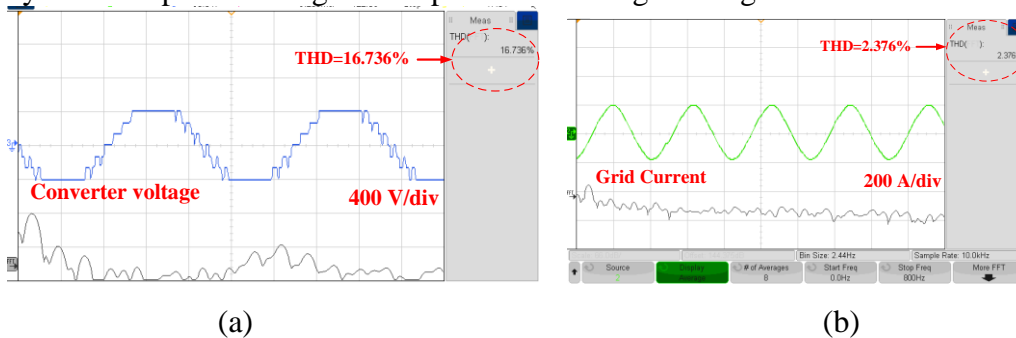


Fig. 4.22. The real-time simulated harmonic response of PEC7 (a) voltage THD (b) Current THD

#### **4.7 CONCLUSIONS**

The main objective of the selection of the best multicarrier scheme for a harmonics reduction in PUC multilevel solar inverter is achieved under all environmental conditions. Switching states, modelling equations, closed-loop proportional control and generation of parabolic, modified triangular are thoroughly discussed. Proportional resonant controllers have shown proper tracking of AC side grid currents. The PUC inverter is analysed with three types of multicarrier PWM schemes, and each multicarrier signal is arranged in three patterns. Modified triangular carrier signal in POD arrangement is found best for PWM switching. The dynamic performance of the PUC inverter with this PWM switching is analysed and validated in real-time. Harmonic performance is found best in modified PWM with THD of converter phase voltage is 14.789% and current THD of 1.77%. The harmonics performance of grid current is within the 5% limit of the IEEE-519 standard.

This PEC7 is simulated in MATLAB/SIMULINK in grid integration mode for medium power application. It has used the ternary configuration to generate seven levels. It is evaluated for the PD, POD and APOD multi-carrier techniques. It is found that the PD modulation is the best for harmonics reduction and used to operate the PEC system. This system's performance is excellent in constant and varying solar irradiance/temperature. This system is evaluated for temperature variation and its performance found proper. This work is done for seven level with the future scope of increasing levels by addition of more power-cell and solar PV arrays. Harmonic performance of converter phase voltage is 16.85% and the current THD is of 2.47%. The harmonic performance of grid current is within the 5% limit of the IEEE-519 standard.

## CHAPTER-V

### CONTROL AND REAL-TIME EXECUTION OF K-TYPE SYMMETRIC SEVEN LEVEL CONVERTER FOR SOLAR PV GENERATION APPLICATIONS

#### 5.1 INTRODUCTION

An enhanced K-type (IK-7) converter is presented in this work that utilizes three solar arrays per phase to produce multilevel waveforms in a staircase pattern. By employing symmetric voltage sources, this converter topology enables the efficient extraction of power from solar photovoltaic array. The proposed IK-7 configuration generates seven distinct voltage levels, utilizing three identical PV sources and eight solid-state switches. The operating modes of the converter, are elucidating the conduction path in detail. The system operates in a grid-tied mode and employs closed-loop control to regulate converter voltage and current, adapting to dynamic solar conditions. To ensure high-quality power output, a specific harmonic elimination strategy is applied in the converter's switching operation, aiming to minimize the total harmonics distortion (THD) of the converter voltage. The system is modeled using MATLAB to evaluate its dynamic performance under varying solar irradiance conditions.

#### 5.2 CIRCUIT CONFIGURATION OF K-TYPE SYMMETRIC SEVEN LEVEL CONVERTER FOR SOLAR PV APPLICATIONS

Fig. 5.1 illustrates the phase 'A' of a seven-level K-type inverter. The ten switches are categorized into three sections: upper ( $T_{1a}$ ,  $T_{2a}$ ,  $T_{3a}$ , and  $T_{4a}$ ), lower ( $T_{5a}$ ,  $T_{6a}$ ,  $T_{7a}$ , and  $T_{8a}$ ), and middle ( $T_{9a}$  and  $T_{10a}$ ). In the upper half cycle, three DC sources ( $V_{S1a}$ ,  $V_{S2a}$ , and  $V_{S3a}$ ) of equal magnitude ( $V_S$ ) generate the voltage levels  $V_S$ ,  $2V_S$ , and  $3V_S$ . Table I provides the switching logic for controlling the switches, while Fig. 5.2(a) demonstrates the various voltage levels obtained through specific combinations.

The voltage levels generated are as follows:

- (i) Peak positive level  $+3V_S = V_{S1} + V_{S2} + V_{S3}$
- (ii) 2nd positive level  $+2V_S = V_{S1} + V_{S2}$
- (iii) 1st positive level  $+V_S = V_{S1}$
- (iv) Zero level obtained by bypassing  $V_{S1}$ ,  $V_{S2}$ , and  $V_{S3}$
- (v) 1st negative level  $-V_S = -V_{S2}$

Table 5.1 Switching Sequence of K-Type Converter

S.No.	Operating Switches	Sources	Vout (V)
1	T1, T3, T6, T8,	VS1+VS2+ VS3	+3VS
2	T1, T6, T7, T8,	VS1+VS2	+2VS
3	T1, T4, T9	VS1	+VS
4	T1, T2, T3, T4	No source	0
5	T4, T5, T6, T7	-VS2	- VS
6	T4, T5, T10	-VS2-VS3	- 2VS
7	T2, T4, T5, T7	-VS1-VS2-VS3	-3VS

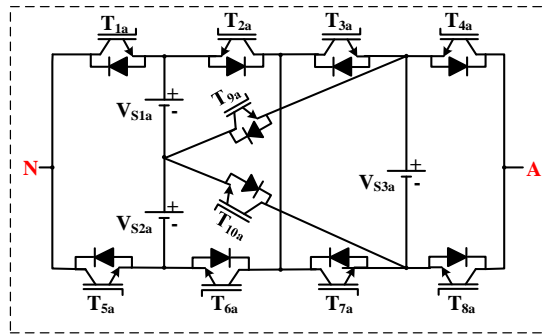


Fig. 5.1. Improved seven-level K-type structure IK-7

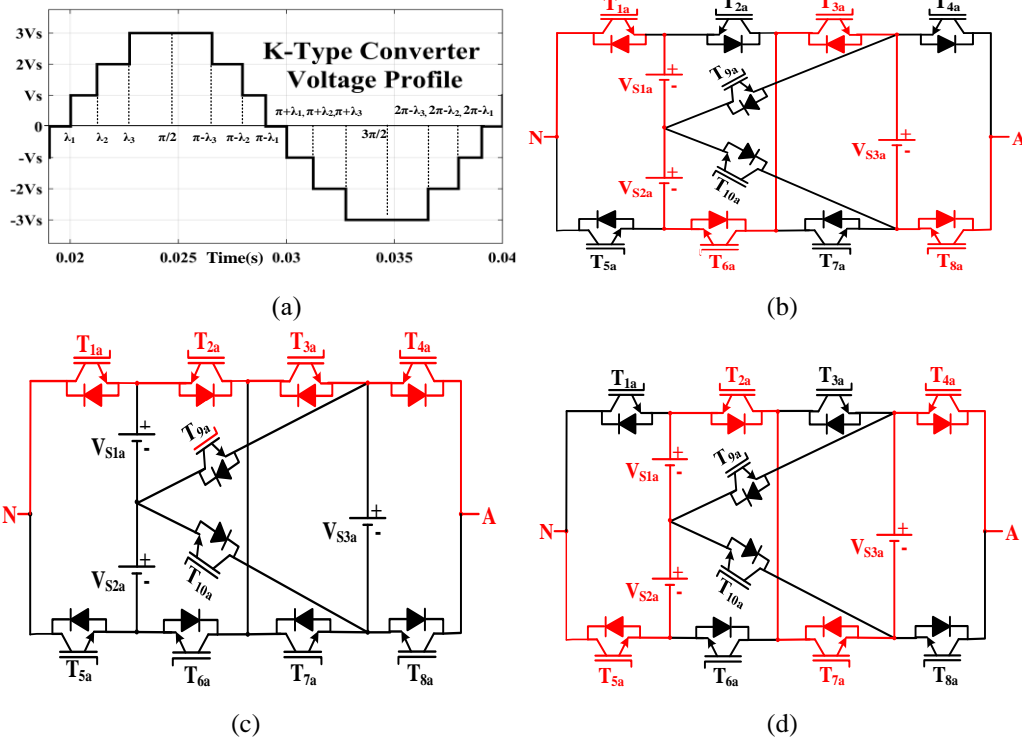


Fig. 5.2. (a) Output voltage profile (b) Positive peak level (c) zero level (d) Negative peak level of IK-7



(vi) 2nd negative level  $-2V_S = -V_{S1} - V_{S2}$

(vii) Peak negative level  $-3V_S = -V_{S1} - V_{S2} - V_{S3}$

To achieve the peak level of  $3V_S$  in the upper half cycle, the switches  $T_{1a}$ ,  $T_{3a}$ ,  $T_{6a}$ , and  $T_{8a}$  are turned ON, connecting all three DC sources in series, as depicted in Fig. 5.2(b). The second level of  $2V_S$  is obtained by activating switches  $T_{1a}$ ,  $T_{6a}$ ,  $T_{7a}$ , and  $T_{8a}$ , creating a series connection of  $V_{S1}$  and  $V_{S2}$ . The first upper half level of  $V_S$  is achieved by turning ON switches  $T_{1a}$ ,  $T_{4a}$ , and  $T_{9a}$ . The zero level is formed by activating switches  $T_{1a}$ ,  $T_{2a}$ ,  $T_{3a}$ , and  $T_{4a}$ , as shown in Fig. 5.2(c). Likewise, three negative levels of the lower half cycle are generated by reversing the connection of the DC sources. The first lower half level is produced by connecting  $V_{S2}$  in reverse through switches  $T_{4a}$ ,  $T_{5a}$ ,  $T_{6a}$ , and  $T_{7a}$ . The second level of ' $-2V_S$ ' is obtained by connecting switches  $T_{4a}$ ,  $T_{5a}$ , and  $T_{10a}$ . To achieve the peak level of the lower half cycle, the switches  $T_{2a}$ ,  $T_{4a}$ ,  $T_{5a}$ , and  $T_{7a}$  are turned ON, connecting  $V_{S1}$ ,  $V_{S2}$ , and  $V_{S3}$  in series, as shown in Fig. 5.2(d). Fig. 5.3 presents a complete three-phase solar PV system integrating the proposed seven-level K-type inverter for direct PV plant integration. The system consists of three single-phase inverters with the DC input from identical solar arrays. Each solar panel incorporates MPPT controllers to maximize power operation. The inverter output is connected to the grid system through series resistances ( $R_a$ ) and inductances ( $L_a$ ) in each phase to mitigate harmonics. The grid's phase angle ' $\theta$ ' is measured using a phase lock logic (PLL).

### **System Parameters**

$V_{S1a-c} = 150.6V$ ,  $V_{S2a-c} = 150.6V$ ,  $V_{S3a-c} = 150.6V$ ,  $P_{PV} = 76 \text{ kW}$ ,  $L_{abc} = 3.5 \text{ mH}$ ,  $f_{sw}$  (SHE) = 50 Hz, Angle 1 =  $11.63^\circ$ , 2 =  $26.09^\circ$ , 3 =  $56.03^\circ$ ,  $V_{abc} = 415V$ .  $K_{pdc} = 2.2$ ,  $K_{idc} = 1.5$ ,  $K_{ppr} = 0.009$ ,  $K_{ipr} = 0.0001$

## **5.3 CONTROL STRATEGY OF K-TYPE SYMMETRIC SEVEN LEVEL CONVERTER FOR SOLAR PV GENERATION APPLICATIONS**

The DC side of the system employs active current control to regulate the voltage  $V_{mpp}$  at the maximum power point tracking (MPPT) of each solar PV array, achieved through proportional-integral (PI) controllers. These controllers generate the current references  $I_{d(S1a)}$ ,  $I_{d(S2a)}$ , and  $I_{d(S3a)}$  for phase 'a', as depicted in Fig. 5.3. The reference currents from all solar PV arrays across the three phases are summed to obtain the total current reference,  $I_{dref}$ . This  $I_{dref}$  is then converted to equivalent AC currents using inverse Park transformation, resulting in the current references  $i_{aref}$ ,  $i_{bref}$ , and  $i_{cref}$ . The proportional resonant (PR) controllers  $PR_a$ ,  $PR_b$ , and  $PR_c$  are responsible for

controlling the reference AC currents in phases 'a', 'b', and 'c', respectively. The generated modulating signals  $M_a$ ,  $M_b$ , and  $M_c$  from these controllers are fed into the selective harmonics elimination (SHE) modulation control.

The SHE modulation technique is highly effective in controlling specific harmonics and switching frequency, thereby enhancing power quality. Fig. 5.3 illustrates the voltage output with seven levels, which can be mathematically expressed as follows:

$$V_o = \frac{4V_{dc}}{w\pi} [\text{Cos}(w\gamma_1) + \text{Cos}(w\gamma_2) + \dots + \text{Cos}(w\gamma_{(L-1)/2})] \quad (5.1)$$

Here L is the number of levels hence for L=7, the output voltage of the improved K-type converter is given as,

$$V_o = \frac{4V_{dc}}{w\pi} [\text{Cos}(w\gamma_1) + \text{Cos}(w\gamma_2) + \text{Cos}(w\gamma_3)] \quad (5.2)$$

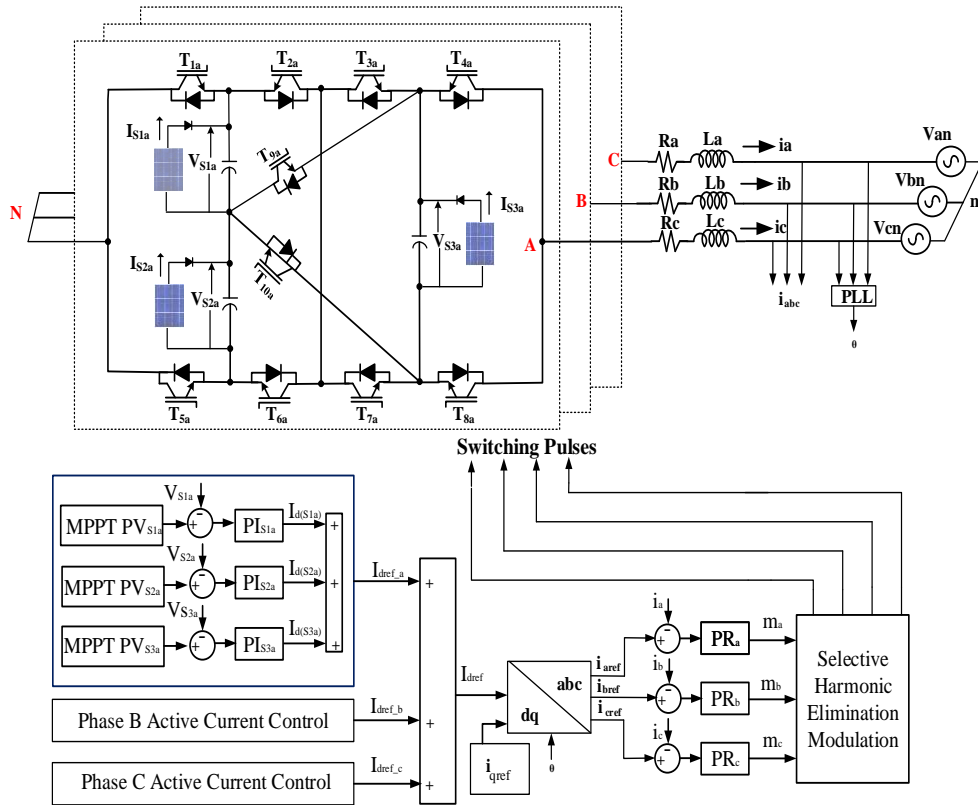


Fig. 5.3. Power and control scheme of solar-grid system of IK-7 multilevel inverter.

$\lambda_1$ ,  $\lambda_2$  and  $\lambda_3$  are the angles of the positive quarter cycle, angles for second quarter cycle are  $(180^\circ - \gamma_1)$ ,  $(180^\circ - \gamma_2)$  and  $(180^\circ - \gamma_3)$ . Similarly,  $(180^\circ + \gamma_1)$ ,  $(180^\circ + \gamma_2)$  and  $(180^\circ + \gamma_3)$  are angles of third negative quarter cycles, angles  $(360^\circ - \lambda_1)$ ,  $(360^\circ - \gamma_2)$  and  $(360^\circ - \gamma_3)$

$\gamma_3$ ) belong to fourth negative quarter cycle. The fundamental voltage output equation of the converter is as,

$$V_{o,(Fund.)} = \frac{4V_{dc}}{w\pi} [\text{Cos}(\gamma_1) + \text{Cos}(\gamma_2) + \text{Cos}(\gamma_3)] \quad (5.3)$$

And equations for 5th and 7th harmonics are,

$$V_{o,(5th)} = \frac{4V_{dc}}{w\pi} [\text{Cos}(5\gamma_1) + \text{Cos}(5\gamma_2) + \text{Cos}(5\gamma_3)] \quad (5.4)$$

$$V_{o,(7th)} = \frac{4V_{dc}}{w\pi} [\text{Cos}(7\gamma_1) + \text{Cos}(7\gamma_2) + \text{Cos}(7\gamma_3)] \quad (5.5)$$

Placing  $w=1$  in equation (3) gives,

$$\text{Cos}(\gamma_1) + \text{Cos}(\gamma_2) + \text{Cos}(\gamma_3) = M_a \quad (5.6)$$

5th and 7th harmonics are eliminated by equating their corresponding equations to zero,

$$\text{Cos}(5\gamma_1) + \text{Cos}(5\gamma_2) + \text{Cos}(5\gamma_3) = 0 \quad (5.7)$$

$$\text{Cos}(7\gamma_1) + \text{Cos}(7\gamma_2) + \text{Cos}(7\gamma_3) = 0 \quad (5.8)$$

$\lambda_1$ ,  $\lambda_2$  and  $\lambda_3$  can be computed from equation (5.7) and (5.8) by using these relations,

$$\text{Cos}(5\gamma) = 16\text{Cos}^5(\gamma) - 20\text{Cos}^3(\gamma) + 5\text{Cos}(\gamma) \quad (5.9)$$

$$\begin{aligned} \text{Cos}(5\gamma) &= 64\text{Cos}^7(\gamma) - 112\text{Cos}^5(\gamma) \\ &+ 5\text{Cos}^3(\gamma) \dots \dots + 7\text{Cos}(\gamma) \end{aligned} \quad (5.10)$$

#### 5.4 MATLAB MODEL OF K-TYPE SYMMETRIC SEVEN LEVEL CONVERTER FOR SOLAR PV GENERATION APPLICATIONS

Fig. 5.4(a) shows the developed MATLAB model of power circuit the seven level K-Type converter. Each phase consist of three solar arrays. The DC link capacitors are connected across the DC terminals of solar arrays and the voltages  $V_{S1a}$ ,  $V_{S2a}$  &  $V_{S3a}$  are measured. The power circuit is formed by the ten switches arranged such that placing resembles with letter 'K'. Phase 'B' & 'C' are formed similar to Phase 'A'. Three phase of converters are connected in the star and are fed to R-L harmonic filter. The measurement of three phase voltages and currents is taken before feeding the power to the grid.

Fig. 5.4(b) shows the control scheme implementation of this converter. The DC link voltage control consists of comparison of average of all reference and actual capacitor voltages to generate the reference currents. Reference currents are then compared with DC equivalent of grid current and PR controllers are employed to track and modulating

signals are generated.

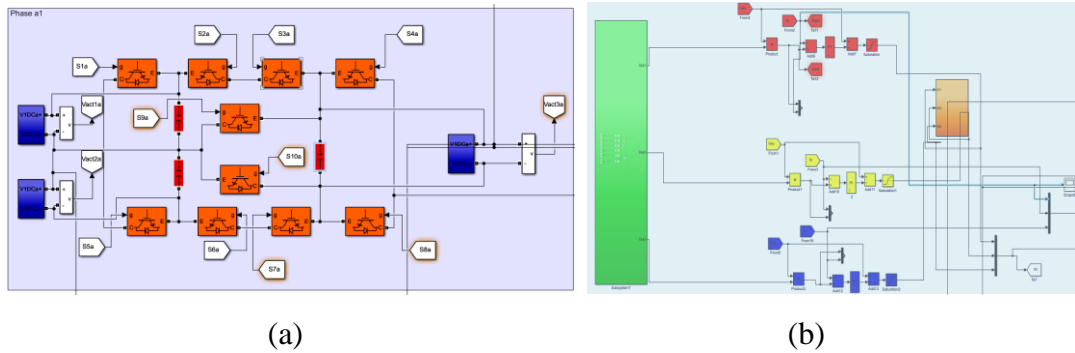


Fig.5.4. MATLAB models of (a) power circuit (b) control circuit

## 5.5 SIMULATED RESULTS OF K-TYPE SYMMETRIC SEVEN LEVEL CONVERTER FOR SOLAR PV GENERATION APPLICATIONS

The performance of the IK-7 solar PV generating system in injecting solar power into the grid is simulated using the MATLAB/SIMULINK platform. The simulation results, depicted in Figs. 5.5-5.7, illustrate the system's behaviour under various solar conditions. Fig. 5.5(a) showcases the steady-state results, where nine solar arrays extract a total of 79.15 kW when exposed to a solar irradiation of 1000W/m<sup>2</sup>. The PV array end power smoothly transfers at 77.57 kW. The IK-7 converter generates seven voltage levels, resulting in a sinusoidal grid current waveform.

In Fig. 5.5(b), the response of the solar PV generation system to a decrease in solar irradiation from 1000W/m<sup>2</sup> to 500W/m<sup>2</sup> is presented. As expected, the PV array power reduces by half, leading to a proportional decrease in the grid power and the current. However, the reactive power remains zero, and although the converter voltage decreases, it maintains the seven levels. Conversely, when solar irradiation increases back to 1000W/m<sup>2</sup> from 500W/m<sup>2</sup>, the solar PV power and electrical powers resume their normal values. Fig. 5.6(a) exhibits the dynamics of solar irradiation during the rise condition. The system's response in the absence of solar PV power generation is depicted in Fig. 5.6(b), where solar irradiation drops to zero from 500W/m<sup>2</sup>, resulting in both solar PV power and grid power falling to zero as well. Figs. 5.7(a)-(b) demonstrate the harmonics response of the IK-7 solar system. Fig. 5.7(a) presents the total harmonic distortion (THD) of the IK-7 output voltage, which measures 13.58%. The fundamental voltage component at 50 Hz is 451.7 V. Fig. 5.7(b) illustrates the current THD, which stands at 1.32%, satisfying the IEEE 519 standard perfectly.

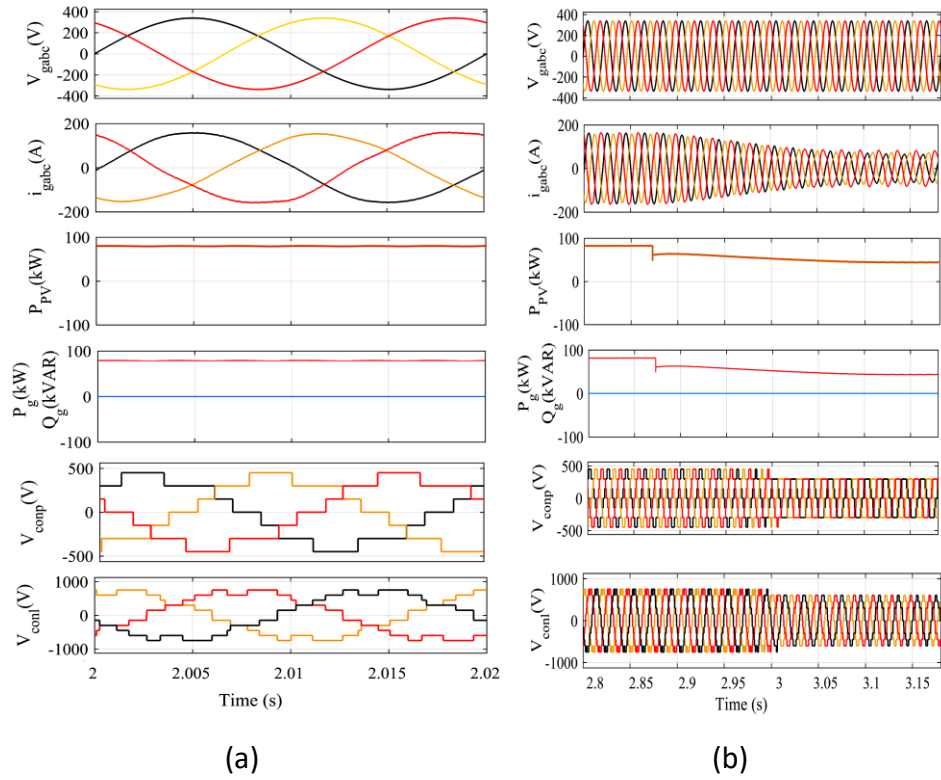


Fig. 5.5. (a) Steady state response (b) dynamic response during irradiation fall of IK-7 multilevel inverter solar-grid system

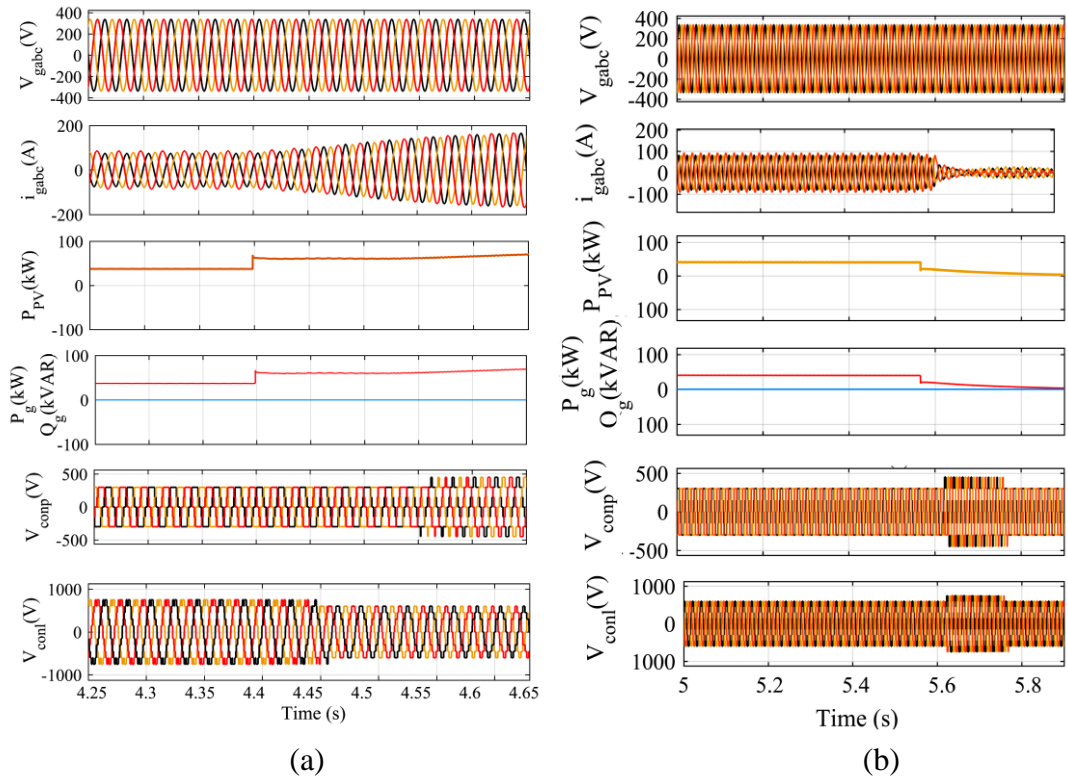
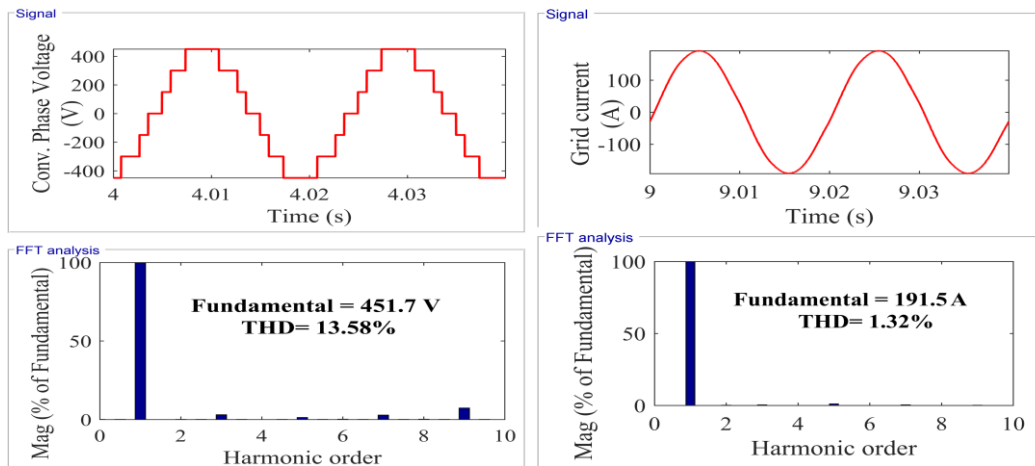


Fig. 5.6. IK-7 multilevel inverter solar-grid system during (a) rise (b) zero irradiation



(a)

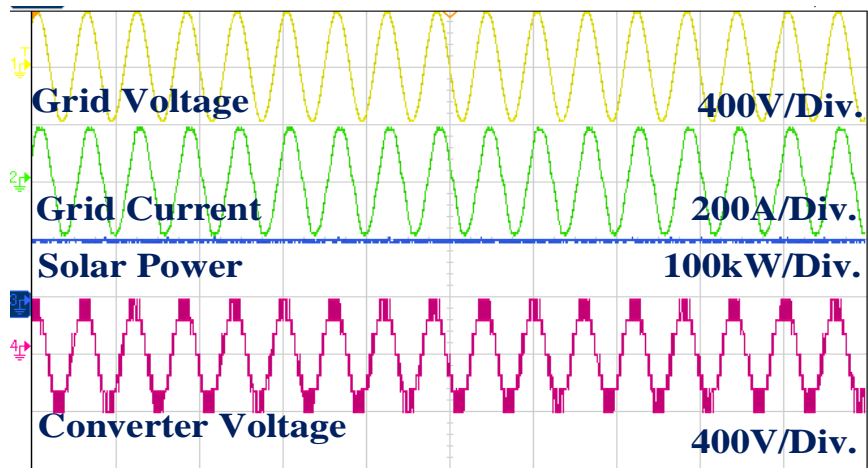
(b)

Fig. 5.7. IK7 converter (a) voltage profile and THD (b) The grid current and its THD.

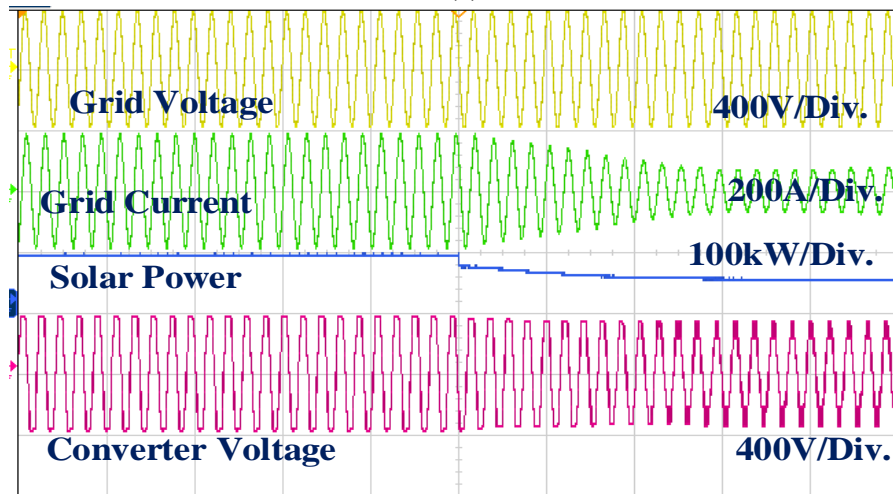
## 5.6 SIMULATED RESULTS OF K-TYPE SYMMETRIC SEVEN LEVEL CONVERTER FOR SOLAR PV GENERATION APPLICATIONS

The solar photovoltaic generation system with seven level K-Type converter simulated responses are validated by the real-time execution on OPAL-RT. Digitally-sampled time control is used to check the control performance with modulating scheme. The real time execution is performed at the sampling time of  $5e^{-5}$  sec. Fig. 5,8(a) shows the steady state response of converter voltage, grid voltage and current at the solar irradiation of  $1000W/m^2$ . These parameters validate the MATLAB simulation response. The dynamic response when solar irradiation decreases to half is depicted in Fig. 5,8(b). The solar PV power also decreases to half. Fig. 5.9 (a) shows the dynamic response when solar irradiation resumes to normal  $1000W/m^2$  from  $500W/m^2$  which is similar to the MATLAB simulated results during the irradiation rise. Fig. 5.9 (b) shows the solar system response during evening when there is no sunlight.

The harmonic response is shown in Fig. 5.10 (a)-(b), which shows the voltage THD of 13.06% and current THD of 1.376%. These values are very close to simulated values.

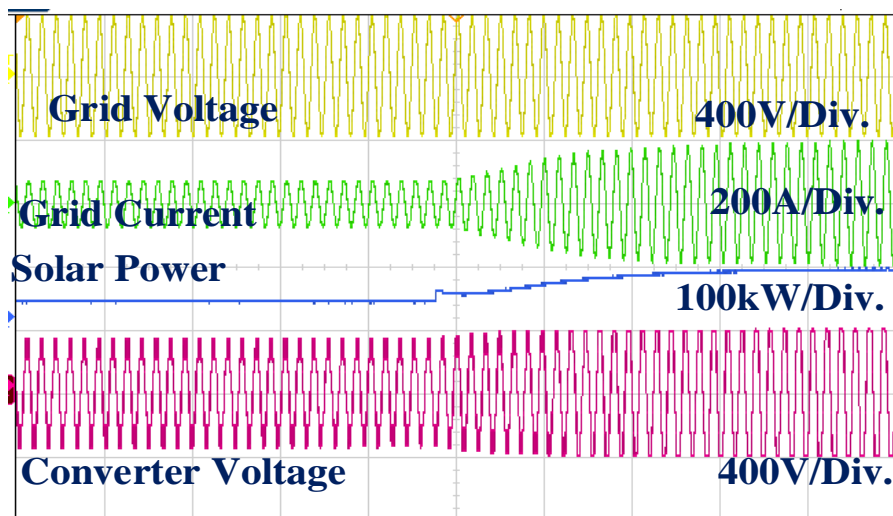


(a)



(b)

Fig. 5.8. OPAL-RT results, (a) Steady state response (b) dynamic response during irradiation fall of IK-7 multilevel inverter solar-grid system



(a)

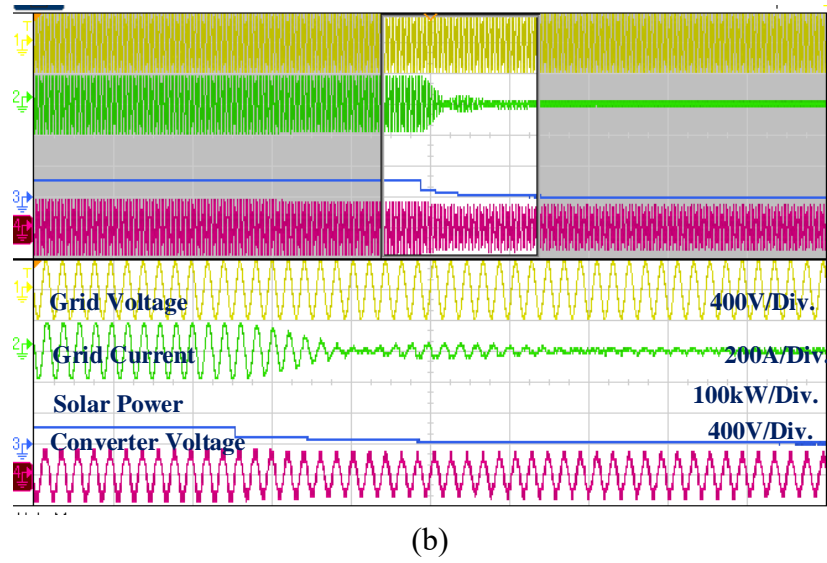


Fig. 5.9. OPAL-RT results of IK-7 multilevel inverter solar-grid system during (a) rise (b) zero irradiation

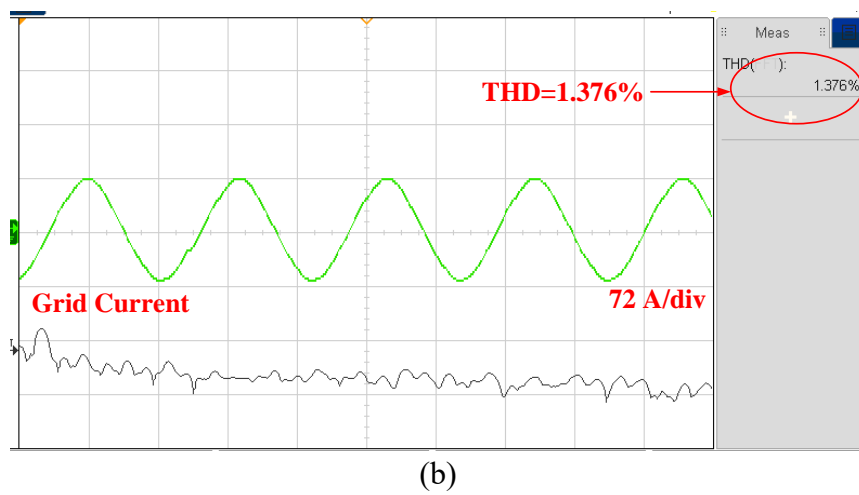
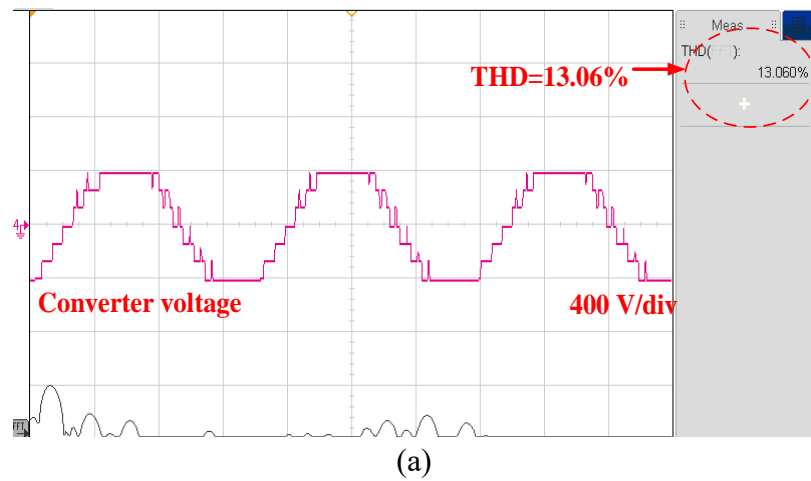


Fig. 5.10. IK7 converter OPAL-RT results (a) voltage profile and THD (b) The grid current and its THD



## 5.7 CONCLUSIONS

Performance of an enhanced K-type multilevel inverter, known as IK-7, has been simulated in MATLAB using a closed-loop configuration. This system operates by harnessing power from solar PV arrays and injecting the electrical energy into the electric grid. To optimize solar power extraction, MPPT controllers are employed, while PI controllers are utilized to maintain voltage balance. The AC power control is achieved through the implementation of PR control, ensuring a straightforward and robust operation. By incorporating SHE modulation, this system has achieved an outstanding harmonics response. The converter phase voltage THD is found 13.58% and current total harmonic distortion (THD) measured 1.32%, within the permissible limits of 5% set by the IEEE-519 standard. This improved harmonic performance ensures a high-quality power output. Furthermore, this system has demonstrated exceptional performance under dynamic conditions caused by varying solar irradiation. It successfully maintained the voltage and current profiles of the converter output and grid, allowing for consistent operation and reliable power injection.

## CHAPTER-VI

### CONTROL AND REAL-TIME EXECUTION OF CASCADED H BRIDGE NINE LEVEL CONVERTER FOR SOLAR PV GENERATION APPLICATIONS

#### 6.1 INTRODUCTION

This work investigates the harmonic analysis of nine level three phase cascaded H-bridge(CHB) multi-level converter by using the nearest level modulation (NLM) and sinusoidal modulating signals are injected with third harmonic. The NLM technique operates at fundamental frequency means improved inverter efficiency due to less switching losses in comparison to the multi-carrier modulation pulse width modulation. The THI combined with the NLM has many advantages, which are increased magnitude of fundamental voltage component, improvement of power quality by mitigation of total harmonics distortion (THD). The THI-NLM provides lesser complexity and performs good in dynamic conditions. The mathematical equations of voltage and current are the basis of modelling of presented CHB inverter generating nine level to explain the operating performance. The robust DQ control along with THI-NLM transfers solar PV power to the grid with improved efficiency and power regulation. System is modeled in MATLAB simulator platform and its solar generating system dynamics is assessed in varying environmental conditions of solar irradiation. The comparison of THI-NLM with normal NLM is made at various solar irradiances. Simulated results are tested in real-time simulator OP-5700.

#### 6.2 CIRCUIT CONFIGURATION OF CASCADED H BRIDGE NINE LEVEL CONVERTER FOR SOLAR PV GENERATION APPLICATIONS

The proposed solar photovoltaic (SPV) generating system is a single stage conversion system as depicted in Fig 6.1, which is formed by a series connection of four H-bridge inverter cells. Each H-bridge inverter cell is powered by a similar solar array of voltage  $V_{PV}$  and output of each inverter cell takes three voltage levels  $+V_{PV}$ , 0 and  $-V_{PV}$

depending on switching states of four switches. Phase voltages of four power cells are given as,

$$V_{con1} = V_{PV1}(S_{a1} - S_{a4}) = D_1 V_{PV1} \quad (6.1)$$

$$V_{con2} = V_{PV2}(S_{a5} - S_{a8}) = D_2 V_{PV2} \quad (6.2)$$

$$V_{con3} = V_{PV3}(S_{a9} - S_{a12}) = D_3 V_{PV3} \quad (6.3)$$

$$V_{con4} = V_{PV4}(S_{a13} - S_{a16}) = D_4 V_{PV4} \quad (6.4)$$

Here  $V_{con1-4}$ ,  $V_{PV1-4}$  are voltage output of H-bridge inverter and PV arrays of power cell 1-4 respectively.  $S_{a1-a16}$  are switch positions, that are 1 and 0 for 'on' and 'off' respectively.  $D_{1-4}$  outcome of power cells and have the values -1,0 or +1 according to the position of  $S_{a1-a16}$  switches. CHB converter dynamics can be expressed by these equations,

$$C_{1a} \frac{dV_{PV1}}{dt} = i_{PV1a} - i_{1a} \quad (6.5)$$

$$C_{2a} \frac{dV_{PV2}}{dt} = i_{PV2a} - i_{2a} \quad (6.6)$$

$$C_{3a} \frac{dV_{PV3}}{dt} = i_{PV3a} - i_{3a} \quad (6.7)$$

$$C_{4a} \frac{dV_{PV4}}{dt} = i_{PV4a} - i_{4a} \quad (6.8)$$

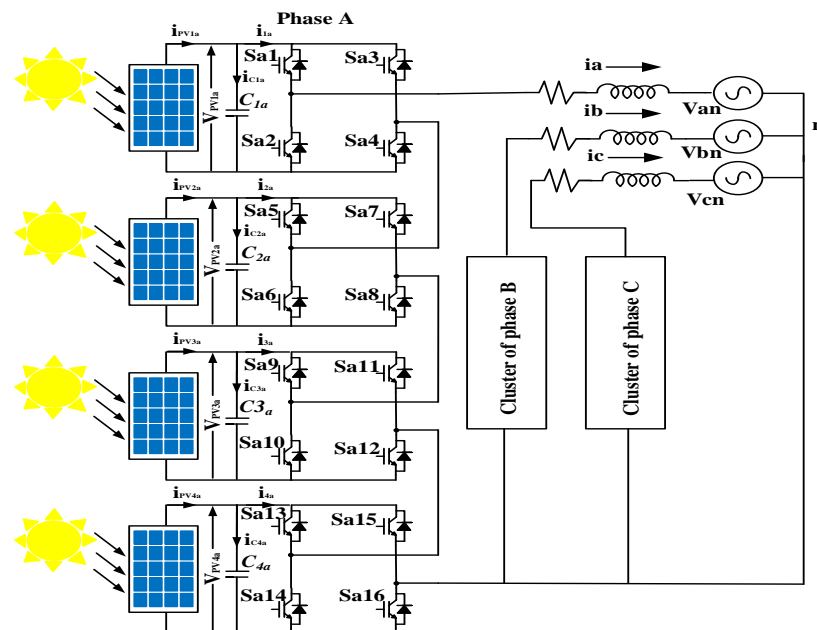


Fig. 6.1. Nine level CHB-PV generating system

Switch logic of all the switches for nine-level stepped output of phase of converter is depicted in Table 6.1. Every PV array is equipped with a maximum power point tracker (MPPT) controller that confirms the maximum solar energy harness from sunlight. The CHB converter output is fed to the power-grid through the harmonic filter.

Table 6.1 Switch Logics of Cascade H-Bridge

S.N.	Operating Switches	V <sub>out</sub> (V)
1	S <sub>a1</sub> , S <sub>a4</sub> , S <sub>a6</sub> , S <sub>a8</sub> , S <sub>a10</sub> , S <sub>a12</sub> , S <sub>a14</sub> , S <sub>a16</sub>	+V <sub>pv</sub>
2	S <sub>a1</sub> , S <sub>a4</sub> , S <sub>a5</sub> , S <sub>a8</sub> , S <sub>a10</sub> , S <sub>a12</sub> , S <sub>a14</sub> , S <sub>a16</sub>	+2V <sub>pv</sub>
3	S <sub>a1</sub> , S <sub>a4</sub> , S <sub>a5</sub> , S <sub>a8</sub> , S <sub>a9</sub> , S <sub>a12</sub> , S <sub>a14</sub> , S <sub>a16</sub>	+3V <sub>pv</sub>
4	S <sub>a1</sub> , S <sub>a4</sub> , S <sub>a5</sub> , S <sub>a8</sub> , S <sub>a9</sub> , S <sub>a12</sub> , S <sub>a13</sub> , S <sub>a16</sub>	+4V <sub>pv</sub>
5	S <sub>a2</sub> , S <sub>a4</sub> , S <sub>a6</sub> , S <sub>a8</sub> , S <sub>a10</sub> , S <sub>a12</sub> , S <sub>a14</sub> , S <sub>a16</sub>	0
6	S <sub>a2</sub> , S <sub>a3</sub> , S <sub>a6</sub> , S <sub>a8</sub> , S <sub>a10</sub> , S <sub>a12</sub> , S <sub>a14</sub> , S <sub>a16</sub>	- V <sub>pv</sub>
7	S <sub>a2</sub> , S <sub>a3</sub> , S <sub>a5s</sub> , S <sub>a8</sub> , S <sub>a10</sub> , S <sub>a12</sub> , S <sub>a14</sub> , S <sub>a16</sub>	- 2V <sub>pv</sub>
8	S <sub>a2</sub> , S <sub>a3</sub> , S <sub>a5s</sub> , S <sub>a8</sub> , S <sub>a9</sub> , S <sub>a12</sub> , S <sub>a14</sub> , S <sub>a16</sub>	-3V <sub>pv</sub>
9	S <sub>a2</sub> , S <sub>a3</sub> , S <sub>a5s</sub> , S <sub>a8</sub> , S <sub>a9</sub> , S <sub>a12</sub> , S <sub>a13</sub> , S <sub>a16</sub>	-4V <sub>pv</sub>

System parameters are as follows.

V<sub>pv</sub>=95.0V, I<sub>pv</sub>=66.21A, P<sub>pv</sub>=75.55kW, R=0.05 ohm, L=1.0mH, V<sub>g</sub>=415V, C=10000 microF, T<sub>s</sub>=10 microS, f<sub>s</sub>=50Hz, PI<sub>dc</sub>: k<sub>pdc</sub>=1.05, k<sub>idc</sub>=0.001, PR<sub>ac</sub>: k<sub>pm</sub>=.0008, k<sub>im</sub>=0.0001.

### 6.3 CONTROL MODULATION TECHNOLOGY OF CASCADED H-BRIDGE NINE LEVEL CONVERTER FOR SOLAR PV GENERATION APPLICATIONS

The control structure of the nine level CHB Solar PV generation system comprises of nearest level PWM coupled with third harmonic injection. The grid tied power control ensures the smooth power transfer at unity power factor. The complete control scheme is presented in the following sub-sections.

#### 6.3.1 Concept of Third Harmonic Injection

The sinusoidal pulse width signals are obtained from the closed loop *dq* controller as (M<sub>a</sub>, M<sub>b</sub>, M<sub>c</sub>). There is a 120° phase difference between the modulating signals, which can be expressed as,

$$M_a = V_{an} \sin(\theta_{an}) \quad (6.9)$$

$$M_b = V_{an} \sin(\theta_{an} - 120^\circ) \quad (6.10)$$

$$M_c = V_{an} \sin(\theta_{an} - 240^\circ) \quad (6.11)$$

Here  $M_{abc}$  are reference for the modulation,  $V_{an}$  &  $\theta_{an}$  are phase voltage of grid and phase-difference of phase a. The reference modulating signals injected with 3<sup>rd</sup> harmonic component are generated. The 3<sup>rd</sup> harmonic injected signals are expressed as,

$$U_{TH1a} = A_{TH1} \sin(\theta_{an}) + \sin(3\theta_{an}) \quad (6.12)$$

$$U_{TH1b} = A_{TH1} \sin(\theta_{an}) + \sin(3(\theta_{an} - 120^\circ)) \quad (6.13)$$

$$U_{TH1c} = A_{TH1} \sin(\theta_{an}) + \sin(3(\theta_{an} - 240^\circ)) \quad (6.14)$$

Where  $U_{TH1a-c}$  are reference modulating signals, which are 3<sup>rd</sup> harmonic injected and reference for the nearest-level-modulation algorithm.

### 6.3.2 3<sup>rd</sup> Harmonic Injected Nearest Level Modulated Switching

Figs. 6.2(a)-(b) depict the algorithm of 3<sup>rd</sup> harmonic injected nearest-level-modulation and 3<sup>rd</sup> harmonic injected carrier signal. The input, three phase 3<sup>rd</sup> harmonic signals can be expressed as,

$$y_{abc} = u_{TH1}(a-c) \quad (6.15)$$

Where  $y_{abc}$  is output response of phases a, b, c while  $u_{TH1}$  are input-variable. The function for the level is expressed as,

$$L_{inv} = \frac{1}{N_p} \quad (6.16)$$

Where  $N_p$  is the count of levels in half cycle of voltage profile. The fraction  $K$  is computed by division of  $u_{TH1}$  and level function, which is given as,

$$K = \frac{u_{TH1}}{L_{inv}} \quad (6.17)$$

The  $R_F$  is obtained by the rounding of fractional value  $K$  to nearest integer by applying the round function, which is expressed as,

$$R_f = \text{round}(K) \quad (6.18)$$

The value of  $R_F$  gives the level of inverter voltage, which is obtained by the switching the sequence given in the Table 6.1.

### 6.3.3 Grid Tied Power Controller

Figs. 6.3 (a)-(b) depict the solar-power and 3<sup>rd</sup> harmonic injected NLM control of CHB-inverter. The capacitors between solar PV array and converter are charged by the solar-irradiation that transfers electric power to the grid. The voltage ripple are caused in the capacitor as power propels to the grid. The power control is implemented by the balancing of solar PV generated power and power transferred to the grid. This control is achieved by generating the DC reference current  $I_{d(ref)}$ , which is obtained by the comparison of average of reference voltages  $V_{d(ref)}$  corresponding to maximum power point and average of actual capacitor voltages  $V_{d(act)}$  of all sixteen solar PV array. The proportional-integral controller  $PI_1$  is employed for tracking of  $V_{d(act)}$  to the  $V_{d(ref)}$ . The control of grid-current injection comprise of direct and quadrature axis currents  $I_d$  and  $I_q$  comparison with reference  $I_{d(ref)}$  and zero respectively, for unity power factor transfer. The direct and quadrature reference voltages are obtained by following equations,

$$V_{dref} = K_p (I_d - I_{dref}) + K_i \int (I_d - I_{dref}) dt - \omega L_f I_q + V_d \quad (6.19)$$

$$V_{qref} = K_p (I_q - I_{qref}) + K_i \int (I_q - I_{qref}) dt - \omega L_f I_d + V_q \quad (6.20)$$

Where  $V_{dref}$  and  $V_{qref}$  are direct and quadrature voltages obtained from Park transformation of grid voltages  $V_{gabc}$ . The reference modulating signals  $M_{abc}$  are obtained by the dq to abc transformation. Fig. 6.2 depicts THI-NLM based switching pulse generation.

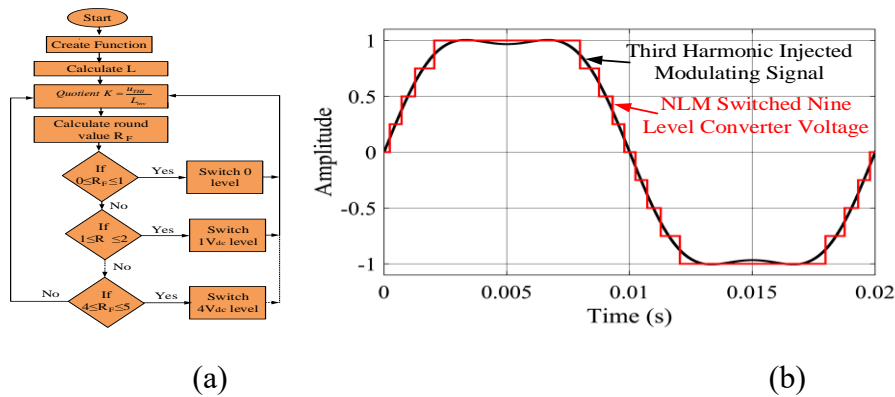
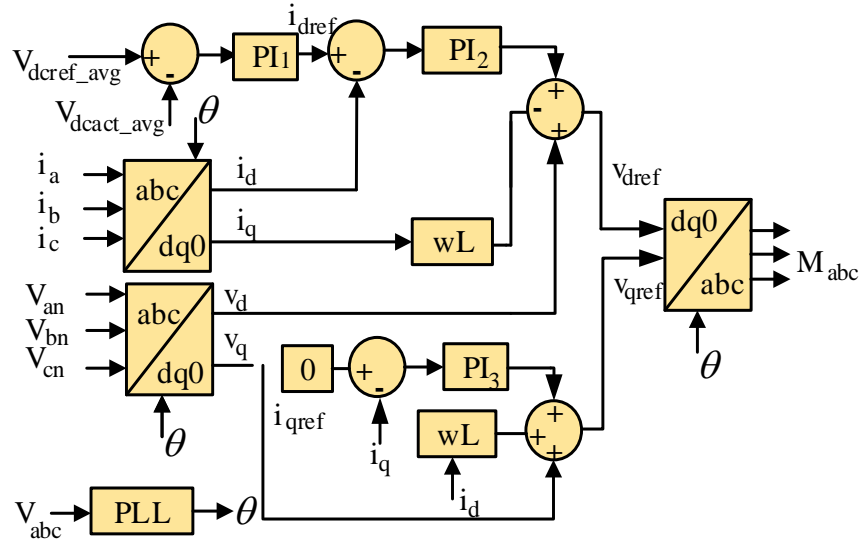
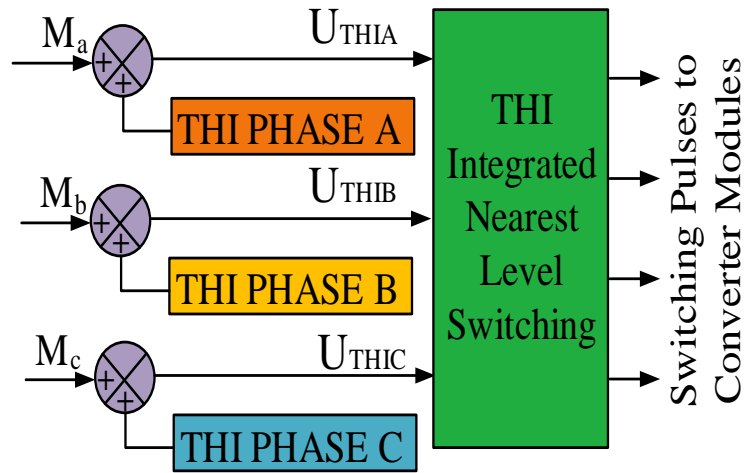


Fig. 6.2. (a) Control algorithm for NLM Switching, (b) THI Modulating signal and converter output voltage



(a)



(b)

Fig. 6.3 Control circuit (a) Grid Power and (b) Switching Controller

#### 6.4 MATLAB MODEL OF CASCADED H-BRIDGE NINE LEVEL CONVERTER FOR SOLAR PV GENERATION APPLICATIONS

Fig. 6.4(a) shows the MATLAB model of power circuit the nine level CHB converter.

Each phase consists of four solar arrays. The DC link capacitors are connected across the DC terminals of solar arrays and the voltage  $V_{PV1a}$ ,  $V_{PV2a}$ ,  $V_{PV3a}$  &  $V_{PV4a}$  are measured. The power circuit is formed by the four H-bridge power cells, which have solar array as DC source in each cell. Phase 'B' & 'C' are formed similar to Phase 'A'. Three phase of converters, are connected in the star and are fed to R-L harmonic filter.





converter performance with THI-NLM and level shifted multi-carrier is presented in detail.

The system performances, under both steady-state and dynamic conditions of solar irradiation are evaluated. Steady state response of the nine level CHB-PV generating system, which is operated at normal  $1000 \text{ W/m}^2$  solar irradiation, is illustrated in various subsections of Fig. 6.5 (a). Subsection (A) demonstrates the balanced power /phase, with grid power ( $P_g$ ) equal to 24.43 kW. In subsection B, a total PV generation ( $P_{PV}$ ) 75.55kW is injected to the grid with a 97.0% efficiency. Sub-section C shows a grid power of 73.28 kW, while section D displays the three phase grid voltages. The section E shows the injected phase currents to the grid. The inverter output phase voltage ( $V_{comp}$ ) is shown in (F), the converter line voltage ( $V_{conl}$ ) is illustrated in (G), and sub-section (H) displays the THI modulating signal.

The solar generating system dynamics are explained in the Figs 6.5 (b)-(c). The section B & C shows the profile of solar PV generated power  $P_{PV}$  and power transferred to the grid  $P_g$  during solar irradiation reduction to  $600 \text{ W/m}^2$  from normal  $1000 \text{ W/m}^2$ , which shows that both  $P_{PV}$  and  $P_g$  varies proportionally with solar irradiation variation, Sub-section A shows that the per phase power transfer to the grid remains uniformly distributed. The section D shows the grid voltages of three phases, which remain stable in the varying solar conditions. In sub-section E, the grid current  $i_g$  falls to 60% of its normal value. The sections F, G, and H show the  $V_{comp}$ ,  $V_{conl}$  and  $M_{abc}$ , phase, line voltage and modulating signal respectively, which remain stable and each phase is  $120^\circ$  apart from one another.

In Fig. 6.5 (c), sub-sections A to H shows magnificent dynamics when solar irradiance rises to normal from 60%. Additionally, during irradiation, as the solar power ( $P_{pv}$ ) rises from  $500 \text{ W/m}^2$  to  $1000 \text{ W/m}^2$ , the system's power output increases to 45.40 kW,

and the grid power also rises to 44.00 kW while maintaining a perfect dynamic balance. The converter output voltage is shown under dynamic conditions. These performance is achieved using feedback-loop control, and a new modified-carrier PWM technique has improved power quality and performance in varying solar conditions.

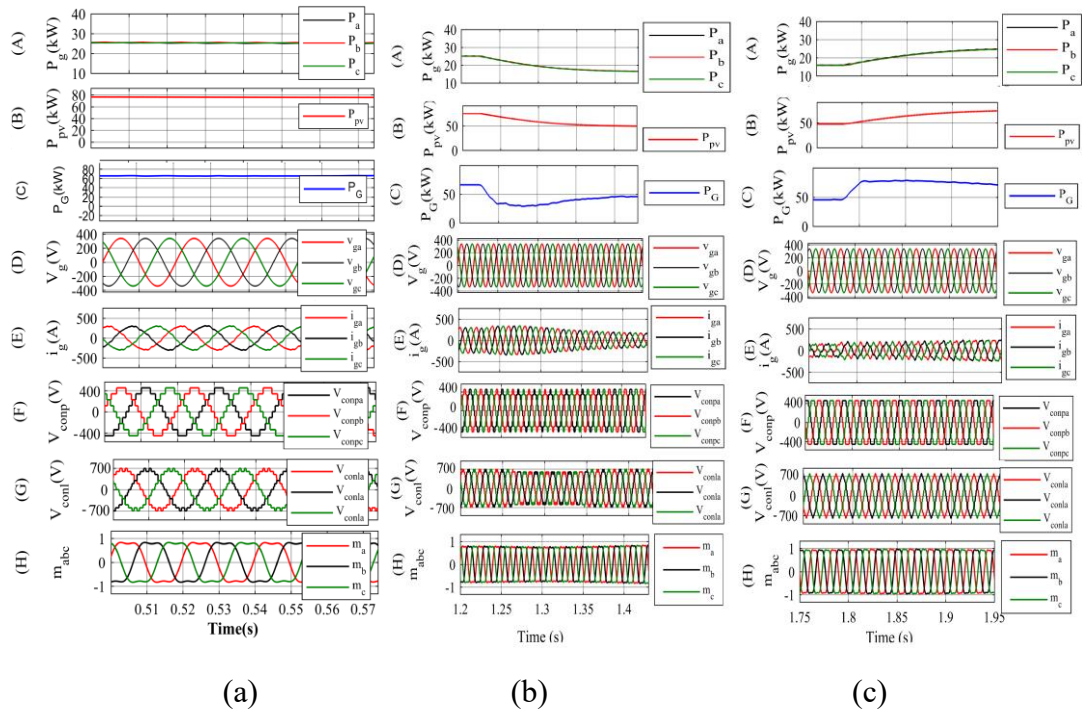


Fig. 6.5. Simulation responses (a) steady-state (b) dynamic reduction solar (c) dynamic increase of solar

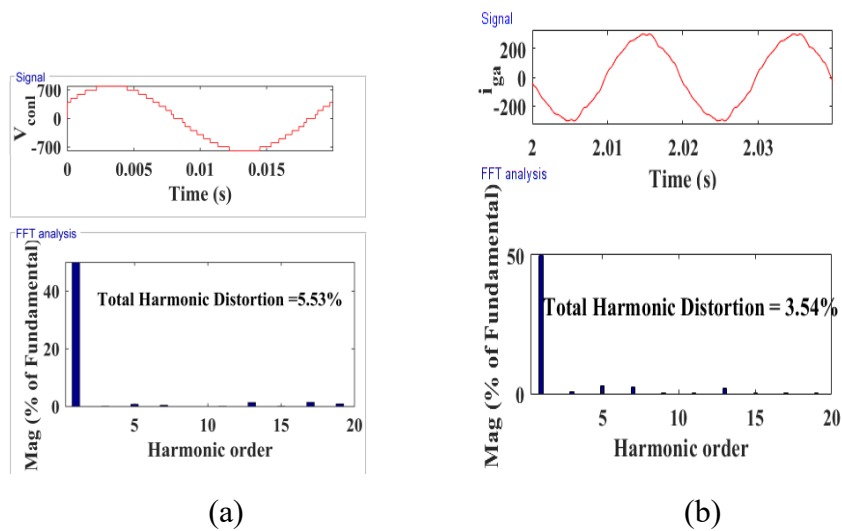


Fig. 6.6. Harmonics spectra of (a) converter voltage (b) grid current

## 6.6 HARMONICS ASSESSMENT OF CASCADED H BRIDGE NINE LEVEL CONVERTER FOR SOLAR PV GENERATION APPLICATIONS

Table 6.2 presents the harmonic performance of a nine level CHB solar PV generating system by using the NLM and multicarrier PWM techniques, with sine wave and 3<sup>rd</sup> harmonic injected sine wave modulated references. The results are obtained for various solar irradiations by adjusting the modulation index. The adopted modulation technique demonstrates improved performance in terms of THD and higher fundamental voltage component. The following subsections provide a detailed analysis of the performance of the two modulation techniques.

### 6.6.1 Analysis with Nearest Level Modulation (NLM)

Table 6.2 illustrates the harmonics of the converter voltage based on NLM. When THI injection is applied in NLM, the converter voltage exhibits a THD of 5.53% (line) and 16.16% (phase) at 1000 W/m<sup>2</sup> solar irradiation. The line and phase voltage THD rise to 10.78% (line) and 28.01% respectively at 600 W/m<sup>2</sup>. When a sinusoidal reference signal is used in NLM, the THD performance is measured at 7.63% (line), 9.37% (phase) for 1000 W/m<sup>2</sup>, and 11.94% (line), 16.72% (phase) for 600 W/m<sup>2</sup> solar irradiation. These results indicate that NLM with the injected third harmonic signal exhibits lower THD compared to sinusoidal reference signal.

Table 6.2 THI-NLM and Multicarrier PWM based Harmonic Comparison

Modulation Scheme	Modulating Signal	1000W/m <sup>2</sup>		900W/m <sup>2</sup>		800W/m <sup>2</sup>		700W/m <sup>2</sup>		600W/m <sup>2</sup>	
		THD	THD	THD	THD	THD	THD	THD	THD	THD	THD
		(V <sub>conl</sub> ) (%)	(V <sub>comp</sub> ) (%)	(V <sub>conl</sub> ) (%)	(V <sub>comp</sub> ) (%)	(V <sub>conl</sub> ) (%)	(V <sub>comp</sub> ) (%)	(V <sub>conl</sub> ) (%)	(V <sub>comp</sub> ) (%)	(V <sub>conl</sub> ) (%)	(V <sub>comp</sub> ) (%)
Nearest Level	THI	5.53	16.16	8.08	19.55	7.27	15.84	6.43	17.82	10.78	28.01
	Sinusoidal	7.63	9.37	10.05	12.55	10.81	11.55	10.87	14.14	11.94	16.72
Multi-Carrier	THI	7.48	19.89	7.87	22.93	9.40	20.01	10.85	25.23	12.86	27.84
	Sinusoidal	8.28	13.46	8.62	16.78	10.58	17.41	12.11	24.41	13.35	27.84

### **6.6.2 Analysis with Multicarrier Modulation**

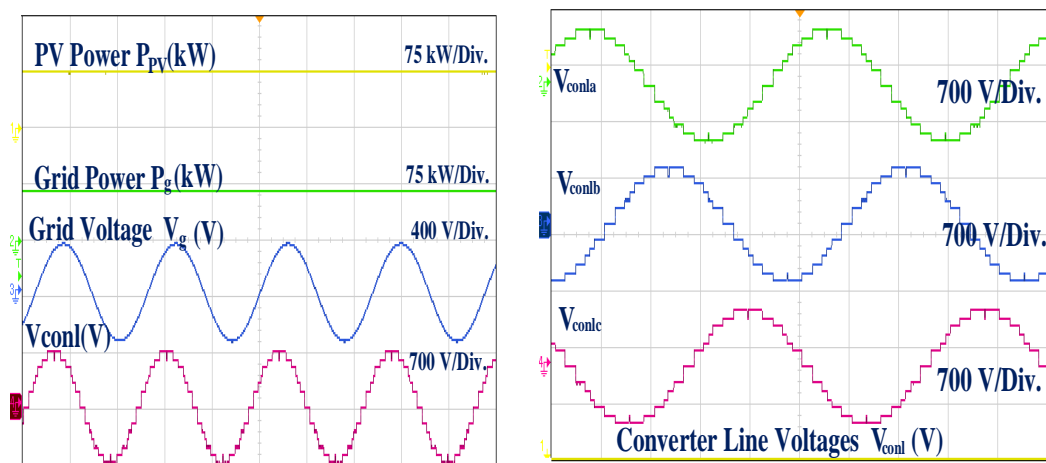
In the multicarrier modulation technique, the THD ranges from 7.48% to 12.86% for line voltage and 19.89% to 27.84% for phase voltage when using a THI sinusoidal reference signal. When a sinusoidal reference signal is employed, the line and phase voltage THD varies from 8.28% - 13.35% and 13.46% - 27.84% respectively.

The 3<sup>rd</sup> harmonic injected NLM performs best with lowest line voltage THD, and hence, it is used for the close loop control of the solar CHB solar PV generation system. Fig. 6.6(a) shows a line voltage THD of 5.53% and an enhanced fundamental voltage component. Additionally, 3.54% grid current THD, as shown in Fig. 6.6(b) is well below of the 5%, IEEE 519 standard.

### **6.7 REAL-TIME EXECUTION OF CASCADED H BRIDGE NINE LEVEL CONVERTER FOR SOLAR PV GENERATION APPLICATIONS**

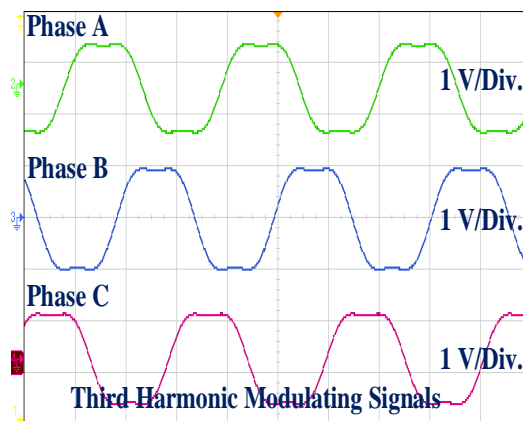
Performance of the system is verified using the real-time simulator OPAL-RT, which employs a physical clock to validate the system's performance in real-time. Figs. 6.7-6.10 exhibit the real time executed responses in the stable and dynamical conditions, real time execution is carried on OPAL-RT simulator. Fig. 6.7 (a) illustrates the voltage profile of inverter stepped output and grid. Fig. 6.7 (a) also shows power transferred to the grid and generated PV power of solar arrays. In Fig. 6.7(b), the line voltage of the nine-level converter is shown, with each voltage waveform being 120 degrees apart from one another. Fig. 6.7(c) displays the modulating signals of the converter's three phases, specifically the third harmonic injected modulating signals. The modulating reference signals are used to generate switching sequence by the nearest level algorithm. Figs. 6.8(a)-(b) demonstrate the system dynamics during the change of solar irradiation. The solar power generating system transfers half of the normal power when solar insolation reduces to half from normal  $1000\text{W}/\text{m}^2$ . Similarly grid power returns to normal when solar irradiation rises to normal from  $500\text{W}/\text{m}^2$ .

Figs. 6.9 (a)-(b) exhibit the dynamic response of the injected grid current. When the solar irradiation decreases by 50% while the grid voltage remains constant, the grid current settles at 50% of its value at  $1000 \text{ W/m}^2$ . Figs. 6.10(a)-(b) present the harmonics performance, with the voltage total harmonic distortion (THD) measuring 5.53%, and the grid current THD measuring 2.78%. The real-time results obtained from the OPAL-RT simulation validate the performance of the PV system based on third harmonic injection and the nearest level algorithm.



(a)

(b)



(c)

Fig. 6.7. Real-time results-I (a) Constant irradiance of  $1000 \text{ W/m}^2$  (b) Converter Line Voltages (c) Modulating signals

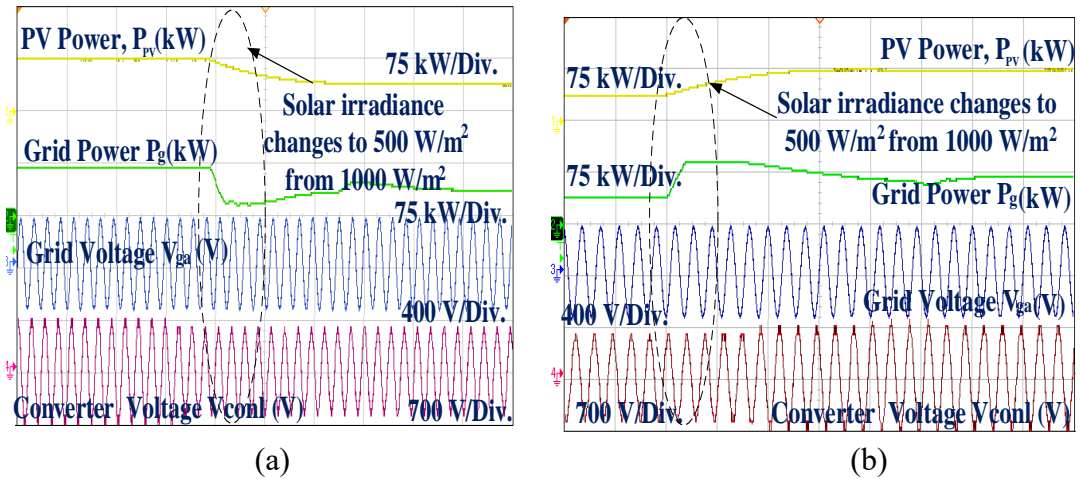


Fig. 6.8. Dynamic results-I (a) Fall in solar power (b) Rise in solar power

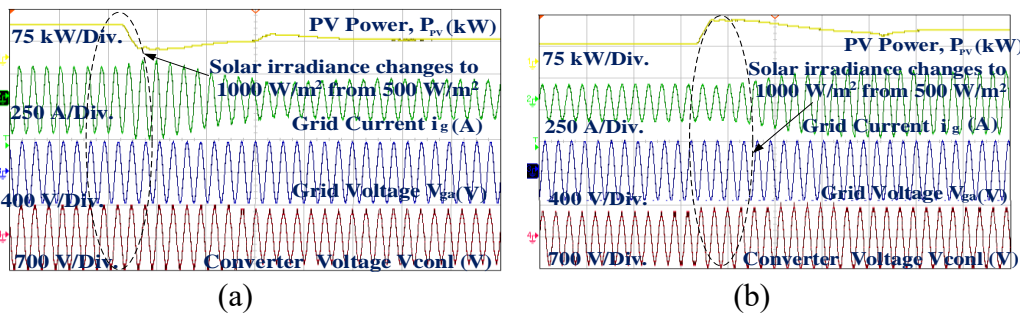


Fig. 6.9. Dynamic results-II (a) Fall in grid current (b) Rise in grid current

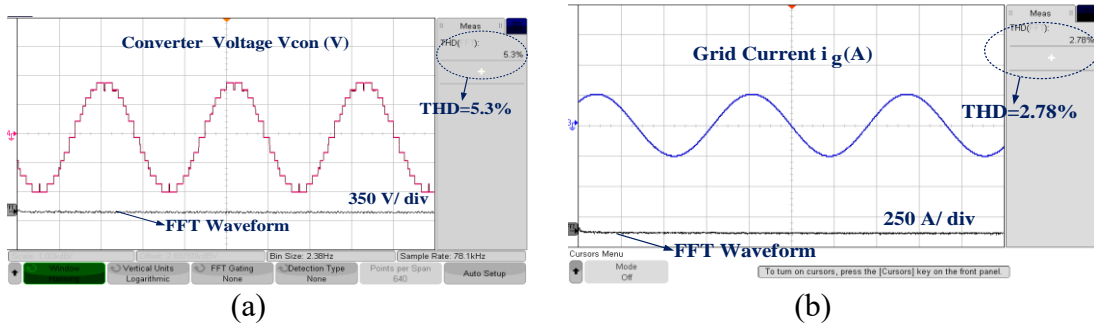


Fig. 6.10. Harmonic analysis (a) Converter voltage (b) Grid Current

## 6.8 CONCLUSIONS

An improved control with 3<sup>rd</sup> harmonic injection and nearest-level PWM is applied for closed loop control of CHB solar PV generating system. Cascaded H-bridge power cells with twelve solar PV arrays have injected the solar PV power to the grid. This work explained the 3<sup>rd</sup> harmonic injection in the modulating signals and performance analysis of harmonics with and without THI. The operational performance results of 3<sup>rd</sup> harmonic injection with nearest level PWM are obtained in the MATLAB platform and verified by the real time execution on RT simulator. This 3<sup>rd</sup> harmonic injected

NLM based feedback-loop controller has shown the excellent response, and grid-power follow the solar PV power during the variation in irradiation. The grid injected current harmonics (THD) are below the IEEE 519 standards of 5% with nearest level PWM. This work has given the improved method for grid integrated solar photovoltaic generating system with harmonics mitigation. The harmonic performance is tested in OPAL-RT test bench with converter line voltage THD of 7.47% and gives a current THD of 2.78%, which is much lower than the permissible limits of 5% as per the IEEE-519 standard.

## **CHAPTER-VII**

### **CONTROL AND DESIGN OF PACKED E-CELL (PEC) ELEVEN LEVEL CONVERTER FOR SOLAR PV GENERATION APPLICATIONS**

#### **7.1 INTRODUCTION**

A novel packed E-Cell (PEC11) converter is introduced, designed specifically for three-phase eleven-level operation. This converter achieves a quintuple voltage ratio (1:5) between the solar photovoltaic arrays. In each phase, the converter comprises of three solar panels, where the highest voltage level is obtained from the top solar panel. The subsequent voltage levels are derived using an algebraic formulation involving the lower two solar panels. The operating modes necessary to obtain each voltage level are explained in detail. The mathematical modelling of the system is presented, incorporating voltage and current equations for the three-phase grid. To feed current into the grid, the PEC11 converter utilizes closed-loop proportional-resonant (PR) controllers. The gating pulses for the PEC converter are generated using the nearest level modulation (NLM) technique. This modulation technique ensures minimal switching losses and enables simple control in grid-tied mode. Performance of the PV generation system is evaluated through simulations conducted on the MATLAB/SIMULINK platform. The power is smoothly delivered to the grid in both steady-state and dynamic conditions. These simulation results are further validated using a real-time simulator (OPAL-RT), confirming the suitability of this converter for solar applications.

#### **7.2 CIRCUIT CONFIGURATION OF PACKED E-CELL (PEC) ELEVEN LEVEL CONVERTER FOR SOLAR PV GENERATION APPLICATIONS**

Fig. 7.1 illustrates a new three-phase solar photovoltaic (SPV) system featuring the PEC11 converter. In this system, each phase incorporates six unidirectional switches and one bidirectional switch. It is supplied power by a primary photovoltaic array,



PV<sub>1a</sub>, and two auxiliary arrays, PV<sub>2a</sub> and PV<sub>3a</sub>, which act as additional DC sources for phase ‘a’. The voltage of first PV array PV<sub>1</sub> (370V) is five times higher than the voltage of PV<sub>2-3</sub> (74V). Each PV array is equipped with a power point tracker to ensure optimal power generation. A harmonic mitigation R-L filter is connected between the converter output and the power grid. Table 7.1 provides an overview of the switching states and operational modes required to generate all the voltage levels in the system.

The voltage output equation for positive half cycle of phase ‘a’ is expressed as,

$$v_{aO} = \begin{pmatrix} V_{PV1} = +5V_{PV} \\ V_{PV1} - V_{PV3} = +4V_{PV} \\ V_{PV1} - V_{PV2} - V_{PV3} = +3V_{PV} \\ V_{PV2} + V_{PV3} = +2V_{PV} \\ V_{PV2} = +V_{PV} \end{pmatrix} \quad (7.1)$$

Similarly negative half cycle is represented as,

$$v_{aO} = \begin{pmatrix} -V_{PV1} = -5V_{PV} \\ -V_{PV1} + V_{PV3} = -4V_{PV} \\ -V_{PV1} + V_{PV2} + V_{PV3} = -3V_{PV} \\ -V_{PV2} - V_{PV3} = +2V_{PV} \\ -V_{PV2} = -V_{PV} \end{pmatrix} \quad (7.2)$$

Grid voltage KVL expression is presented as,

$$v_{abc} = R i_{abc} + L \frac{di_{abc}}{dt} + v_{gabc} \quad (7.3)$$

Figs. 7.2 and 7.3 illustrate the various modes of operation for the PEC11 converter.

Fig. 7.2 focuses on the positive half cycle of the eleven-level converter output voltage.

In Fig. 7.2(a), the peak step of +5V<sub>PV</sub> is achieved by activating switches S<sub>1a</sub>, S<sub>5a</sub>, and S<sub>6a</sub>, connecting the main solar panel PV<sub>1a</sub> to the converter output. Fig. 7.2(b) demonstrates the +4V<sub>PV</sub> step by turning on switches S<sub>1a</sub>, S<sub>5a</sub>, S<sub>7a</sub>, and S<sub>8a</sub>. This combination opposes PV<sub>3a</sub> to PV<sub>1a</sub>, resulting in an output voltage of +4V<sub>PV</sub> (+5V<sub>PV</sub> - V<sub>PV</sub>). Fig. 7.2(c) showcases level +3V<sub>PV</sub> obtained by activating switches S<sub>1a</sub>, S<sub>4a</sub>, and



Table 7.1 Switching states of PEC11

Switching and Levels								
S <sub>1a</sub>	S <sub>2a</sub>	S <sub>3a</sub>	S <sub>4a</sub>	S <sub>5a</sub>	S <sub>6a</sub>	S <sub>7a</sub>	S <sub>8a</sub>	V <sub>out</sub> (V)
1	0	0	0	1	1	0	0	+5V <sub>PV</sub>
1	0	0	0	1	0	1	1	+4V <sub>PV</sub>
1	0	0	1	1	0	0	0	+3 V <sub>PV</sub>
1	1	0	0	0	1	0	0	+2 V <sub>PV</sub>
1	1	0	0	0	0	1	1	+ V <sub>PV</sub>
1	1	1	0	0	0	0	0	0
0	0	0	1	1	1	0	0	0
0	0	0	1	1	0	1	1	- V <sub>PV</sub>
0	0	1	1	1	0	0	0	-2 V <sub>PV</sub>
0	1	0	1	0	1	0	0	-3 V <sub>PV</sub>
0	0	1	1	0	0	1	1	-4 V <sub>PV</sub>
0	1	1	1	0	0	0	0	-5 V <sub>PV</sub>

obtained by connecting the negative terminal of PV<sub>1a</sub> to the converter output through switch S<sub>4a</sub>, while PV<sub>2a</sub> and PV<sub>3a</sub> are connected in series opposing PV<sub>1a</sub>, resulting in a net converter voltage of -3V<sub>PV</sub>. Fig. 7.3(e) showcases the -4V<sub>PV</sub> level achieved by connecting PV<sub>1a</sub> and PV<sub>2a</sub> in series through switches S<sub>2a</sub>, S<sub>4a</sub>, S<sub>7a</sub>, and S<sub>8a</sub>. Finally, the -5V<sub>PV</sub> level is shown in Fig. 7.3(f), obtained by connecting PV<sub>1a</sub> through switches S<sub>2a</sub>, S<sub>3a</sub>, and S<sub>4a</sub>. These figures provide a comprehensive visualization of various voltage levels generated by the PEC11 converter during both the positive and negative cycles.

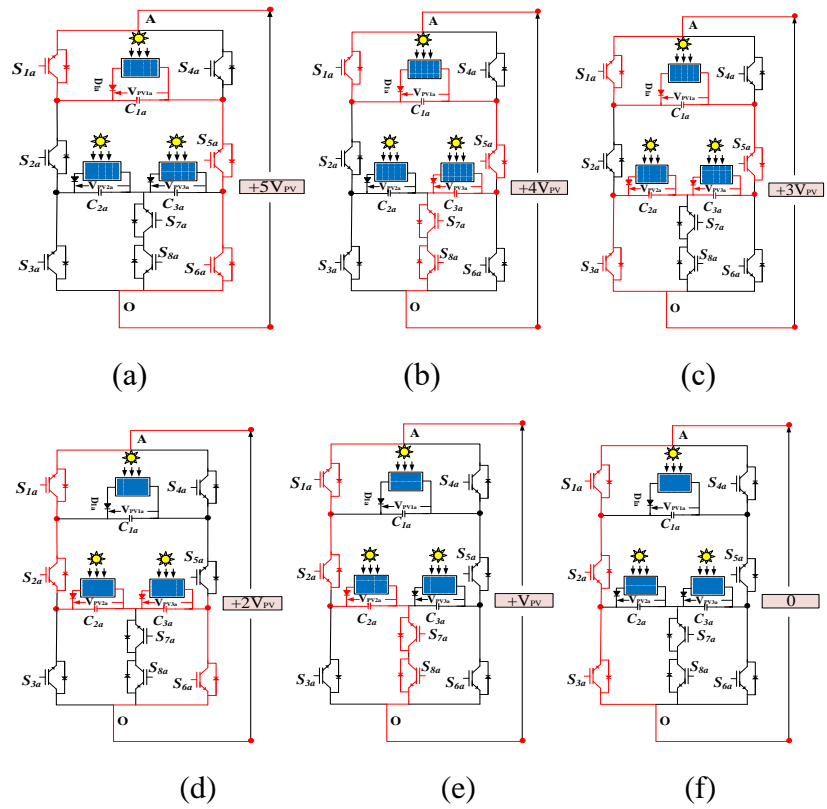


Fig. 7.2. Positive cycle operating path

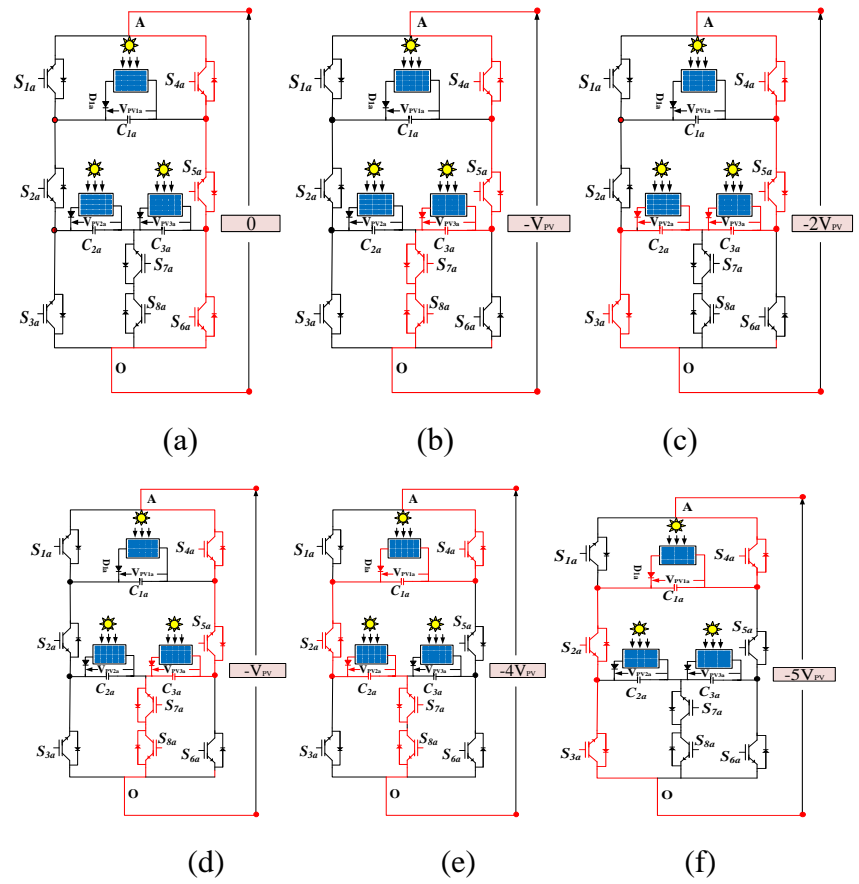


Fig. 7.3. Negative cycle operating path

Table 7.2 System parameters of PEC11

S.N.	Parameter	Value
1	VMPP (V)	37.01
2	IMPP (A)	7.47
3	No. of series modules in main	10
4	No. of series modules in	2
5	No. of parallel modules in all	10
6	Grid voltage (V)	415
7	Labc of harmonic filter (mH)	2.0
8	Kp, Ki (AC side control)	0.002,0.0015
9	Kp, Ki (DC side control)	2.1, 0.35

### 7.3 CONTROL STRATEGY OF PACKED E-CELL (PEC) ELEVEN LEVEL CONVERTER FOR SOLAR PV GENERATION APPLICATIONS

The control structure of PEC11 includes the DC-link voltage control, power control, and NLM. Fig. 7.4 illustrates the complete scheme. Each solar panel's MPPT controller utilizes the perturb and observe (P&O) method to generate a reference voltage. These reference voltages, namely  $V_{REF1a}$ ,  $V_{REF2a}$ , and  $V_{REF3a}$  for  $PV_{1a}$ ,  $PV_{2a}$ , and  $PV_{3a}$  respectively, are then compared with the measured voltages  $V_{C1a}$ ,  $V_{C2a}$ , and  $V_{C3a}$  in phase 'a' to determine the reference currents. Likewise, the DC-link voltages of phases 'b' and 'c' are compared with their respective charge controllers' reference

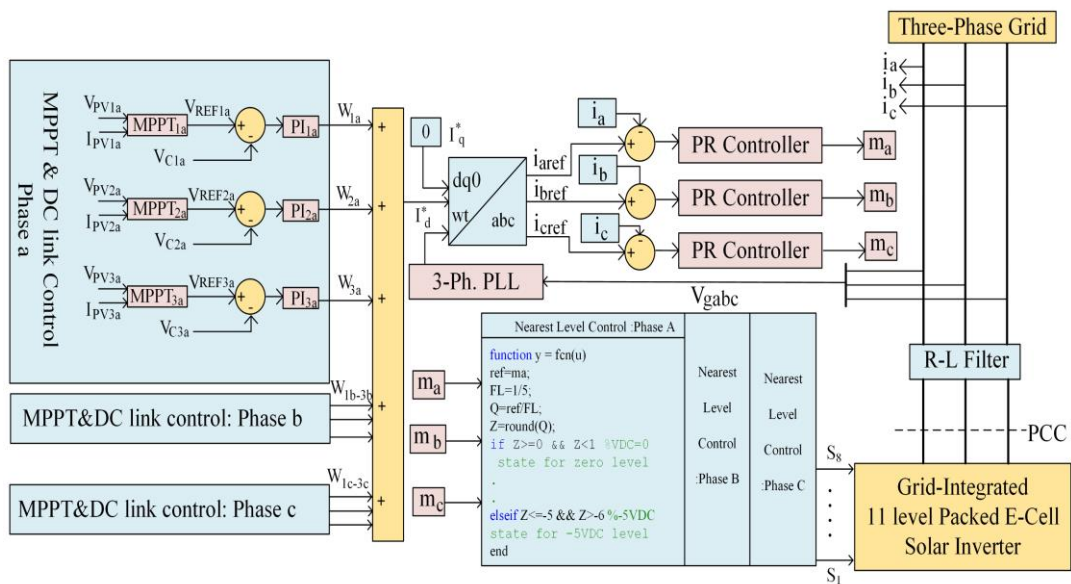


Fig. 7.4. Control structure of PEC11.

voltages. To minimize the discrepancy between the reference and actual DC-link voltages, PI controllers are employed. Mathematically, a PI controller to regulate error, is presented as,

$$W_{1a}(k+1) = W_{1a}(k) + k_{p(PV1a)}\{e_{PV1a}(k+1) - e_{PV1a}(k)\} + k_{i(PV1a)}e_{PV1a}(k+1) \quad (7.4)$$

Here  $e_{PV1a}$ ,  $k_{p(PV1a)}$  and  $k_{i(PV1a)}$  are error, proportional gain and integral gain controller  $PI_{1a}$  of main solar PV array of phase 'a'

Reference d-axis current of all the solar arrays are added and total reference current  $I_d^*$  is given as,

$$I_d^* = \sum_{k=1}^n W_{ka} + \sum_{k=1}^n W_{kb} + \sum_{k=1}^n W_{kc} \quad (7.5)$$

In the system, where "n" represents the number of solar panels in each phase, the total current " $I_d$ " is decomposed using the dq-abc transformation. This transformation yields three reference phase currents, namely " $i_{aref}$ ," " $i_{bref}$ ," and " $i_{cref}$ ." The reference quadrature axis current, " $I_q$ ," is maintained at zero to only supply active power to the grid. Furthermore, a phase-locked loop (PLL) is employed to synchronize the phase of the grid voltage with the converter voltage. To compare the grid currents " $i_a$ ," " $i_b$ ," and " $i_c$ " with the reference values, proportional-resonant (PR) controllers are utilized. These controllers modulate the signals " $m_a$ ," " $m_b$ ," and " $m_c$ ." The ideal mathematical representation of the PR controllers is as follows:

$$F(s) = K_p + K_i \frac{s}{s^2 + (2\pi f_0)^2} \quad (7.6)$$

While practical PR controller with damping is represented as,

$$G_{PR}(s) = K_p + K_i \frac{4\pi f_c s}{s^2 + 4\pi f_c s + (2\pi f_0)^2} \quad (7.7)$$

Where  $K_p$  and  $K_i$  are control inputs,  $f_0$  is system frequency and  $f_c$  is bandwidth.

The implementation of the carrier-less nearest level modulation (NLM) technique is

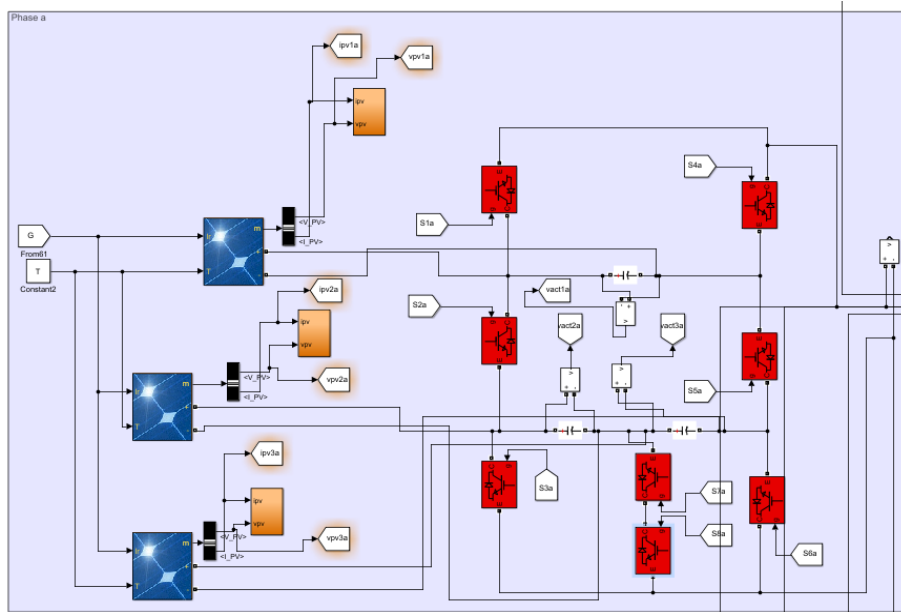
utilized to generate the switching pulses for the inverter. Fig. 7.4 illustrates the code for each phase. The reference signal "m<sub>abc</sub>" is divided into five levels in the positive half, denoted as "FL." A quotient (Q) is calculated by dividing "m<sub>a</sub>" by "FL," which effectively divides the running reference waveform. In the positive half, the reference waveform varies from 0 to 1, while in the negative half, it varies from 0 to -1. Since the value of "FL" is 1/5, the value of "Q" ranges from 0 to 5 for the positive half and 0 to -5 for the negative half. To obtain discrete values, the value of "Q" is rounded off, resulting in five integer values for each half, denoted as "Z." Five levels in each half cycle are generated from Z as,

$$v_{aO} = \begin{cases} 0, & \text{for } 0 \leq Z < 1 \\ +V_{PV} & \text{for } 1 \leq Z < 2 \\ +2V_{PV} & \text{for } 2 \leq Z < 3 \\ +3V_{PV} & \text{for } 3 \leq Z < 4 \\ +4V_{PV} & \text{for } 4 \leq Z < 5 \\ +5V_{PV} & \text{for } 5 \leq Z < 6 \end{cases} \quad (7.8)$$

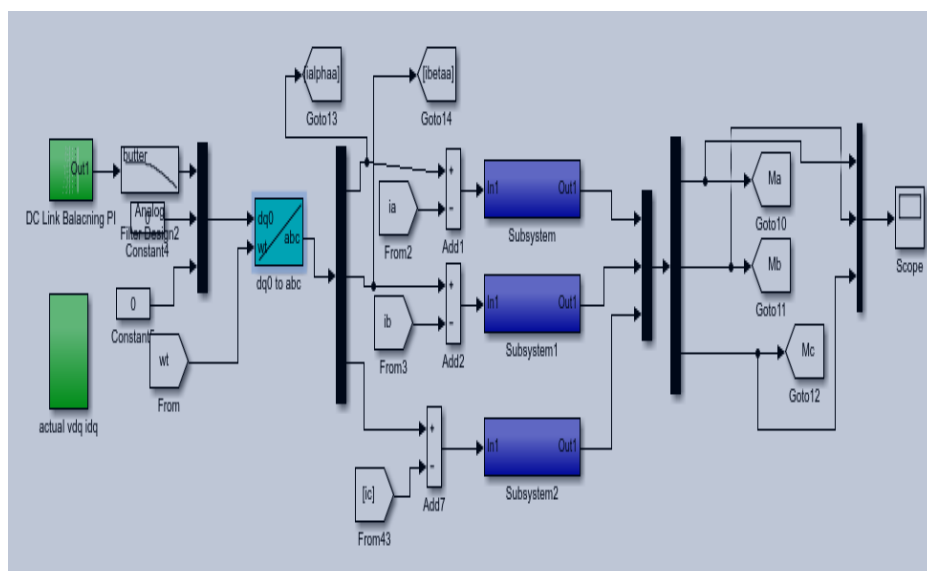
The quintuple operation is maintained in between the reference output voltages of the MPPT controller blocks. The proper tracking of actual voltages with the reference provides a perfect eleven level generation. Similarly, each phase controls the power keeping the quintuple progression.

#### **7.4 MATLAB MODEL OF PACKED E-CELL (PEC) ELEVEN LEVEL CONVERTER FOR SOLAR PV GENERATION APPLICATIONS**

Fig. 7.5(a) shows the developed MATLAB model of power circuit of the eleven level PEC converter. Each phase consists of three solar arrays and eight switches. The power circuit is formed by the two merged H-bridge power cells with six switches and two switches act as a bi-directional switch and converter has solar arrays as DC source in each cell. Phase 'B' & 'C' are formed similar to Phase 'A'. Three phases of converter are connected in the star and are fed to R-L harmonic filter. The measurement of three phase voltage and current is taken.



(a)



(b)

Fig.7.5. MATLAB models of (a) power circuit (b) control circuit

Fig. 7.5 (b) shows the control scheme implementation of this converter. The DC link control consists of comparison of average of all reference and actual capacitor voltages to generate the reference current. Reference current are then transformed to equivalent AC currents and compared with grid current and PR controllers are employed to track and modulating signals are generated.



## 7.5 SIMULATED RESULTS OF OF PACKED E-CELL (PEC) ELEVEN LEVEL CONVERTER FOR SOLAR PV GENERATION APPLICATIONS

The PEC11 converter operates in a grid-solar integrated mode, and its performance is simulated. The system is subjected to a solar irradiation of  $1000\text{W}/\text{m}^2$  using the NLM technique. Various parameters are measured and monitored under steady-state conditions, including converter voltage (line and phase), active and reactive powers transferred by the converter, and the grid voltage and the current. These results are depicted in Fig. 7.6(a). The converter's phase voltage ( $V_{\text{comp}}$ ) and line voltage ( $V_{\text{conl}}$ ) are maintained at their designated values, with eleven levels of  $V_{\text{comp}}$ . The active power transferred to the grid amounts to 36.50 kW, achieving a remarkable 97% efficiency with no reactive power transfer. The grid current is injected at a voltage of 415V and an RMS value of 50.5 A. Performance of the PEC11 converter is then analyzed under varying solar irradiation conditions. Fig. 7.6(b) illustrates the dynamic response when the solar irradiation increases from  $500\text{W}/\text{m}^2$  to  $1000\text{W}/\text{m}^2$ . The solar power doubles to 36.5 kW, resulting in the grid current also doubling to 25.25A (RMS)

The converter voltages,  $V_{\text{comp}}$  and  $V_{\text{conl}}$ , remain unchanged. Fig. 7.7(a) showcases the dynamic response when the solar irradiation decreases from  $1000\text{W}/\text{m}^2$  to  $500\text{W}/\text{m}^2$ . The injected power decreases to half its value corresponding to  $1000\text{W}/\text{m}^2$ , while the converter phase voltages ( $V_{\text{comp}}$ ) maintain the voltage profile of eleven levels. The PEC11 converter is also evaluated for its harmonic response, and the results are presented in Fig. 7.7(b). The current total harmonic distortion (THD) shown in the top section is 2.92%, which falls below the 5% limit established by the IEEE-519 standard. The peak value of the fundamental grid current is 71.4 A. The bottom section of Fig. 7.7(b) displays the line voltage THD, which amounts to 7.96%, with a fundamental voltage of 370V. This converter proposes new voltage ratios (5:1:1) to achieve successful power conversion.

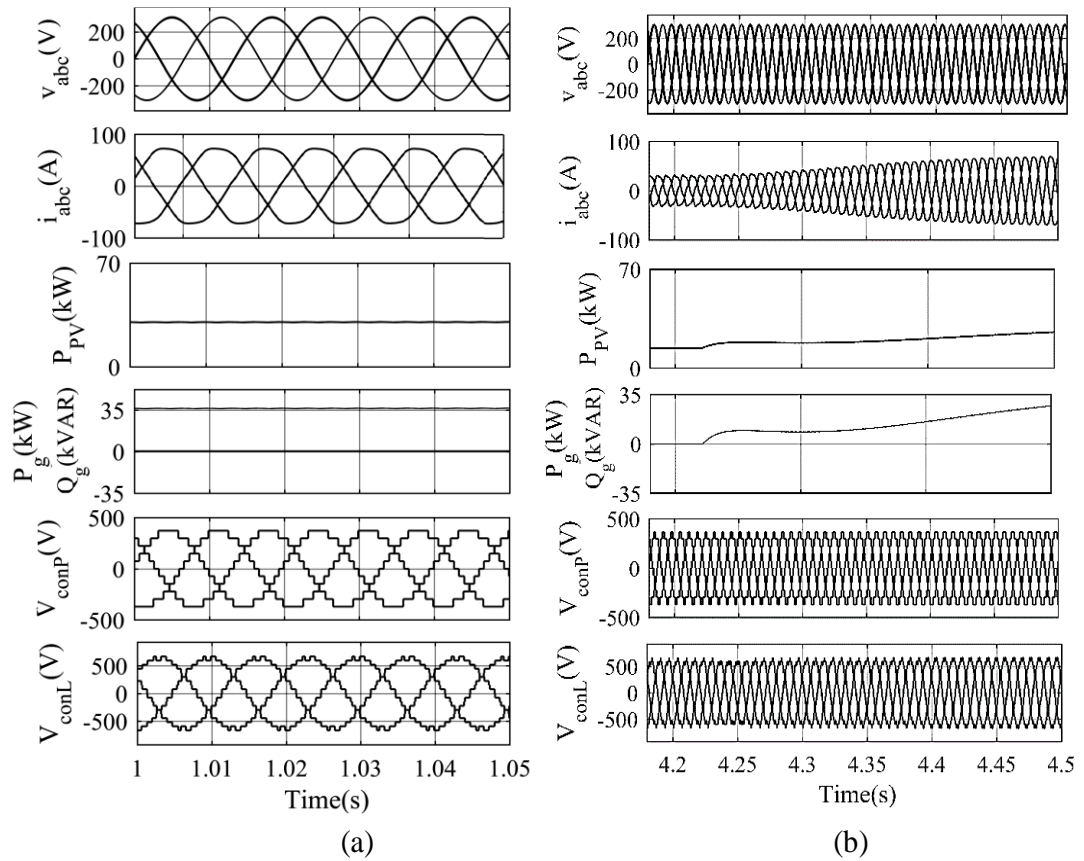


Fig. 7.6. Simulation results set I (a) Steady-state response of PEC11 (b) Dynamic response of PEC11 during the rise of irradiation.

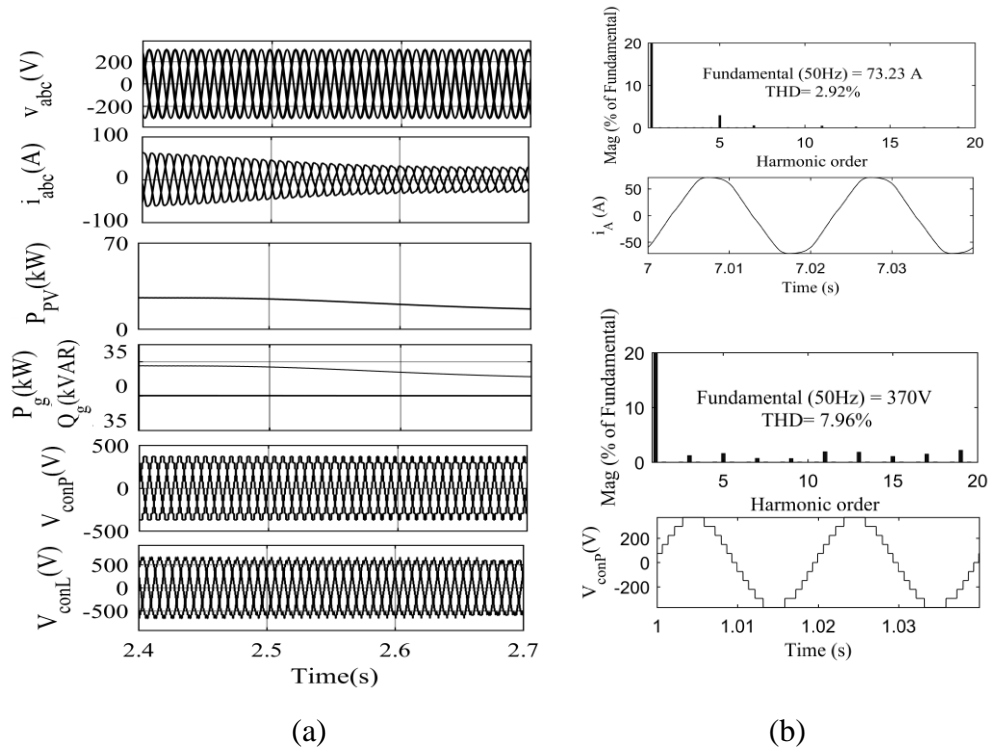
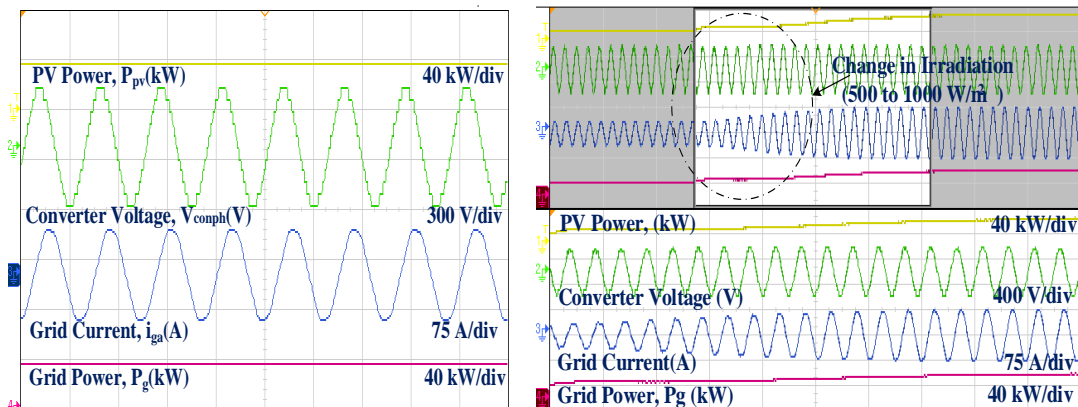


Fig. 7.7. Simulation results set II (a) Dynamic response of PEC11 during irradiation fall. (b) Grid current and converter voltage THD

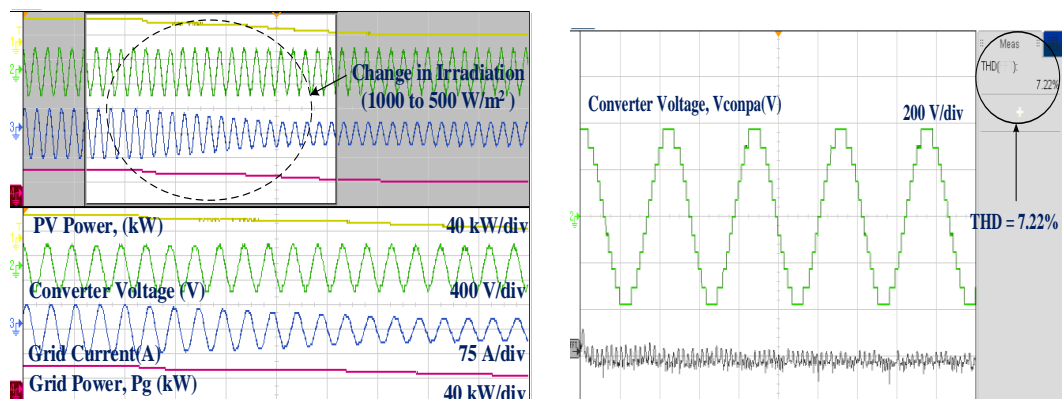
## 7.6 REAL-TIME EXECUTION OF PACKED E-CELL (PEC) ELEVEN LEVEL CONVERTER FOR SOLAR PV GENERATION APPLICATIONS

To validate its performance, the solar-powered PEC11 converter is tested in real-time using the OPAL-RT simulator. Fig. 7.8(a) illustrates the steady response obtained under a solar irradiation of  $1000 \text{ W/m}^2$ . The dynamic responses, corresponding to an increase in solar power from  $500 \text{ W/m}^2$  to  $1000 \text{ W/m}^2$ , are depicted in Fig. 7.8(b). Similarly, the real-time system dynamics when solar power decreases from  $1000 \text{ W/m}^2$  to  $500 \text{ W/m}^2$  are shown in Fig. 7.8(c). These real-time results serve to validate the MATLAB/SIMULINK outcomes, affirming the excellent performance of the PEC11 converter. The harmonic response of the converter voltage and injected current is displayed in Fig. 7.8(d), showcasing THD values of 7.22% and 3.014% for voltage and current, respectively.



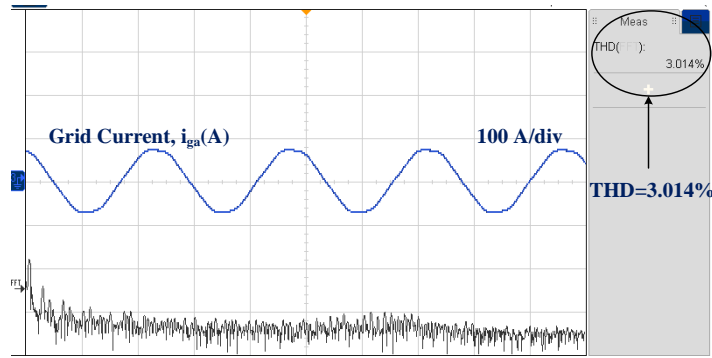
(a)

(b)



(c)

(d)



(e)

Fig. 7.8. PEC11 response in Real-time simulator; (a) Steady state, (b) Rise in irradiation, (c), Fall in irradiation, (d) THD in real-time simulator, Voltage harmonic distortion and (e) Current harmonic distortion

## 7.7 CONCLUSION

A new 11-level PEC (Power Electronic Converter) based solar PV system has been developed by selecting a quintuple voltage ratio for the voltage sources. The number of switches and PV arrays remains the same as in a PEC9 system. The converter voltage is represented using relevant equations. The switching states of the converter are organized in a table, and the operating modes for each state are explained through PEC11 diagrams. To regulate grid currents, PR (Proportional-Resonant) controllers are employed, and the governing mathematical equations are provided. The complete control scheme, including the DC-link voltage of the top and bottom PV arrays, resonant current controllers, and the NLM (Nearest Level Modulation) code, is presented for the PEC11 system. Simulated results showcasing the DC and AC side performance of the PEC11 system under steady and varying solar conditions are demonstrated. The harmonic performance, determined by using FFT (Fast Fourier Transform), is presented in the results. Performance of the new PEC11 system is verified using real-time OPAL-RT simulation, which offers an improved solution for solar PV generation-grid integrated systems. The harmonic performance (THD) is determined by FFT with converter phase voltage THD as 7.22% and grid current THD as 3.014%.

## CHAPTER-VIII

### CONTROL AND REAL-TIME EXECUTION OF LADDER TYPE THIRTEEN LEVEL CONVERTER FOR SOLAR PV GENERATION APPLICATIONS

#### 8.1 INTRODUCTION

In this work, practical implementation of a grid-tied solar photovoltaic (PV) generation system utilizing a thirteen-level inverter is explored. This system introduces a ladder-type topology that effectively addresses common issues such as harmonica distortion and low power quality. The term "ladder" refers to the series connection of PVarray fed converter cells arranged in a staircase-like manner. Each phase of the system consists of six cells, with an H-bridge module employed to change the converter voltage polarity. Unlike the conventional Cascaded H-bridge (CHB) approach that requires twenty-four switches for thirteen-level operation, the proposed system achieves the same functionality with only fifteen switches. To evaluate its performance, the system is analyzed under varying solar irradiation conditions and to conduct simulations to validate its effectiveness. The results obtained demonstrate that thirteen-level inverter-based system significantly reduces total harmonics distortion and voltage imbalance, thereby improving the overall power quality of the grid-tied solar PV generation system. These findings indicate that the proposed system holds considerable potential for widespread application in the renewable energy sector, making a significant contribution towards the realization of a more sustainable future.

#### 8.2 CIRCUIT CONFIGURATION OF LADDER TYPE THIRTEEN LEVEL CONVERTER FOR SOLAR PV GENERATION APPLICATIONS

Fig. 8.1 illustrates the solar ladder converter system, utilizing fifteen switches and six identical solar arrays per phase. In the ladder structure of phase 'a', there are eleven switches ( $T_{1a}$ - $T_{11a}$ ), and the phase inversion module employs four switches ( $T_{HB1a}$ -

$T_{HB4a}$ ). Among the switches,  $T_{1a}$ ,  $T_{4a}$ ,  $T_{7a}$ , and  $T_{10a}$  serve as bypass switches (BS), while  $T_{2a}$ ,  $T_{5a}$ ,  $T_{8a}$ , and  $T_{11a}$  act as series connecting switches (SCS). The BS is responsible for bypassing the solar PV array voltage, while the SCS connects the solar PV arrays in series. The converter voltage polarity depends on the state of the switches. When

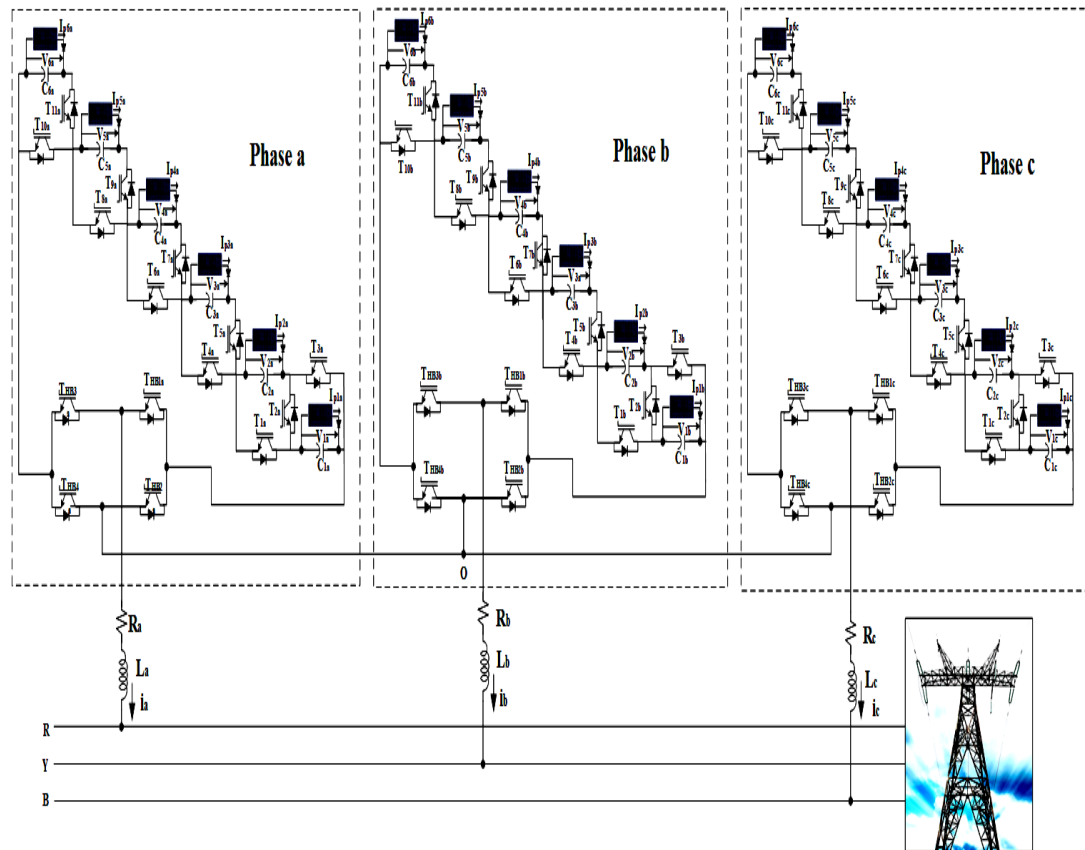


Fig. 8.1. Ladder type thirteen level solar PV System.

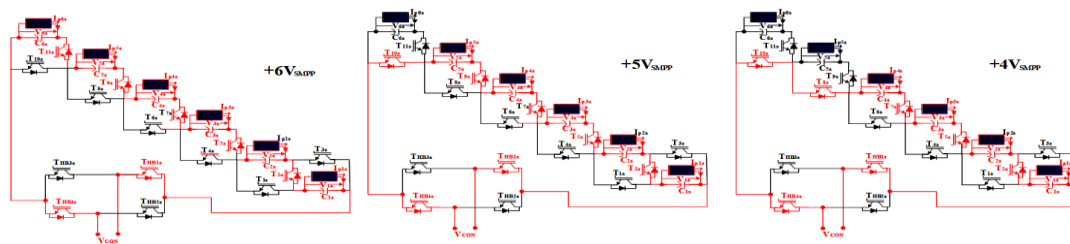


Fig. 8.2. Operating modes of six, five and four level

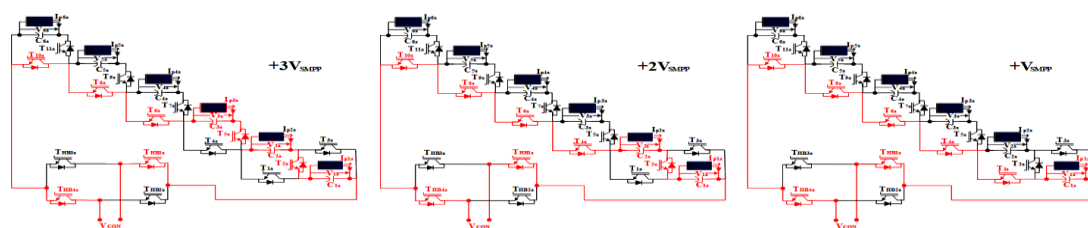


Fig. 8.3. Operating modes of three, two, and one level

$T_{HB1a}$  and  $T_{HB4a}$  conduct, the converter voltage is positive, and when  $T_{HB2a}$  and  $T_{HB3a}$  are in the ON state, the converter voltage is negative. The generation of positive peak, negative peak, and zero voltage steps are explained as follows. The peak step of the converter occurs when all SCS switches are turned ON, connecting all the solar arrays in series. If  $V_{SMPP}$  represents the voltage of each solar array at the maximum power point, the peak voltage step of the converter output voltage of phase 'a',  $V_{con}$ , can be expressed as shown in equation (8.1).

$$V_{con} = V_{a1} + V_{a2} + V_{a3} + V_{a4} + V_{a5} + V_{a6} \quad (8.1)$$

This converter voltage,  $V_{con}$ , is positive when the phase inversion switches  $T_{HB1}$  and  $T_{HB4}$  are turned ON, and negative when  $T_{HB2}$  and  $T_{HB3}$  are closed. The zero voltage step is achieved by bypassing all the solar sources. Switching ON all BS switches bypasses the last five solar arrays of the ladder, while the first solar array is bypassed by closing the first SCS switch  $T_{2a}$  and the bypass switch of the first solar panel  $T_{3a}$ . Fig. 8.2-8.3 demonstrate the generation of the remaining converter voltage profiles for the positive cycle. Table 8.1 provides the corresponding switch positions for each step. Each voltage step involves the activation of five switches, except for the zero converter voltage, which requires the conduction of seven switches. To achieve the fifth voltage level, the last or sixth solar array is disconnected by opening  $T_{11a}$  and closing  $T_{10a}$ , as depicted in Fig. 8.2(a). Fig. 8.2(b) illustrates the attainment of the fourth level by removing the fifth array, achieved by switching OFF its SCS  $T_{9a}$  and turning ON the BS  $T_{8a}$ . Similarly, Fig. 8.2(c) demonstrates the fourth level. The third, second, and first levels are explained in Figs. 8.3(a-c). The negative voltage levels of the converter are realized by changing the phase inversion switches from  $T_{HB1a}$  and  $T_{HB4a}$  to  $T_{HB2a}$  and  $T_{HB3a}$  for each level. Table 8.2 shows the system parameters of the converter.

Table 8.1 Switching modes of ladder converter

Level	T <sub>1</sub>	T <sub>2</sub>	T <sub>3</sub>	T <sub>4</sub>	T <sub>5</sub>	T <sub>6</sub>	T <sub>7</sub>	T <sub>8</sub>	T <sub>9</sub>	T <sub>10</sub>	T <sub>11</sub>	T <sub>HB1</sub>	T <sub>HB2</sub>	T <sub>HB3</sub>	T <sub>HB4</sub>
+6		ON			ON		ON		ON		ON	ON			ON
+5		ON			ON		ON		ON	ON		ON			ON
+4		ON			ON		ON	ON		ON		ON			ON
+3		ON			ON	ON		ON		ON		ON			ON
+2		ON		ON		ON		ON		ON		ON			ON
+1	ON			ON		ON		ON		ON		ON			ON
0	ON	ON	ON	ON		ON		ON		ON			ON		ON
-1	ON			ON		ON		ON		ON			ON	ON	
-2		ON		ON		ON		ON		ON			ON	ON	
-3		ON			ON	ON		ON		ON			ON	ON	
-4		ON			ON		ON	ON		ON			ON	ON	
-5		ON			ON		ON		ON	ON			ON	ON	
-6		ON			ON		ON		ON		ON		ON	ON	

Table 8.2 Parameters for ladder type solar multilevel converter

S.N.	Parameter	Value
1	V (Max power point)	47.76V
2	I (Max power point)	8.23A
3	N <sub>S</sub> (series connected solar modules)	11
4	N <sub>P</sub> (parallel connected solar modules)	5
5	C (DC link)	700 μF
6	V(Grid Voltage)	3.3 kV
8	L (harmonic filter)	20.0 mH
9	AC side PR controllers' K <sub>pac</sub> , K <sub>iac</sub>	0.0017,0.0005
10	DC side PI controllers' K <sub>pdc</sub> , K <sub>idc</sub>	0.5, 0.035



### 8.3 CONTROL STRATEGY OF LADDER TYPE THIRTEEN LEVEL CONVERTER FOR SOLAR PV GENERATION APPLICATIONS

Fig. 8.4 depicts the control of proposed system, consisting of two control blocks. The first block, shown in Fig. 8.4(a), regulates the DC-link voltage. Each solar module's voltage is optimized using an MPPT controller, which calculates the maximum power extraction from the solar module's voltage ( $V_{PV}$ ) and current ( $I_{PV}$ ). Individual proportional-integral (PI) controllers are employed to maintain the maximum power point voltage of all solar panels at the DC link. The DC-link voltage of all solar modules is summed to obtain the reference DC current  $I_{d(ref)}$ . The second control block converts the DC-side current ( $I_{d(ref)}$ ) into reference AC-side currents ( $i_{a-ref}$ ,  $i_{b-ref}$ , and  $i_{c-ref}$ ). A phase-locked loop (PLL) is utilized to synchronize the utility grid and the converter. The PLL ensures precise and rapid detection of the grid phase angle ( $\omega t$ ) for generating the converter reference signal. The AC reference phase currents are compared with the actual grid currents ( $i_{ga}$ ,  $i_{gb}$ , and  $i_{gc}$ ), and difference between the two is minimized by proportional-resonant (PR) controllers ( $PR_a$ ,  $PR_b$ , and  $PR_c$ ) in the 'a', 'b', and 'c' phases, respectively. PR controllers are preferred for AC-side control as they offer a faster tracking response compared to PI controllers. The modulating signals ( $M_a$ ,  $M_b$ , and  $M_c$ ) for phase 'a', 'b', and 'c', respectively, are generated from the PR controllers. The transfer function of the PR controller for phase 'a' is expressed.

$$H_{PRa}(s) = \frac{M_a(s)}{I_{PR(e_a)}} = (K_{PR})_{pea} + (K_{PR})_{kea} \left( \frac{s}{s^2 + 2W_\sigma s + W_n^2} \right) \quad (8.2)$$

$$I_{PR(e_a)} = i_{a-ref} - i_a \quad (8.3)$$

Here  $I_{PR(e_a)}$  error current signal,  $w_n$  is resonant frequency,  $\omega\sigma$  is corner frequency,  $(K_{PR})_{pea}$  &  $(K_{PR})_{kea}$  are control parameters. Hence the modulating signal of phase 'a' is given as,

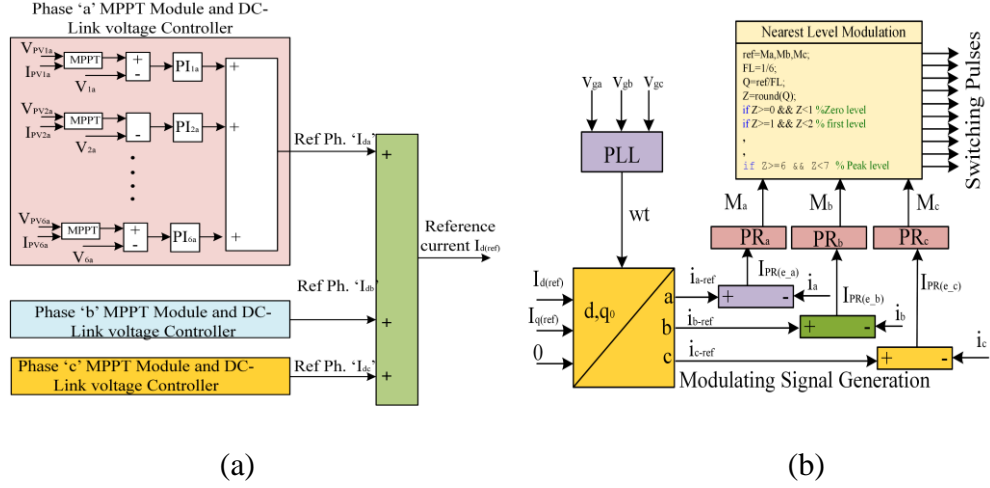


Fig 8.4. The Control Scheme (a) DC side control (b) AC side NLM-PR controller.

$$M_a(s) = I_{PR(e_a)} \left\{ (K_{PR})_{pea} + (K_{PR})_{kea} \left( \frac{s}{s^2 + 2w_\sigma s + w_n^2} \right) \right\} \quad (8.4)$$

$$H_{PRb}(s) = \frac{M_b(s)}{I_{PR(e_b)}} = (K_{PR})_{peb} + (K_{PR})_{keb} \left( \frac{s}{s^2 + 2w_\sigma s + w_n^2} \right) \quad (8.5)$$

$$I_{PR(e_b)} = i_{b-ref} - i_b \quad (8.6)$$

Modulating signal of phase 'b' is given as,

$$M_b(s) = I_{PR(e_b)} \left\{ (K_{PR})_{peb} + (K_{PR})_{keb} \left( \frac{s}{s^2 + 2w_\sigma s + w_n^2} \right) \right\} \quad (8.7)$$

Transfer function of phase 'c' is given as,

$$H_{PRc}(s) = \frac{M_c(s)}{I_{PR(e_c)}} = (K_{PR})_{pec} + (K_{PR})_{kec} \left( \frac{s}{s^2 + 2w_\sigma s + w_n^2} \right) \quad (8.8)$$

$$I_{PR(e_c)} = i_{c-ref} - i_c \quad (8.9)$$

And modulating signal of phase 'c' is given as,

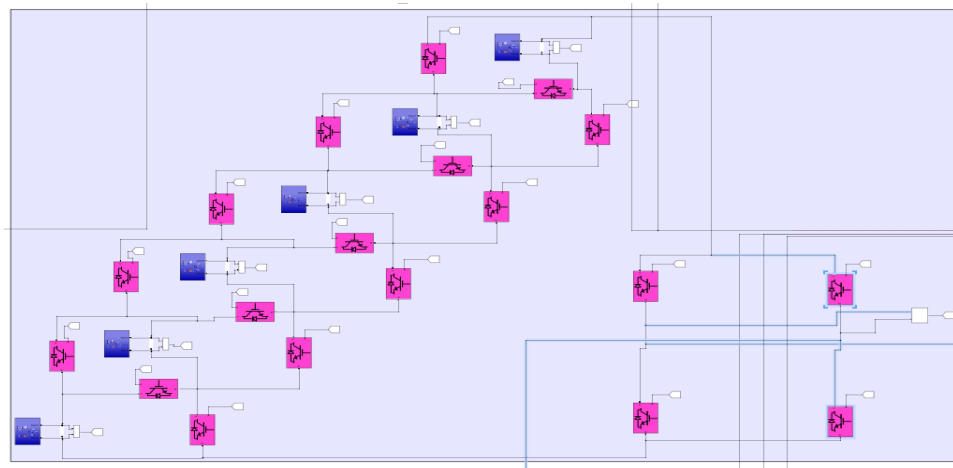
$$M_c(s) = I_{PR(e_c)} \left\{ (K_{PR})_{pec} + (K_{PR})_{kec} \left( \frac{s}{s^2 + 2w_\sigma s + w_n^2} \right) \right\} \quad (8.10)$$

Fundamental frequency switching nearest level modulation (NLM) is applied for converter switching pulse generation and  $M_a$ ,  $M_b$  and  $M_c$  are references for the NLM algorithm. The implementation of the NLM algorithm is shown in Fig. 8.4(b). The NLM function is executed by the following steps.

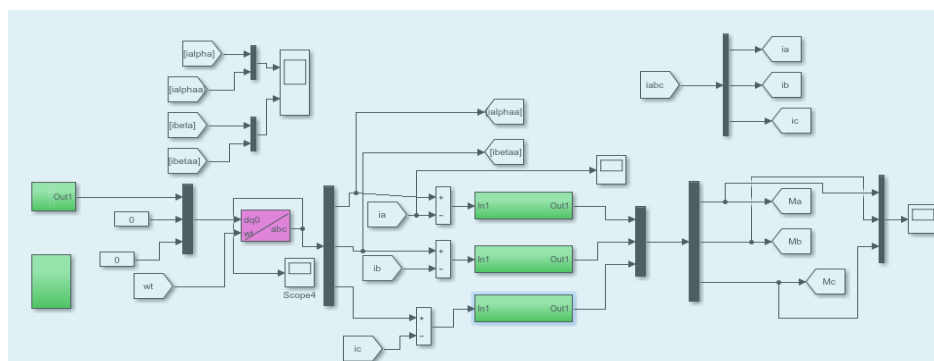
- (i) The FL is set as  $1/6$  as there are six levels in each half of the cycle.
- (ii)  $Q = \text{Ref}/\text{FL}$  where ref is  $M_a$ ,  $M_b$  and  $M_c$  for phase 'a' 'b' and 'c', respectively.
- (iii)  $Z = \text{round}(Q)$  and value of  $Z$  determines the level.
- (iv) For  $0 \leq Z < 1$  the switches T1-T4 ,T6, T8, T10, THB2, THB4 are turned ON for zero converter voltage as shown in Table 8.1.
- (v) For  $1 \leq Z < 2$  the switches T1,T4 ,T6, T8, T10, THB1, THB4 are turned ON for  $V_{a1}$  first level converter voltage as shown in Table 8.1.
- (vi) Value of  $Z$  goes up to seven for positive half of modulating signals, second, third, fourth, fifth and sixth levels are generated when  $2 \leq Z < 3$ ,  $3 \leq Z < 4$ ,  $4 \leq Z < 5$ ,  $5 \leq Z < 6$  and  $6 \leq Z < 7$ , respectively by turning ON switches for corresponding level as shown in Table 8.1.
- (vii) Similarly,  $Z$  varies zero to negative seven for the negative half of modulating signal and six negative levels are formed for values of  $Z$  from zero to negative seven.

#### **8.4 MATLAB MODEL OF LADDER TYPE THIRTEEN LEVEL CONVERTER FOR SOLAR PV GENERATION APPLICATIONS**

Fig. 8.5(a) shows the developed MATLAB model of power circuit of the thirteen level PEC converter. Each phase consists of six solar arrays and nineteen switches. The power circuit is formed by the switching, which either connect the solar array in series or bypass it. Phase 'B' & 'C' are formed similar to Phase 'A'. Three phases of converter are connected in the star and are fed to R-L harmonic filter. The measurement of three phase voltage and current is taken before feeding the power to the grid.



(a)



(b)

Fig. 8.5. MATLAB models of (a) power circuit (b) control circuit

Fig. 8.5 (b) shows the control scheme implementation of this converter. The DC link voltage is converted to the equivalent AC values which are then compared with AC current of grid and PR controller are used to minimize the error signal.

### 8.5 SIMULATED RESULTS OF LADDER TYPE THIRTEEN LEVEL CONVERTER FOR SOLAR PV GENERATION APPLICATIONS

The performance of proposed solar photovoltaic generating system is assessed in both steady-state and transient conditions. Various parameters are monitored, including grid voltages ( $v_{gabc}$ ), grid currents ( $i_{abc}$ ), solar photovoltaic power ( $P_{PV}$ ), active power transferred to the grid ( $P_g$ ), reactive power (P-Q), converter voltages ( $V_{con(Ph.)}$ ,  $V_{conL}$ ), and the power quality indicators of voltage and current total harmonic distortion (THD). The evaluation is carried out using MATLAB/SIMULINK.

### 8.5.1 Operating Performance Analysis

Fig. 8.6(a) shows the steady-state response at a solar irradiation level of  $1000 \text{ W/m}^2$ . A total of  $383.50 \text{ kW}$   $P_{PV}$  is generated across all three phases, and  $373.90 \text{ kW}$  of active power ( $P_g$ ) is efficiently transferred in the grid with a 98.5% efficiency. The converter output waveform exhibits a total of thirteen levels. Fig. 8.6(b) demonstrates the transient response when the solar irradiance is reduced by half to  $500 \text{ W/m}^2$ . Consequently, the  $P_{PV}$  decreases to half of its value at  $1000 \text{ W/m}^2$ , and the grid-injected current ( $i_{abc}$ ) also settles at half of its previous value. The voltage profiles of  $V_{\text{con(Ph.)}}$  and  $V_{\text{conL}}$  remain unchanged. In Fig. 8.7(a), the transient response under increased solar irradiation from  $500 \text{ W/m}^2$  to  $1000 \text{ W/m}^2$  is presented. The system's behaviour in this scenario is similar to the case of decreased solar irradiation. The  $P_{PV}$  increases back to  $383.50 \text{ kW}$ , and the  $i_{abc}$  stabilizes, reaching the same values observed at  $1000 \text{ W/m}^2$ . Fig. 8.7(b) highlights the evening effect on the solar arrays. As the solar irradiation diminishes to zero, both the  $P_{PV}$  and  $P_g$  decline to zero. Overall, the performance analysis provides valuable insights into the behaviour of the proposed solar photovoltaic generating system under steady-state and transient conditions, demonstrating its effectiveness in different operating scenarios.

### 8.5.2 Harmonic Performance Analysis

The power quality of the injected power is assessed by evaluating the total harmonics distortion (THD) of voltage and current. The THDs are calculated using the fast Fourier method, and the results are depicted in Fig. 8.8(a). The THD of the ladder output voltage is measured to be 7.47%, with a fundamental voltage component of  $3546 \text{ V}$ . The current THD is 1.72% Fig. 8.8(b)). It is worth noting that the current THD limit, according to the IEEE standard 519, is set at 5%.

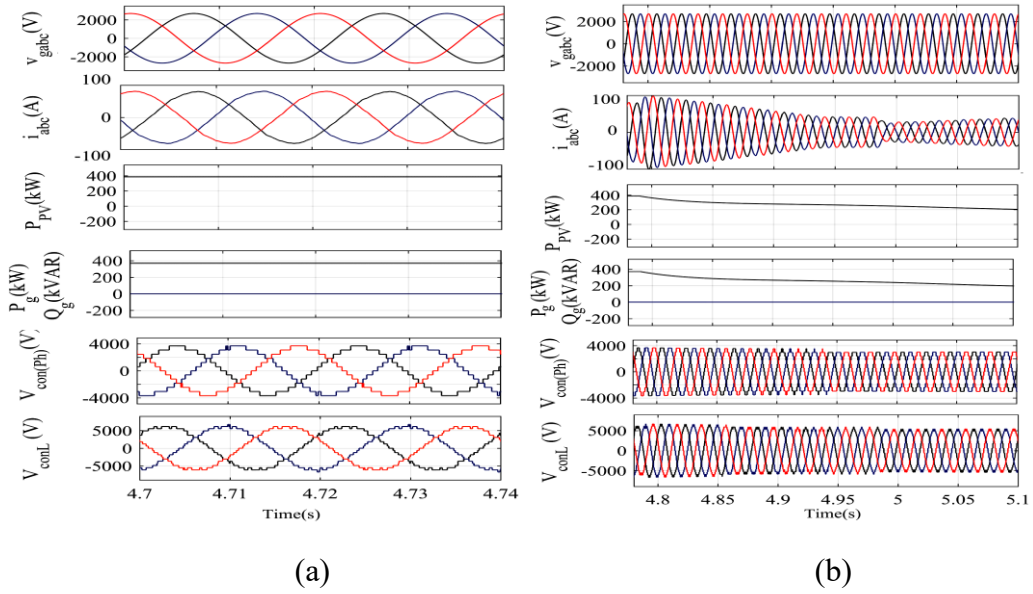


Fig. 8.6. Ladder type converter result (a) at constant irradiance (b) with insolation fall.

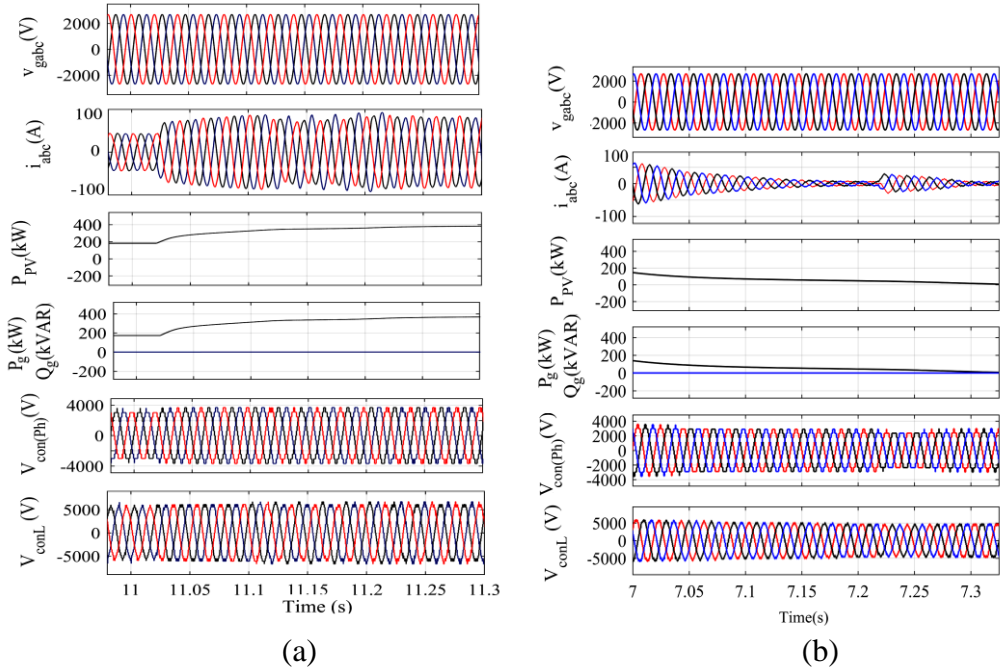


Fig. 8.7. Ladder type converter result with (a) insolation rise (b) insolation to zero.

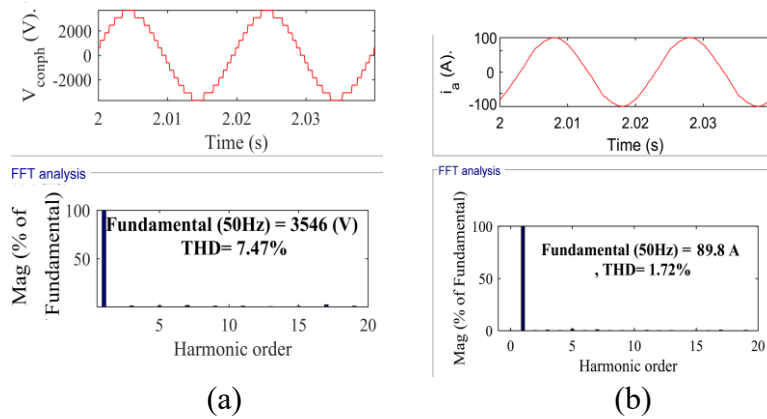


Fig. 8.8 Converter harmonics (a) Ladder converter voltage (b) grid side current

## 8.6 REAL-TIME EXECUTION OF LADDER TYPE THIRTEEN LEVEL CONVERTER FOR SOLAR PV GENERATION APPLICATIONS

The presented system is tested with the real-time simulator OPALRT for the validation of results obtained by the MATLAB/SIMULINK. The results of OPALRT are presented in Figs. 8.9-8.12 The steady state performance is shown in Figs. 8.9(a)-(b) which validates the power transfer at unity power factor and while thirteen level converter voltage profile is maintained. Transient state of falling and rising irradiation is shown in Figs. 8.10(a)-(b) and 8.11(a)-(b) and power transfer changes corresponding to increase and decrease of solar irradiation that is 1000 W/m<sup>2</sup> to 500 W/m<sup>2</sup> and 500 W/m<sup>2</sup> to 1000 W/m<sup>2</sup>. Figs. 8.12(a)-(b) show the harmonic performance in terms of voltage and current THD. The operating and harmonics performance matches the results obtained from the simulations.

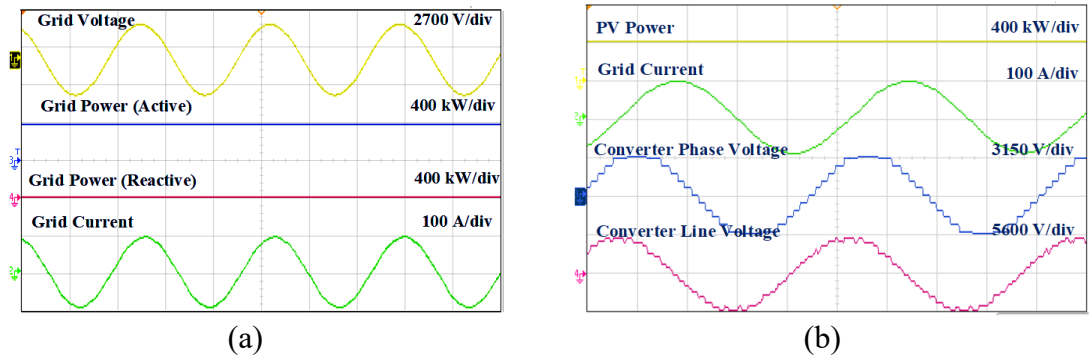


Fig. 8.9. RT simulator results (a) grid voltage, power(Active and reactive) and current (b) PV power, grid current, Converter voltage (Line and Phase) at steady state.

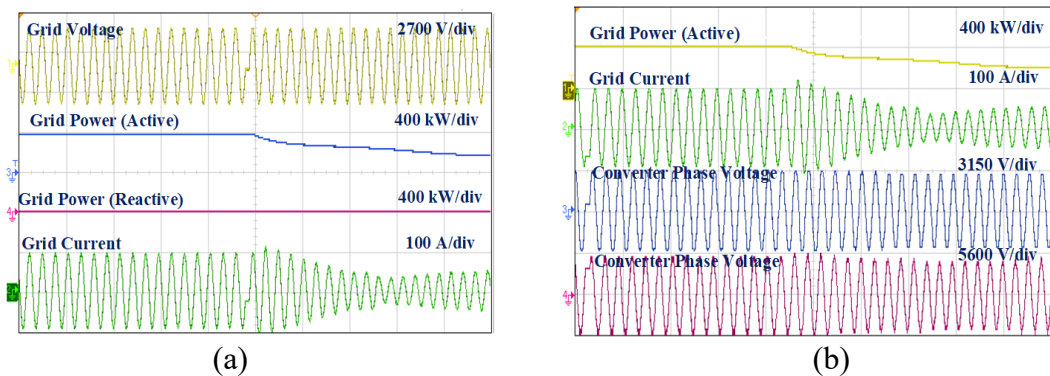


Fig. 8.10. RT simulator result (a) Grid voltage, power(Active and reactive) and current (b)PV power, grid current, Converter voltage (Line and Phase) at irradiation fall.

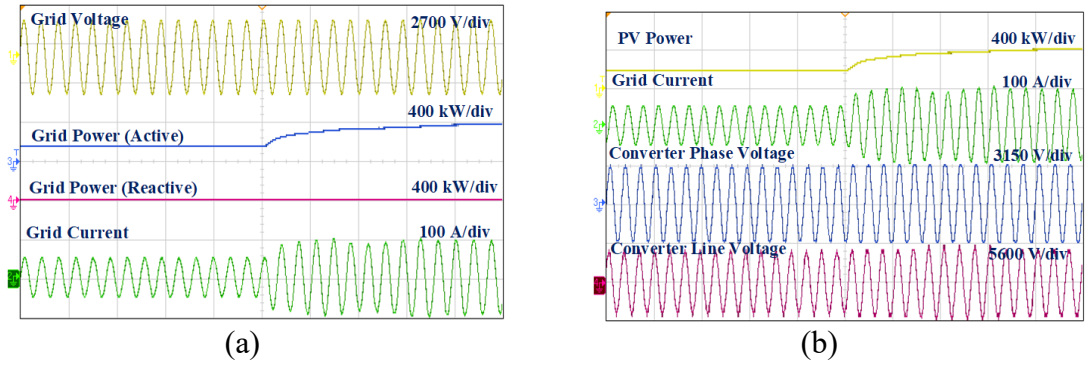


Fig. 8.11. RT simulator result (a) Grid voltage, power(Active and reactive) and current (b)PV power, grid current, Converter voltage (Line and Phase) at irradiation rise.

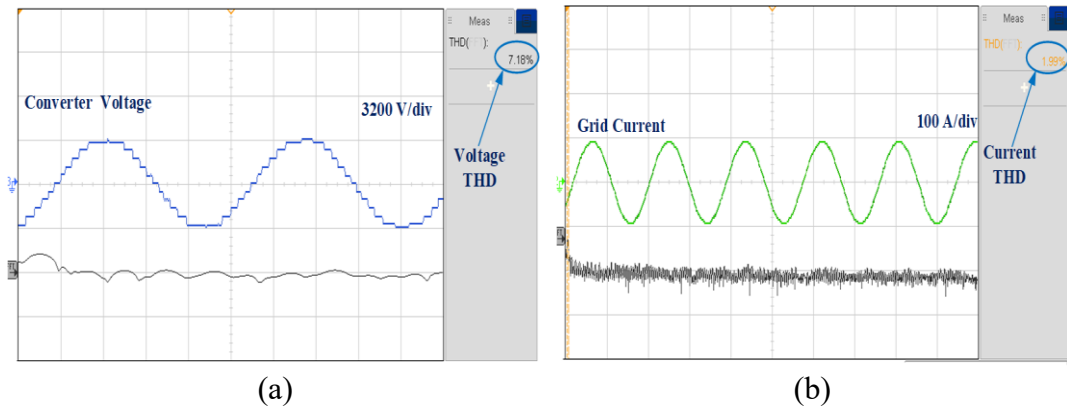


Fig. 8.12. RT simulator result of (a) Voltage harmonic response (b) Grid current harmonic.

## 8.7 CONCLUSIONS

The primary objective of reducing the switch count in a thirteen-level solar inverter has been successfully achieved. Nearest-level modulation is employed for fundamental frequency switching. The control strategies for DC voltage regulation using proportional-integral (PI) control and proportional resonant (PR) control for the AC side have been comprehensively discussed. The PI controllers have effectively tracked the actual DC-link voltage to the reference MPPT voltage. The harmonic performance (THD) is determined by FFT with converter phase voltage THD as 7.47% and grid current THD as 1.72% well below the IEEE-519 standard of 5%.



## CHAPTER IX

### COMPARATIVE STUDY OF DIFFERENT MULTILEVEL CONVERTERS FOR SOLAR PV GENERATION APPLICATIONS

#### 9.1 INTRODUCTION

This chapter presents a comparison of different topologies of PV generation systems covered in the work. The comparison is made on the basis of circuit configuration of the inverters presented in this work with other same level topologies. The number of switches, diodes, capacitors, are compared for each type of configuration. Control method, grid-integration, switching frequency are also considered for the comparison. The results are depicted in the tables for all levels inverters. The summary of comparison provides the new findings for solar photovoltaic systems as follows.

- A symmetric five level T-Type inverter, modified NPC topology is used. This configuration uses the switches in place of diode to clamp the voltage. A new modified triangular carrier signal is generated as a contribution, which has given the excellent harmonics performance.
- A asymmetric PUC topology is used for seven level solar PV plant. PUC is a modification to the CHB configuration and uses less switches. This solar PV generation system is tested for different modulation techniques with various patterns as a contribution.
- A symmetric seven level K-Type converter is used for the medium power solar PV plant. The SHE modulation method is applied for the voltage level generation. Performance of the solar PV generation system is analyzed in steady, rising, falling and no irradiation conditions.
- Well known CHB topology is used in nine level solar PV plant. The THI-NLM

PWM is applied for the switching of converter as a contribution in modulation side.

- A asymmetric eleven level converter based on PEC topology is used for the a grid integrated solar system. The PEC topology is a modification to PUC topology by nesting of bidirectional switch branch to generate eleven levels.
- A symmetric thirteen level ladder type converter based solar PV system is formed for high power. The ladder type topology uses lesser number of switches than conventional CHB. Fundamental frequency switching is achieved by the nearest level modulation, which improves the efficiency of power transfer.

## **9.2 FIVE LEVEL T-TYPE CONVERTER COMPARISON WITH OTHER FIVE LEVEL CONVERTERS**

The proposed T-Type inverter generates the five levels by using the six number of switches per phase, which are lowest among the other five level topologies. The proposed topology is analysed in grid integrated mode and switching of inverter is done with new multicarrier at 500 Hz which is lowest in other converters and gives the higher efficiency and power quality. The detailed comparison is shown in Table 9.1.

## **9.3 SEVEN LEVEL PUC, PEC AND K-TYPE CONVERTER COMPARISON WITH OTHER SEVEN LEVEL CONVERTERS**

The seven level topologies of PUC, PEC and K-Type are compared with other widely used topologies CHB, FC and others. The presented converters are operated in grid integrated mode by using the various modulation techniques with lower frequencies and maintaining the power quality with THD below the IEEE standard limit. PUC, PEC and K-Type converters need only six, eight and ten switches per phase for generating the seven levels. The detailed comparison of presented seven level inverters are depicted in Table 9.2.

## **9.4 NINE LEVEL CHB CONVERTER COMPARISON WITH OTHER NINE LEVEL CONVERTERS**

The nine level CHB converter is compared with other nine level topologies,

presented converter is operated in grid integrated mode while other converter are operated in stand-alone mode. The third harmonic is injected to the modulating signal to improve the DC-link utilization. The fundamental frequency switching of converter is done by the implementation of nearest level modulation. The detailed comparison of presented nine level inverters is shown in the Table 9.3.

### **9.5 ELEVEN LEVEL PEC CONVERTER COMPARISON WITH OTHER ELEVEN LEVEL CONVERTERS**

The eleven level converter PEC 11 is formed by twenty four switches and nine sources in all three phases which is among the lowest with most of the inverters. This converter utilizes the voltage ratio of five to one and switched at power frequency of fifty hertz. A simple and robust PI controllers are used for grid voltage synchronization, which have given the excellent operating performance. The detailed comparison of presented nine level inverters is shown in Table 9.4.

### **9.6 THIRTEEN LEVEL LADDER-TYPE CONVERTER COMPARISON WITH OTHER THIRTEEN LEVEL CONVERTERS**

The presented thirteen level converter is operated in grid tied mode and switched at fundamental frequency. The switching frequency in most of other similar level inverters is very high. The other work in thirteen level converters discussed converter in standalone mode. The detailed comparison of presented nine level inverters is shown in Table 9.5.

Table 9.1 Comparison of other converters with T-Type five level converter for solar PV generation applications

<b>Parameter</b>	<b>[109] HERI C Active- Clamp ed</b>	<b>[110] CHB</b>	<b>[111] Boost Invert er</b>	<b>[112] LLC Boost</b>	<b>[113] FC</b>	<b>[1114] NPC</b>	<b>Propos ed T- Type</b>
No. of levels	5	5	5	5	5	5	5

No. of Switches/Ph	8	8	8	8	7	8	6
No. of Sources/Ph.	1	2	1	2	2	1	2
No. of diodes	Nil	Nil	2	4	Nil	4	nil
No. of Capacitors/Ph.	2	2	3	2	2	2	2
Voltage ratio	1	1:1	1	1:1	1:1	1:1	1:1
Closed/Open Loop Control	Closed Loop	Closed Loop	Closed Loop	Closed Loop	Closed Loop	Closed Loop	Closed Loop
PWM Technique	Phase shifted PWM	Carrier	PCC	PDCPWM	Carrier	Synchronous optimized	New carrier PWM
Switching Frequency	50 kHz	70 kHz	-	8 kHz	1 kHz	350 Hz	500 Hz
Control Method	PR	DSP	PCC	PI	RT-PI	Not discussed	PI
Grid Tied Implementation	Discussed	Not Discussed	Discussed	Not Discussed	Discussed	Not Discussed	Discussed

Table 9.2 Comparison of other converters with PUC and K-Type seven level converter for solar PV generation applications

Parameter	[115] Multiple xed	[116] FC	[117] Hybrid Dual Inv.	[118] CHB	[119] Triple Boost	Proposed PUC	Proposed K- Type
No. of levels	7	7	7	7	7	7	7
No. of Switches/Ph	8	12	8	8	8	6	10
No. of	1	1	1	1	1	2	3

Sources/Ph.							
No. of diodes	2	Nil	Nil	Nil	2	Nil	Nil
No. of Capacitors/ Ph.	2	2	Nil	Nil	3	2	3
Voltage ratio	1	1	1	1	1:1	2:1	1:1:1
Closed/Open Loop Control	Closed Loop	Closed Loop	Closed Loop	Closed Loop	Closed Loop	Closed Loop	Closed Loop
PWM Technique	SPWM	PD-PWM	Space Vector PWM	Carrier PWM	Carrier	New Carrier	SHE
Switching Frequency	5 kHz	5 kHz	fundamental	80 kHz	Not Discussed	1 kHz	50 Hz
Control Method	OPAL-RT and DSP	DSP	DSP	PI	PR	PR	PR
Grid Tied Implementation	Not Discussed	Not Discussed	Not Discussed	Not Discussed	Discussed	Discussed	Discussed

Table 9.3 Comparison of other converters with CHB nine level converter for solar PV generation applications

Parameter	[120] FC	[121] Series connected capacitor	[122] ANPC	[123] Quadruple Boost Inv.	Proposed CHB
No. of levels	9	9	9	9	9
No. of Switches/Ph	8	20 (three ph.)	9	8	16
No. of Sources/Ph.	1	1	1	1	4
No. of diodes	Nil	3(three ph.)	Nil	Nil	Nil

No. of Capacitors/Ph.	2	7(three ph.)	4	2	4
Voltage ratio	1	1	1	1	1:1:1:1
Closed/Open Loop Control	Closed Loop	Closed Loop	Closed Loop	Closed Loop	Closed Loop
PWM Technique	SPWM	SPWM	Space Vector PWM	SPWM	THI-NLM
Switching Frequency	5 kHz	2 kHz	10 kHz	5 kHz	50 Hz
Control Method	dSpace and DSP	DSP	MPC	ARDUINO	PI
Grid Tied Implementation	Not Discussed	Not Discussed	Not Discussed	Not Discussed	Discussed

Table 9.4 Comparison of other converters with PEC eleven level converter for solar PV generation applications

Parameter	[124] HI	[125] MMLI	[126] HC-MLI	[127] Cascaded MLI	[128] PUC11	[129] UXE11	[130] H-NPC-HB	Proposed PEC11
No. of levels	11	11	11	11	11	11	11	11
No. of Switches	36	36	36	18	24	36	30	24
No. of Sources	3	15	9	9	9	3	6	9
No. of diodes	Nil	12	Nil	Nil	Nil	Nil	12	Nil
No. of Capacitors	6	Nil	Nil	Nil	Nil	6	3	Nil
Voltage ratio	1:1:1	1:1:1:1:1	2:2:1	1:2:2	5:3:1	4:1:1	2:1:1	5:1:1
Closed/Open Loop Control	Closed Loop	Closed Loop	Closed Loop	Open Loop	Closed Loop	Open Loop	Open Loop	Closed Loop

PWM Technique	Carrier	Carrier	SHE-PSO	SHE	Carrier	Carrier	Carrier	NLM
Switching Frequency	2 kHz	10 kHz	50 Hz	50 Hz	1 kHz	5 kHz	10 kHz	50 Hz
Control Method	dSpace PI	dSpace PI	DSP	DSP	RT-PI	DSP	DSP	PI
Grid Tied Implementation	Discussed	Not Discussed	Not Discussed	Not Discussed	Discussed	Not Discussed	Not Discussed	Discussed

Table 9.5 Comparison of other converters with PEC eleven level converter for solar PV generation applications

Parameter	[131] PEC	[132] FC	[133] UXE	[134] Dual Boost	[135] SCMLI	Proposed Ladder-Type
No. of levels	13	13	13	13	13	13
No. of Switches/Ph	10	13	12	29	10	15
No. of Sources/Ph.	1	1	1	1	1	6
No. of diodes	Nil	2	Nil	Nil	2	Nil
No. of Capacitors/Ph.	4	4	2	5	1	6
Voltage ratio	1	1	1	1	1	1
Closed/Open Loop Control	Closed Loop	Closed Loop	Closed Loop	Closed Loop	Closed Loop	Closed Loop
PWM Technique	Not Discussed	SPWM	SPWM	SPWM	NLM	NLM
Switching Frequency	Not Discussed	2 kHz	5 kHz	10 kHz	50Hz	50 Hz
Control Method	PI	Not Discussed	PI	PI, PR, Fuzzy	DSP	PR
Grid Tied Implementation	Discussed	Not Discussed	Not Discussed	Not Discussed	Not Discussed	Discussed

## 9.7 CONCLUSIONS

In this chapter, converters from five to thirteen level for the grid integration of solar PV power generation are discussed. The converters are operated by using various modulation techniques, power balance control methods. The converters are operated for the medium to high power transfer handling capacities. Modulation techniques of switching frequency of fifty to order of kHz are tested for the objective of containing the THD to the standard limits. Power balance control is achieved by implementing the PI and PR controllers. This work is done for solar PV generation based grid application with various environmental conditions of rising, falling solar irradiation and temperature change. This work also analyses the power quality during the dynamic conditions. The selection of the best multilevel inverter depends upon the requirement of total power to be transferred to the grid. The increase in number of levels increases power quality and power handling capability.



## CHAPTER X

### MAIN CONCLUSIONS AND FUTURE WORK

#### 10.1 INTRODUCTION

The multilevel converter-based solar photovoltaic generation system has performed better in power conversion efficiency and reduced harmonic distortions compared to traditional converters. The system's modular and scalable architecture allows for easy integration with various PV array configurations and the grid. Control strategies applied to the converter successfully have managed voltage levels and ensured seamless grid synchronization in all environmental conditions. Various modulation techniques have shown the better power quality.

#### 10.2 MAIN CONCLUSIONS

The main conclusions of this thesis are listed here.

➤ Five level symmetric T-Type topology converter is investigated for grid-tied solar PV generation applications. The new multi-carrier modulation method is applied with unit template based AC control. The results are recorded for new PWM along with other commonly used techniques. Harmonic performance is tested with THD of converter phase voltage of 23.19% and current THD of 2.07%. The harmonics performance of grid current is within the 5% limit of the IEEE-519 standard. The T-Type converter with new multi-carrier modulation is found suitable over CHB and NPC topologies.

➤ Seven level asymmetric PUC topology converter is investigated for grid-tied applications. Proportional resonant controllers have shown proper tracking of AC side grid currents. The PUC inverter is analyzed with three types of multicarrier PWM schemes, and each multicarrier signal is arranged in three patterns (PD, POD, APOD). The results are recorded for SPWM, parabolic PWM and modified PWM.

Harmonic performance is found best in modified PWM with THD of converter phase voltage of 14.789% and current THD of 1.77%. The harmonic performance of grid current is found within the 5% limit of IEEE-519 standard.

➤ Seven level symmetric K-Type topology converter is investigated for grid-tied solar applications. The PR control provides simple and robust AC power control. The implementation of SHE modulation ensures an excellent harmonics response with converter phase voltage THD of 13.58% and gives a current THD of 1.32%, which is much lower than the permissible limits of 5% as per the IEEE-519 standards. These results have shown that the grid power is fed smoothly at steady state and dynamic conditions.

➤ Nine level symmetric CHB topology converter is investigated for grid-tied solar PV generation applications. Proportional resonant controllers have shown proper tracking of AC side grid currents. An improved control with 3<sup>rd</sup> harmonic injection and nearest-level PWM is applied for closed loop control of CHB solar PV generating system. Cascaded H-bridge power cells with twelve solar PV arrays have injected the solar PV power to the grid. This work explained the 3<sup>rd</sup> harmonic injection in the modulating signals and performance analysis of harmonics with and without THI. The harmonic performance is tested in OPAL-RT test bench with converter line voltage THD of 7.47% and gives a current THD of 2.78%, which is much lower than the permissible limits of 5% as per the IEEE-519 standard.

➤ Eleven level asymmetric (1:5, Quintuple) PEC topology converter is investigated for grid-tied solar applications. The complete control scheme with DC-link voltage of top and bottom PV arrays, resonant current controllers, and code of NLM is shown for PEC11. The simulated results of DC and AC side of the PEC11 in steady and varying solar conditions are demonstrated in detail. The harmonic

performance (THD) is determined by FFT with converter phase voltage THD as 7.22% and grid current THD as 3.014%. The performance of the new PEC11 is verified on real-time OPALRT successful.

➤ Thirteen level symmetric ladder type topology converter is investigated for grid-tied solar applications. The fundamental frequency switching is done with nearest-level modulation. The DC voltage control by proportional-integral control and proportional resonant control for the AC side have been achieved. The harmonic performance (THD) is determined by FFT with converter phase voltage THD as 7.47% and grid current THD as 1.72%.

### **10.3 FURTHER WORK**

Following are the possible research directions for further research in solar multilevel converters.

- Hybrid topologies are to be explored for increasing the number of levels with lesser count of the switches for better conversion efficiency.
- Control strategies involving the neural network and artificial intelligence are to be explored for faster response to varying solar irradiation conditions.
- Development of new modulation techniques for the mitigation of harmonic distortion.
- The inclusion of solar irradiation forecasting into the control algorithm of solar PV system.

## REFERENCES

- [1] B. K. Bose, "Power Electronics, Smart Grid, and Renewable Energy Systems," *Proc. IEEE*, vol. 105, no. 11, pp. 2011-2018, Nov. 2017.
- [2] A. Kumar, M. Alaraj, M. Rizwan and U. Nangia, "Novel AI Based Energy Management System for Smart Grid With RES Integration," *IEEE Access*, vol. 9, pp. 162530-162542, 2021.
- [3] F. Blaabjerg, Z. Chen and S. B. Kjaer, "Power electronics as efficient interface in dispersed power generation systems," *IEEE Trans. Pow. Electron.*, vol. 19, no. 5, pp. 1184-1194, Sept. 2004.
- [4] J. M. Carrasco, L. G. Franquelo, J. T. Bialasiewicz, E. Galvan, R. C. P. Guisado, Ma. A. M. Prats, J. I. Leon and N. Moreno-Alfonso, "Power- Electronic Systems for the Grid Integration of Renewable Energy Sources: A Survey", *IEEE Trans. Ind. Electron.*, vol. 53, no. 4, pp. 1002-1016, June 2006.
- [5] J. T. Bialasiewicz, "Renewable energy systems with photovoltaic power generators: operation and modeling," *IEEE Trans. Ind. Electron.*, vol. 55, no. 7, pp.2752-2758, July 2008.
- [6] S. Kouro, M. Malinowski, K. Gopakumar, J. Pou, L. G. Franquelo, B. Wu, J. Rodriguez, M. A. Perez and J. L. Leon, "Recent advances and industrial applications of multilevel converters", *IEEE Trans. Ind. Electron.*, vol. 57, no 8, August 2010.
- [7] F. Blaabjerg, Z. Chen and S. B. Kjaer, "Power electronics as efficient interface in dispersed power generation systems," *IEEE Trans. Ind. Electron.*, vol. 19, no 5, pp.1184-1194, September, 2006.

- [8] S. Kouro, M. Malinowski, K. Gopakumar, J. Pou, L. G. Franquelo, B. Wu, J. Rodriguez, M. A. Perez and J. L. Leon, "Recent advances and industrial applications of multilevel converters", *IEEE Trans. Ind. Electron.*, vol. 57, no 8, August 2010.
- [9] S. K. Yadav and B. Singh, "Topological Analysis and Solar Grid-Tied Integration of Level Building Network Based Extendable High Power Multilevel Converter," *IEEE Trans. Ind. Applications*, vol. 59, no. 4, pp. 4215-4224, July-Aug. 2023.
- [10] M. Badoni, A. Singh, A. K. Singh, H. Saxena and R. Kumar, "Grid Tied Solar PV System with Power Quality Enhancement Using Adaptive Generalized Maximum Versoria Criterion," *CSEE Journ. Pow. & Ener. Sys.*, vol. 9, no. 2, pp. 722-732, March 2023.
- [11] Y. Lu, W. Xiao and D. D. -C. Lu, "Optimal Dynamic and Steady-State Performance of PV-Interfaced Converters Using Adaptive Observers," *IEEE Trans. Circuits and Sys. II: Express Briefs*, vol. 69, no. 12, pp. 4909-4913, Dec. 2022.
- [12] K. Kumari and A. K. Jain, "Performance Assessment of Three-Phase NPC-Based Grid Integrated Single-Stage Solar PV System With Reduced DC Bus Capacitor," *IEEE Trans. Ind. Electron.*, vol. 70, no. 4, pp. 3773-3781, April 2023.
- [13] A. Zorig, S. Barkat and A. Sangwongwanich, "Neutral Point Voltage Balancing Control Based on Adjusting Application Times of Redundant Vectors for Three-Level NPC Inverter," *IEEE Journ. Emerg. & Selec. Topics Pow. Electron.*, vol. 10, no. 5, pp. 5604-5613, Oct. 2022.

- [14] J. Li, J. Chen and C. Gong, "An Optimized Reactive Power Compensation Strategy to Extend the Working Range of CHB Multilevel Grid-Tied Inverters," *IEEE Trans. Pow. Electron.*, vol. 38, no. 4, pp. 5500-5512, April 2023.
- [15] H. Katir, A. Abouloifa, E. Elbouchikhi, A. Fekih, K. Noussi and A. El Aroudi, "Robust Control of Cascaded H-Bridge Multilevel Inverters for Grid-Tied PV Systems Subject to Faulty Conditions," *IEEE Control Sys. Letters*, vol. 7, pp. 2683-2688, 2023.
- [16] W. Zhang and Y. He, "A Simple Open-Circuit Fault Diagnosis Method for Grid-Tied T-Type Three-Level Inverters With Various Power Factors Based on Instantaneous Current Distortion," *IEEE Journ. Emerg. & Select. Topics Pow. Electron.*, vol. 11, no. 1, pp. 1071-1085, Feb. 2023.
- [17] R. Vasu, S. K. Chattopadhyay and C. Chakraborty, "Seven-Level Packed U-Cell (PUC) Converter With Natural Balancing of Capacitor Voltages," *IEEE Trans. Ind. Applications*, vol. 56, no. 5, pp. 5234-5244, Sept.-Oct. 2020.
- [18] J. Zeng, W. Lin, D. Cen and J. Liu, "Novel K-Type Multilevel Inverter With Reduced Components and Self-Balance," *IEEE Journ. Emerg. & Select. Topics in Pow. Electron.*, vol. 8, no. 4, pp. 4343-4354, Dec. 2020.
- [19] F. Sebaaly, M. Sharifzadeh, H. Y. Kanaan and K. Al-Haddad, "Multilevel Switching-Mode Operation of Finite-Set Model Predictive Control for Grid-Connected Packed E-Cell Inverter," *IEEE Trans. Ind. Electron.*, vol. 68, no. 8, pp. 6992-7001, Aug. 2021.
- [20] M. M. Shobini, D. P. Winston, S. S. Kumar, M. Pravin, A. G. Aakash and B. G. Babu, "S-Connected Ladder Fashion Multilevel Topology With Reduced Device

- Count,” *IEEE Canadian Journ. Elect. & Comp. Engg.*, vol. 45, no. 3, pp. 285-292, Summer 2022.
- [21] Y. Wang, C. Wang, Y. Guo, K. Wang and J. Liang, “An X-type Boost Multilevel Inverter Based on Switched Capacitor Cells with Low Voltage Stress and High Frequency Applications,” *IEEE Journ. Emerg. & Select. Topics Pow. Electron.*, Early Access.
- [22] “IEEE Standard for Harmonic Control in Electric Power Systems,” *IEEE Std 519-2022 (Revision of IEEE Std 519-2014)*, vol., no., pp.1-31, 5 Aug. 2022.
- [23] S. Karmakar and B. Singh, “48-Pulse Voltage-Source Converter Based on Three-Level Neutral Point Clamp Converters for Solar Photovoltaic Plant,” *IEEE Journ. Emerg. & Select. Topics Pow. Electron.*, vol. 10, no. 5, pp. 5894-5903, Oct. 2022.
- [24] M. K. Mishra and V. N. Lal, “A Multiobjective Control Strategy for Harmonic Current Mitigation With Enhanced LVRT Operation of a Grid-Tied PV System Without PLL Under Abnormal Grid Conditions,” *IEEE Journ. Emerg. & Select. Topics Pow. Electron.*, vol. 11, no. 2, pp. 2164-2177, April 2023
- [25] S. K. Baksi and R. K. Behera, “A Reduced Switch Count Seven-Level Boost ANPC Based Grid Following Inverter Topology With Photovoltaic Integration,” *IEEE Trans. Ind. Applica.* vol. 59, no. 4, pp. 4238-4251, July-Aug. 2023
- [26] A. Iqbal, M. Meraj, M. Tariq, K. A. Lodi, A. I. Maswood and S. Rahman, “Experimental Investigation and Comparative Evaluation of Standard Level Shifted Multi-Carrier Modulation Schemes With a Constraint GA Based SHE Techniques for a Seven-Level PUC Inverter,” *IEEE Access*, vol. 7, pp. 100605-100617, 2019.

- [27] H. B. Gobburi, V. B. Borghate and P. M. Meshram, "A Level Enhanced Nearest Level Control for Modular Multilevel Converter Without Using Sensors," *IEEE Trans. Ind. Applic.*, vol. 59, no. 4, pp. 4364-4374, July-Aug. 2023
- [28] G. Li, Z. Wu, D. Cao and J. Li, "Random PWM Selective Harmonic Elimination Method With Master-Slave Mode for Seven-Level MPUC Inverter," *CPSS Trans. Pow. Electron. & Applications*, vol. 8, no. 1, pp. 87-96, March 2023
- [29] Z. Salam, "An Enhanced Adaptive P&O MPPT for Fast and Efficient Tracking Under Varying Environmental Conditions," *IEEE Trans. Sustainable Energy*, vol. 9, no. 3, pp. 1487-1496, July 2018.
- [30] M. Kermadi, Z. Salam, J. Ahmed and E. M. Berkouk, "An Effective Hybrid Maximum Power Point Tracker of Photovoltaic Arrays for Complex Partial Shading Conditions," *IEEE Trans. Ind. Electron.*, vol. 66, no. 9, pp. 6990-7000, Sept. 2019.
- [31] A. Sangwongwanich and F. Blaabjerg, "Mitigation of Interharmonics in PV Systems With Maximum Power Point Tracking Modification," *IEEE Trans. Pow. Electron.*, vol. 34, no. 9, pp. 8279-8282, Sept. 2019.
- [32] M. Alsumiri, "Residual Incremental Conductance Based Nonparametric MPPT Control for Solar Photovoltaic Energy Conversion System," *IEEE Access*, vol. 7, pp. 87901-87906, 2019.
- [33] A. Sangwongwanich, Y. Yang, F. Blaabjerg and H. Wang, "Benchmarking of Constant Power Generation Strategies for Single-Phase Grid-Connected Photovoltaic Systems," *IEEE Trans. Ind. Applications*, vol. 54, no. 1, pp. 447-457, Jan.-Feb. 2018.



- [34] M. J. Alshareef, "An Effective Falcon Optimization Algorithm Based MPPT Under Partial Shaded Photovoltaic Systems," *IEEE Access*, vol. 10, pp. 131345-131360, 2022.
- [35] A. Ballaji, R. Dash, V. Subburaj, J. R. Kalvakurthi, D. Swain and S. C. Swain, "Design & Development of MPPT Using PSO With Predefined Search Space Based on Fuzzy Fokker Planck Solution," *IEEE Access*, vol. 10, pp. 80764-80783, 2022.
- [36] P. Venugopal, M. K. Rajendran and G. Chowdary, "A Constant-Energy-Packet-Extraction-Based MPPT Technique With 98% Average Extraction Efficiency for Wide Range Generic Ambient Energy Scavenging Supporting  $1000 \times$  Source Resistance Range," *IEEE Journ. Solid-State Circuits*, vol. 57, no. 10, pp. 3150-3163, Oct. 2022
- [37] S. R. Kiran, C. H. H. Basha, V. P. Singh, C. Dhanamjayulu, B. R. Prusty and B. Khan, "Reduced Simulative Performance Analysis of Variable Step Size ANN Based MPPT Techniques for Partially Shaded Solar PV Systems," *IEEE Access*, vol. 10, pp. 48875-48889, 2022.
- [38] P. A. R. Freitas, L. P. Pires, L. C. Freitas, G. B. Lima and L. C. G. Freitas, "Design and Development of a Grid-Tied PV Inverter With GMPPT Technique and Reduced Number of Sensors," *IEEE Access*, vol. 10, pp. 48810-48823, 2022.
- [39] V. K. Dunna, K. P. B. Chandra, P. K. Rout and B. K. Sahu, "Design and Real-Time Validation of Higher Order Sliding Mode Observer-Based Integral Sliding Mode MPPT Control for a DC Microgrid," *IEEE Canadian Jour. Electrical Comp Engg.*, vol. 45, no. 4, pp. 418-425, Fall 2022.

- [40] R. H. Morales et al., "A Novel Global Maximum Power Point Tracking Method Based on Measurement Cells," *IEEE Access*, vol. 10, pp. 97481-97494, 2022.
- [41] D. Prasad and D. C., "Solar PV-Fed Multilevel Inverter With Series Compensator for Power Quality Improvement in Grid-Connected Systems," *IEEE Access*, vol. 10, pp. 81203-81219, 2022.
- [42] S. Xu, R. Shao, B. Cao and L. Chang, "Single-phase grid-connected PV system with golden section search-based MPPT algorithm," *Chinese Journ. Elect. Engg*, vol. 7, no. 4, pp. 25-36, Dec. 2021.
- [43] J. Y. Fam, S. Y. Wong, H. B. M. Basri, M. O. Abdullah, K. B. Lias and S. Mekhilef, "Predictive Maximum Power Point Tracking for Proton Exchange Membrane Fuel Cell System," *IEEE Access*, vol. 9, pp. 157384-157397, 2021.
- [44] H. K. Mehta and A. K. Panchal, "PV Panel Performance Evaluation via Accurate V-I Polynomial With Efficient Computation," *IEEE Journ. Photovoltaics*, vol. 11, no. 6, pp. 1519-1527, Nov. 2021.
- [45] M. Z. Malik, H. M. H. Farh, A. M. Al-Shaalan, A. A. Al-Shamma'a and H. H. Alhelou, "A Novel Single-Input-Multi-Output Converter for Flexible-Order Power-Distributive With MPPT Capability," *IEEE Access*, vol. 9, pp. 131020-131032, 2021.
- [46] S. A. Ibrahim, A. Nasr and M. A. Enany, "Maximum Power Point Tracking Using ANFIS for a Reconfigurable PV-Based Battery Charger Under Non-Uniform Operating Conditions," *IEEE Access*, vol. 9, pp. 114457-114467, 2021.

- [47] T. Sutikno, A. C. Subrata and A. Elkhateb, "Evaluation of Fuzzy Membership Function Effects for Maximum Power Point Tracking Technique of Photovoltaic System," *IEEE Access*, vol. 9, pp. 109157-109165, 2021.
- [48] A. Govindharaj, A. Mariappan, A. Ambikapathy, V. S. Bhadoria and H. H. Alhelou, "Real-Time Implementation of Adaptive Neuro Backstepping Controller for Maximum Power Point Tracking in Photo Voltaic Systems," *IEEE Access*, vol. 9, pp. 105859-105875, 2021.
- [49] A. Jakhar, N. Sandeep and A. K. Verma, "A Nine-Level Common-Ground Type Boost Inverter for PV Applications," *2022 IEEE 1st Ind. Electron. Society Annual On-Line Conf. (ONCON)*, kharagpur, India, pp. 1-6, 2022.
- [50] M. O. Saad et al., "Design and Control of Novel Grid Tied Multilevel Filter-Less Inverter Using Current Based Sliding Mode Control," *IEEE Access*, vol. 10, pp. 115555-115570, 2022.
- [51] I. Harbi, M. Ahmed, M. L. Heldwein, R. Kennel and M. Abdelrahem, "Enhanced Fault-Tolerant Robust Deadbeat Predictive Control for Nine-Level ANPC-Based Converter," *IEEE Access*, vol. 10, pp. 108492-108505, 2022.
- [52] N. Tak, S. K. Chattopadhyay and C. Chakraborty, "Single-Sourced Double-Stage Multilevel Inverter for Grid-Connected Solar PV Systems," *IEEE Open Journ. Ind. Electron. Society*, vol. 3, pp. 561-581, 2022.
- [53] M. Ye, W. Ren, L. Chen, Q. Wei, G. Song and S. Li, "Research on Power-Balance Control Strategy of CHB Multilevel Inverter Based on TPWM," *IEEE Access*, vol. 7, pp. 157226-157240, 2019.

- [54] L. Zhou, F. Gao and T. Xu, "Implementation of Active NPC Circuits in Transformer-Less Single-Phase Inverter With Low Leakage Current," *IEEE Trans. Ind. Applications*, vol. 53, no. 6, pp. 5658-5667, Nov.-Dec. 2017
- [55] S. S. Lee, "Single-Stage Switched-Capacitor Module (S3CM) Topology for Cascaded Multilevel Inverter," *IEEE Trans. Pow. Electron.*, vol. 33, no. 10, pp. 8204-8207, Oct. 2018.
- [56] M. Tariq, M. Meraj, A. Azeem, A. I. Maswood, A. Iqbal and B. Chokkalingam, "Evaluation of level-shifted and phase-shifted PWM schemes for seven level single-phase packed U cell inverter," *CPSS Trans. on Pow. Electron. & Applications*, vol. 3, no. 3, pp. 232-242, Sept. 2018
- [57] M. Sharifzadeh and K. Al-Haddad, "Packed E-Cell (PEC) Converter Topology Operation and Experimental Validation," *IEEE Access*, vol. 7, pp. 93049-93061, 2019.
- [58] Y. Ye, G. Zhang, X. Wang, Y. Yi and K. W. E. Cheng, "Self-Balanced Switched-Capacitor Thirteen-Level Inverters With Reduced Capacitors Count," *IEEE Trans. Industrial Electron.*, vol. 69, no. 1, pp. 1070-1076, Jan. 2022.
- [59] Y. Tian, H. R. Wickramasinghe, P. Sun, Z. Li, J. Pou and G. Konstantinou, "Assessment of Low-Loss Configurations for Efficiency Improvement in Hybrid Modular Multilevel Converters," *IEEE Access*, vol. 9, pp. 158155-158166, 2021.
- [60] S. Kumari, A. K. Verma, S. N, U. R. Yaragatti and H. R. Pota, "A Five-Level Transformer-Less Inverter With Self-Voltage Balancing and Boosting Ability," *IEEE Trans. Ind. Applications*, vol. 57, no. 6, pp. 6237-6245, Nov.-Dec. 2021.

- [61] D. Lumbreras, E. L. Barrios, J. Balda, M. Navarrete, R. González and P. Sanchis, "Medium-Voltage Cascaded Sequential Topology for Large-Scale PV Plants," *IEEE Access*, vol. 9, pp. 130601-130614, 2021.
- [62] N. Panda, B. Das, A. Chakrabarti, P. R. Kasari, A. Bhattacharya and D. Chatterjee, "A New Grid Interactive 11-Level Hybrid Inverter Topology for Medium-Voltage Application," *IEEE Trans. Ind. Applications*, vol. 57, no. 1, pp. 869-881, Jan.-Feb. 2021.
- [63] R. Goel, T. T. Davis and A. Dey, "Thirteen-Level Multilevel Inverter Structure Having Single DC Source and Reduced Device Count," *IEEE Trans. Ind. Applications*, vol. 58, no. 4, pp. 4932-4942, July-Aug. 2022.
- [64] K. Jena, C. K. Panigrahi and K. K. Gupta, "A 6X-Voltage-Gain 13-Level Inverter With Self-Balanced Switched-Capacitors," *CPSS Trans. Power Electron. & Applications*, vol. 7, no. 1, pp. 94-102, March 2022.
- [65] L. Kurinjimalar, S. Pooja, R. Sivaprasad, B. Meenakshi, J. S. Priya and T. Porselvi, "Design and Analysis of Fifteen Level Inverter for Renewable Applications," *2022 Int. Conf. on Power, Energy, Control and Transmission Systems (ICPECTS)*, Chennai, India, pp. 1-4, 2022.
- [66] P. S. V. Kishore, N. Jayaram, S. Jakkula, Y. R. Sankar, J. Rajesh and S. Halder, "A New Reduced Switch Seven-Level Triple Boost Switched Capacitor Based Inverter," *IEEE Access*, vol. 10, pp. 73931-73944, 2022.
- [67] A. Salem, H. Van Khang, I. N. Jiya and K. G. Robbersmyr, "Hybrid Three-Phase Transformer-Based Multilevel Inverter With Reduced Component Count," *IEEE Access*, vol. 10, pp. 47754-47763, 2022.

- [68] M. T. Islam, M. F. Rahman, S. Barua, A. Shihavuddin, M. H. Maruf and R. H. Ashique, "Harmonic Reduction of Cascaded H -Bridge Multilevel Inverter Using Advanced Level Shifted Pulse Width Modulation Technique," *2021 Int. Conf. Electron., Comm. and Info. Tech. (ICECIT)*, Khulna, Bangladesh, pp. 1-4, 2021.
- [69] K. Suresh and E. Parimalasundar, "A Modified Multi Level Inverter With Inverted SPWM Control," *IEEE Canadian Journ. Elect. & Comp. Engg.*, vol. 45, no. 2, pp. 99-104, Spring 2022.
- [70] Y. Li, Y. Wang and B. Q. Li, "Generalized Theory of Phase-Shifted Carrier PWM for Cascaded H-Bridge Converters and Modular Multilevel Converters," *IEEE Journ. Emerg. & Select. Topics Pow. Electron.*, vol. 4, no. 2, pp. 589-605, June 2016.
- [71] N. Mishra, S. K. Yadav, B. Singh, S. Padmanaban and F. Blaabjerg, "Binary-Quintuple Progression Based 12-Switch 25-Level Converter With Nearest Level Modulation Technique for Grid-Tied and Standalone Applications," *IEEE Trans. Ind. Applications*, vol. 57, no. 3, pp. 3214-3223, May-June 2021
- [72] M. Sadoughi, A. Pourdashednia, M. Farhadi-Kangarlu and S. Galvani, "PSO-Optimized SHE-PWM Technique in a Cascaded H-Bridge Multilevel Inverter for Variable Output Voltage Applications," *IEEE Trans. Pow. Electron.*, vol. 37, no. 7, pp. 8065-8075, July 2022.
- [73] V. Jayakumar, B. Chokkalingam and J. L. Munda, "A Comprehensive Review on Space Vector Modulation Techniques for Neutral Point Clamped Multi-Level Inverters," *IEEE Access*, vol. 9, pp. 112104-112144, 2022.

- [74] A. Poorfakhraei, M. Narimani and A. Emadi, "A Review of Modulation and Control Techniques for Multilevel Inverters in Traction Applications," *IEEE Access*, vol. 9, pp. 24187-24204, 2021.
- [75] A. Moeini, S. Wang, B. Zhang and L. Yang, "A Hybrid Phase Shift-Pulsewidth Modulation and Asymmetric Selective Harmonic Current Mitigation-Pulsewidth Modulation Technique to Reduce Harmonics and Inductance of Single-Phase Grid-Tied Cascaded Multilevel Converters," *IEEE Trans. Ind. Electron.*, vol. 67, no. 12, pp. 10388-10398, Dec. 2020.
- [76] Z. Liu, K. -J. Li, Z. Guo, J. Wang and J. Qian, "A Comprehensive Study on the Modulation Ratio for Modular Multilevel Converters," *IEEE Trans. on Ind. Applications*, vol. 58, no. 3, pp. 3205-3216, May-June 2022.
- [77] T. Younis, P. Mattavelli, P. Magnone, I. Toigo and M. Corradin, "Enhanced Level-Shifted Modulation for a Three-Phase Five-Level Modified Modular Multilevel Converter (MMC)," *IEEE Journ. Emerg. & Selected Topics Power Electron.*, vol. 10, no. 1, pp. 704-716, Feb. 2022.
- [78] J. I. Leon, S. Vazquez, S. Kouro, L. G. Franquelo, J. M. Carrasco and J. Rodriguez, "Unidimensional Modulation Technique for Cascaded Multilevel Converters," *IEEE Trans. Ind. Electron.*, vol. 56, no. 8, pp. 2981-2986, Aug. 2009.
- [79] D. Alex Bao Zambra and J. Renes Pinheiro, "Comparison of Phase-Shift and Step Wave Modulation Technique applied to Symmetrical Cascaded Multilevel Inverter," *IEEE Latin America Trans.*, vol. 11, no. 5, pp. 1156-1162, Sept. 2013.
- [80] A. Edpuganti and A. K. Rathore, "A Survey of Low Switching Frequency Modulation Techniques for Medium-Voltage Multilevel Converters," *IEEE Trans. Ind. Applications*, vol. 51, no. 5, pp. 4212-4228, Sept.-Oct. 2015.

- [81] K. Gnanasambandam, A. K. Rathore, A. Edpuganti, D. Srinivasan and J. Rodriguez, "Current-Fed Multilevel Converters: An Overview of Circuit Topologies, Modulation Techniques, and Applications," *IEEE Trans. Power Electron.*, vol. 32, no. 5, pp. 3382-3401, May 2017.
- [82] X. Shi, C. Zhang, R. Li and X. Cai, "Control Scheme for Second Harmonic Current Elimination in Single-Star Configuration Based Cascade Multilevel Energy Storage System," *IEEE Journ. Emerg. & Selected Topics Ind. Electron.*, vol. 3, no. 4, pp. 1210-1216, Oct. 2022.
- [83] H. Azeem, S. Yellasiri, V. Jammala, B. S. Naik and A. K. Panda, "A Fuzzy Logic Based Switching Methodology for a Cascaded H-Bridge Multi-Level Inverter," *IEEE Trans. Power Electron.*, vol. 34, no. 10, pp. 9360-9364, Oct. 2019.
- [84] Y. Oto, T. Noguchi, T. Sasaya, T. Yamada and R. Kazaoka, "Space Vector Modulation of Dual-Inverter System Focusing on Improvement of Multilevel Voltage Waveforms," *IEEE Trans. on Ind. Electron.*, vol. 66, no. 12, pp. 9139-9148, Dec. 2019.
- [85] S. Sharma, J. Kumar, V. Sirohi and G. L. Jat, "Performance evaluation of multilevel inverters for low switching frequency modulation techniques," *2022 IEEE Delhi Section Conf. (DELCON)*, New Delhi, India, 2022.
- [86] P. R. Bute and S. K. Mittal, "Simulation Study of Cascade H-bridge Multilevel Inverter 7-Level Inverter by SHE Technique," *2020 4th Int. Conf. Computing Methodologies and Comm. (ICCMC)*, Erode, India, 2020.
- [87] R. Majdoul, A. Touati, A. Aitelmahjoub, M. Zegrari, A. Taouni and A. Ouchatti, "A Nine-Switch Nine-Level Voltage Inverter New Topology with Optimal



- Modulation Technique,” *2020 Int. Conf. Electrical and Info. Tech. (ICEIT)*, Rabat, Morocco, 2020, pp. 1-6.
- [88] L. R. Ch and S. L. G, “Analysis of THD for Multilevel Inverters with Novel Pulse Width Modulation Techniques,” *2021 IEEE Int. Conf. Intelligent Sys., Smart & Green Technologies (ICISSGT)*, Visakhapatnam, India, pp. 150-155, 2021.
- [89] A. M. Mahfuz-Ur-Rahman, M. R. Islam, K. M. Muttaqi and D. Sutanto, “Model Predictive Control for a New Magnetic Linked Multilevel Inverter to Integrate Solar Photovoltaic Systems With the Power Grids,” *IEEE Trans. Ind. Applications*, vol. 56, no. 6, pp. 7145-7155, Nov.-Dec. 2020.
- [90] A. Taghvaie, M. E. Haque, S. Saha and M. A. Mahmud, “A New Step-Up Switched-Capacitor Voltage Balancing Converter for NPC Multilevel Inverter-Based Solar PV System,” *IEEE Access*, vol. 8, pp. 83940-83952, 2020.
- [91] E. Villanueva, P. Correa, J. Rodriguez and M. Pacas, “Control of a Single-Phase Cascaded H-Bridge Multilevel Inverter for Grid-Connected Photovoltaic Systems,” *IEEE Trans. Ind. Electron.*, vol. 56, no. 11, pp. 4399-4406, Nov. 2009.
- [92] A. Laib, A. Krama, A. Sahli, A. Kihal and H. Abu-Rub, “Reconfigurable Model Predictive Control for Grid Connected PV Systems Using Thirteen-Level Packed E-Cell Inverter,” *IEEE Access*, vol. 10, pp. 102210-102222, 2022.
- [93] D. Upadhyay, M. Ali, M. Tariq, S. A. Khan, B. Alamri and A. Alahmadi, “Thirteen-Level UXE-Type Inverter With 12-Band Hysteresis Current Control Employing PSO Based PI Controller,” *IEEE Access*, vol. 10, pp. 29890-29902, 2022.

- [94] S. Sahoo, S. Prakash and S. Mishra, "Investigation of voltage template based control of a grid connected DC microgrid under different grid conditions," *2016 IEEE 6th Int. Conf. Pow. Sys. (ICPS)*, New Delhi, India, 2016.
- [95] M. Parvez, M. F. M. Elias, N. A. Rahim, F. Blaabjerg, D. Abbott and S. F. Al-Sarawi, "Comparative Study of Discrete PI and PR Controls for Single-Phase UPS Inverter," *IEEE Access*, vol. 8, pp. 45584-45595, 2020.
- [96] M. Ebrahimi, S. A. Khajehoddin and M. Karimi-Ghartemani, "Fast and Robust Single-Phase DQ Current Controller for Smart Inverter Applications," *IEEE Trans. on Pow. Electron.*, vol. 31, no. 5, pp. 3968-3976, May 2016.
- [97] M. Trabelsi, S. Bayhan, K. A. Ghazi, H. Abu-Rub and L. Ben-Brahim, "Finite-Control-Set Model Predictive Control for Grid-Connected Packed-U-Cells Multilevel Inverter," *IEEE Trans. Ind. Electron.*, vol. 63, no. 11, pp. 7286-7295, Nov. 2016.
- [98] R. Hemmati, H. Faraji and N. Y. Beigvand, "Multilevel and Advanced Control Scheme for Multimicrogrid Under Healthy-Faulty and Islanded-Connected Conditions," *IEEE Sys. Journ.*, vol. 16, no. 2, pp. 2639-2647, June 2022.
- [99] A. A. Stonier, S. Murugesan, R. Samikannu, S. K. Venkatachary, S. Senthil Kumar and P. Arumugam, "Power Quality Improvement in Solar Fed Cascaded Multilevel Inverter With Output Voltage Regulation Techniques," *IEEE Access*, vol. 8, pp. 178360-178371, 2020.
- [100] P. K. Sahu and M. D. Manjrekar, "Controller Design and Implementation of Solar Panel Companion Inverters," *IEEE Trans. Ind. Applications*, vol. 56, no. 2, pp. 2001-2011, March-April 2020.

- [101] Y. P. Siwakoti, A. Palanisamy, A. Mahajan, S. Liese, T. Long and F. Blaabjerg, "Analysis and Design of a Novel Six-Switch Five-Level Active Boost Neutral Point Clamped Inverter," *IEEE Trans. Ind. Electron.*, vol. 67, no. 12, pp. 10485-10496, Dec. 2020.
- [102] N. Arab, H. Vahedi and K. Al-Haddad, "LQR Control of Single-Phase Grid-Tied PUC5 Inverter With LCL Filter," *IEEE Trans. on Ind. Electronics*, vol. 67, no. 1, pp. 297-307, Jan. 2020.
- [103] C. A. Rojas, M. Aguirre, S. Kouro, T. Geyer and E. Gutierrez, "Leakage Current Mitigation in Photovoltaic String Inverter Using Predictive Control With Fixed Average Switching Frequency," *IEEE Trans. Ind. Electron.*, vol. 64, no. 12, pp. 9344-9354, Dec. 2017.
- [104] N. Kumar, T. K. Saha and J. Dey, "Sliding-Mode Control of PWM Dual Inverter-Based Grid-Connected PV System: Modelling and Performance Analysis," *IEEE Journ. Emerg. & Selected Topics Pow. Electron.*, vol. 4, no. 2, pp. 435-444, June 2016.
- [105] M. Coppola, F. Di Napoli, P. Guerriero, D. Iannuzzi, S. Daliento and A. Del Pizzo, "An FPGA-Based Advanced Control Strategy of a Grid-Tied PV CHB Inverter," *IEEE Trans. Pow. Electron.*, vol. 31, no. 1, pp. 806-816, Jan. 2016.
- [106] M. Chen, K. K. Afridi and D. J. Perreault, "A Multilevel Energy Buffer and Voltage Modulator for Grid-Interfaced Microinverters," *IEEE Trans. Pow. Electron.*, vol. 30, no. 3, pp. 1203-1219, March 2015.
- [107] G. Buticchi, D. Barater, E. Lorenzani, C. Concari and G. Franceschini, "A Nine-Level Grid-Connected Converter Topology for Single-Phase Transformer-less PV Systems," *IEEE Trans. Ind. Electron.*, vol. 61, no. 8, pp. 3951-3960, Aug. 2014.

- [108] N. M. C. M. and J. P., “Realization of Cascaded H-Bridge Multilevel Inverter Based Grid Integrated Solar Energy System With Band Stop Generalized Integral Control,” *IEEE Trans. on Ind. Applications*, vol. 57, no. 1, pp. 764-773, Jan.-Feb. 2021.
- [109] Y. Y. Syasegov et al., “HERIC-Clamped and PN-NPC Inverters With Five-Level Output Voltage and Reduced Grid-Interfaced Filter Size,” *IEEE Open Journ. Pow. Electron.*, vol. 4, pp. 306-318, 2023.
- [110] G. Schettino, A. O. Di Tommaso, R. Miceli, C. Nevoloso, G. Scaglione and F. Viola, “Dead-Time Impact on the Harmonic Distortion and Conversion Efficiency in a Three-Phase Five-Level Cascaded H-Bridge Inverter: Mathematical Formulation and Experimental Analysis,” *IEEE Access*, vol. 11, pp. 32399-32426, 2023.
- [111] M. G. Marangalu, N. V. Kurdkandi, P. Alavi, S. Khadem, H. Tarzamni and A. Mehrizi-Sani, “A New Single DC Source Five-Level Boost Inverter Applicable to Grid-Tied Systems,” *IEEE Access*, vol. 11, pp. 24112-24127, 2023.
- [112] A. Bughneda, M. Salem, E. Hossain, D. Ishak and N. Prabakaran, “Design Considerations and Performance Investigation of a Five-Level Cascaded Multilevel LLC Boost DC–DC Converter,” *IEEE Access*, vol. 11, pp. 40441-40456, 2023.
- [113] S. Mondal, S. P. Biswas, M. R. Islam and S. M. Muyeen, “A Five-Level Switched-Capacitor Based Transformerless Inverter With Boosting Capability for Grid-Tied PV Applications,” *IEEE Access*, vol. 11, pp. 12426-12443, 2023.
- [114] H. Fang, C. Qiu and D. Wang, “Synchronous Optimal Pulse-Width Modulation Method for Three-Phase Five-Level NPC-H Bridge Inverter,” *2021 IEEE 4th*

- International Electrical and Energy Conference (CIEEC)*, Wuhan, China, pp. 1-5, 2021
- [115] A. Lidozzi, M. di Benedetto, T. A. Meynard and L. Solero, "Medium-Voltage Seven-Level Multiplexed Converter for AC Applications," *IEEE Open Journal of Power Electronics*, vol. 4, pp. 81-90, 2023.
- [116] A. K. Singh, R. K. Mandal and R. Anand, "Quasi-Resonant Switched-Capacitor-Based Seven-Level Inverter With Reduced Capacitor Spike Current," *IEEE Journal of Emerging and Selected Topics in Power Electronics*, vol. 11, no. 2, pp. 1953-1965, April 2023.
- [117] S. Pal, K. Gopakumar, U. Loganathan, H. Abu-Rub and D. Zielinski, "A Hybrid Seven-Level Dual-Inverter Scheme With Reduced Switch Count and Increased Linear Modulation Range," *IEEE Transactions on Power Electronics*, vol. 38, no. 2, pp. 2013-2021, Feb. 2023.
- [118] L. Ren, L. Zhang, L. Wang and S. Dai, "Capacitor Voltage Regulation Strategy for 7-Level Single DC Source Hybrid Cascaded Inverter," *IEEE Journal of Emerging and Selected Topics in Power Electronics*, vol. 10, no. 5, pp. 5773-5784, Oct. 2022
- [119] A. Srivastava and J. Seshadrinath, "A Single-Phase Seven-Level Triple Boost Inverter for Grid-Connected Transformerless PV Applications," *IEEE Transactions on Industrial Electronics*, vol. 70, no. 9, pp. 9004-9015, Sept. 2023.
- [120] D. S. M. Osheba, A. M. E. Lashine, H. A. Nagi, J. Rodriguez and M. Abdelrahem, "A Quadruple Boost Nine-Level Switched Capacitor Inverter With a Low Count of Components," *IEEE Access*, vol. 11, pp. 55569-55581, 2023

- [121] T. Debnath, K. Gopakumar, L. Umanand, D. Zielinski and K. Rajashekara, "A Nine-Level Inverter With Single DC-Link and Low-Voltage Capacitors as Stacked Voltage Sources With Capacitor Voltage Control Irrespective of Load Power Factor," *IEEE Open Journ. Ind. Electron. Society*, vol. 3, pp. 522-536, 2022.
- [122] Harbi, M. Ahmed, C. M. Hackl, J. Rodriguez, R. Kennel and M. Abdelrahem, "Low-Complexity Dual-Vector Model Predictive Control for Single-Phase Nine-Level ANPC-Based Converter," *IEEE Transactions on Power Electronics*, vol. 38, no. 3, pp. 2956-2971, March 2023.
- [123] A. K. Singh, R. Raushan, R. K. Mandal and M. W. Ahmad, "A New Single-Source Nine-Level Quadruple Boost Inverter (NQBI) for PV Application," *IEEE Access*, vol. 10, pp. 36246-36253, 2022.
- [124] N. Panda, B. Das, A. Chakrabarti, P. R. Kasari, A. Bhattacharya and D. Chatterjee, "A New Grid Interactive 11-Level Hybrid Inverter Topology for Medium-Voltage Application," *IEEE Transactions on Industry Applications*, vol. 57, no. 1, pp. 869-881, Jan.-Feb. 2021
- [125] A. M. M. Hassan, X. Yang, A. I. M. Ali, T. A. Ahmed and A. M. Azmy, "A Study of Level-Shifted PWM Single-phase 11-Level Multilevel Inverter," *2019 21st Int. Middle East Pow. Sys. Conf. (MEPCON)*, Cairo, Egypt., pp. 170-176, 2019.
- [126] A. Routray, R. Kumar Singh and R. Mahanty, "Harmonic Minimization in Three-Phase Hybrid Cascaded Multilevel Inverter Using Modified Particle Swarm Optimization," *IEEE Trans. Ind. Informatics*, vol. 15, no. 8, pp. 4407-4417, Aug. 2019.

- [127] M. D. Siddique, S. Mekhilef, N. M. Shah, A. Sarwar, A. Iqbal and M. A. Memon, "A New Multilevel Inverter Topology With Reduce Switch Count," *IEEE Access*, vol. 7, pp. 58584-58594, 2019.
- [128] N. Mishra, S. K. Yadav, B. Singh, M. Tariq, S. Padmanaban and F. Blaabjerg, "Performance Assessment of Eight-Switch 11-Level Packed U Cell Converter Under Dynamic Solar Photovoltaic Environment," *IEEE Journ. Emerg. & Select. Topics in Pow. Electron.*, vol. 10, no. 4, pp. 3851-3860, Aug. 2022.
- [129] M. Ali, M. Tariq, A. Sarwar and B. Alamri, "A 13-, 11-, and 9-Level Boosted Operation of a Single-Source Asymmetrical Inverter With Hybrid PWM Scheme," *IEEE Trans. Ind. Electron.*, vol. 69, no. 12, pp. 12817-12828, Dec. 2022.
- [130] Q. Ren, A. Chen, J. Chen and C. Zhang, "A Novel Neutral-Point-Clamped Half-Bridge Eleven-level Inverter With High DC Voltage Utilization Ratio and Fewer Switches," *2020 IEEE Applied Pow. Electron. Conf. Exposition (APEC)*, New Orleans, LA, USA, pp. 1148-1153, 2020.
- [131] A. Laib, A. Krama, A. Sahli, A. Kihal and H. Abu-Rub, "Reconfigurable Model Predictive Control for Grid Connected PV Systems Using Thirteen-Level Packed E-Cell Inverter," *IEEE Access*, vol. 10, pp. 102210-102222, 2022.
- [132] K. Jena, C. K. Panigrahi and K. K. Gupta, "A 6X-Voltage-Gain 13-Level Inverter With Self-Balanced Switched-Capacitors," *CPSS Trans. Pow. Electron. & Applications*, vol. 7, no. 1, pp. 94-102, March 2022.
- [133] D. Upadhyay, M. Ali, M. Tariq, S. A. Khan, B. Alamri and A. Alahmadi, "Thirteen-Level UXE-Type Inverter With 12-Band Hysteresis Current Control

- Employing PSO Based PI Controller," *IEEE Access*, vol. 10, pp. 29890-29902, 2022.
- [134] S. G. Basha, V. Mani and S. Mopidevi, "Single-phase Thirteen-level Dual-boost Inverter Based Shunt Active Power Filter Control Using Resonant and Fuzzy Logic Controllers," *CSEE Journ. Pow. & Energy Sys.*, vol. 8, no. 3, pp. 849-863, May 2022.
- [135] D. J. Almakhles, J. S. M. Ali, S. Selvam, M. S. Bhaskar and N. Sandeep, "Switched Capacitor-Based 13L Inverter Topology for High-Frequency AC Power Distribution System," *IEEE Journ. Emerg. & Select. Topics Pow. Electron.*, vol. 9, no. 5, pp. 5883-5894, Oct. 2021.



## APPENDIX

In the RT-LAB environment, a MATLAB model operates as the master and console, while OPALRT empowers it to run at physical clock time. Refer to Fig.1 for the schematic representation. After a successful execution, Fig. 1 displays the automatically generated real-time window. The remarkable high sampling speed of OPAL-RT turns it into a dynamic real-time system. For detailed specifications of the real-time OPAL-RT simulator. Difference between offline and online simulation is discusses here.

### **Offline MATLAB Simulation**

The time taken to compute all equations and functions representing a system during a given time-step in real-time may vary, being either shorter or longer than the duration of the simulation time step.

### **Real-time Test Bench Execution**

The real-time simulator precisely generates the internal variables and outputs of the simulation in the same time frame as its physical counterpart would.

These are the advantages of real time execution:

**Early Discovery of Design Issues:** It enables the identification of design issues at an earlier stage in the process, facilitating timely corrections and improvements.

**Reduced Development Costs:** Real-time execution helps in reducing overall development costs by streamlining testing and validation processes.

**Cost-Effective:** Real-time test benches are more economical compared to physical setups, and they can be utilized for multiple applications, maximizing their utility.

**Table: OPAL-RT software block-sets and features**

Key Parameters	Hyper-sim	Phasor-sim	FPGA-sim	Mega-sim
Application	Power system	Power system	Power System	Power electronics and power system
Network Scale	9000 real-time nodes	-	-	900 real-time nodes
Processing Time	200 ns-100 s	1-10 ms	200 ns-2 s	200 ns-100 s
Mode of Simulation	EMT Mode	Phasor Mode	EMT Mode	EMT Mode
Compatibility	Simulink and Sim-scape	Simulink, CYME, Power	Psim, PLECS	Simulink and Sim-scape



**Fig. Real-Time Test Bench**

Fig. Real-Time Test Bench

Substitution for Risky or Expensive Tests: Real-time execution allows for the substitution of risky or costly tests that would otherwise require physical test benches, enhancing safety and cost-effectiveness.

# LIST OF PUBLICATIONS

## ❖ Publications in National/International Journals

1. S. Upreti., B. Singh and N. Kumar, “Third Harmonic Injected Nearest Level Control of Nine-Level Grid-Tied PV-CHB Converter” *J. Inst. Eng. India Ser. B*, vol. 104, pp. 935–943 2023. <https://doi.org/10.1007/s40031-023-00893-0>
2. S. Upreti., B. Singh and N. Kumar., “A new three-phase eleven level packed e-cell converter for solar grid-tied applications” *e-Prime - Advances in Electrical Engineering, Electronics and Energy*, Vol.4, 2023 , pp. 1-8. ISSN 2772-6711, <https://doi.org/10.1016/j.prime.2023.100152.reti>,
3. S. Upreti., B. Singh and N. Kumar, “Harmonics Minimization in PUC Type Solar Multilevel Converter with Multicarrier Switching Schemes” *IETE Journal of Research*, 0377-2063 pp. 1-10 , 2022, <https://doi.org/10.1080/03772063.2022.2081625>
4. S. Upreti, S.K. Yadav, B. Singh and N. Kumar, “New Multicarrier Modulation Scheme for Harmonics Mitigation of T-Type Solar Multilevel Inverter” *J. Inst. Eng. India Ser. B* vol.103, pp. 903–911, 2022. <https://doi.org/10.1007/s40031-021-00708-0>

## ❖ Publications in International Conferences

1. S. Upreti, S.K. Yadav, B. Singh and N. Kumar, “An Improved K-Type Seven-Level Converter Topology for Direct Grid Integration of Solar Photovoltaic Plant,” 2023 *IEEE IAS Global Conference on Renewable Energy and Hydrogen Technologies (GlobConHT)*, Male, Maldives, 2023, pp. 1-6 doi: [10.1109/GlobConHT56829.2023.10087497](https://doi.org/10.1109/GlobConHT56829.2023.10087497)
2. S. Upreti, S. Kumar Yadav, B. Singh and N. Kumar, "Power Quality Improvement with Seven Level Packed-E Cell for Renewable Applications," 2022 *IEEE Global Conference on Computing, Power and Communication Technologies (GlobConPT)*, New Delhi, India, 2022, pp. 1-5, doi: [10.1109/GlobConPT57482.2022.9938315](https://doi.org/10.1109/GlobConPT57482.2022.9938315).
3. S. Upreti, B. Singh and N. Kumar, “A thirteen level ladder type grid-tied solar power converter in varying irradiance conditions,” 2023 *IEEE Renewable Energy and Sustainable E-Mobility Conference (RESEM)*, Bhopal, India, 2023 pp. 1-6

## **BIODATA**

**NAME:** SANJAY UPRETI

**DATE OF BIRTH:** 12<sup>TH</sup> DECEMBER 1966

**NATIONALITY:** INDIAN

### **QUALIFICATIONS:**

<b>EDUCATIONAL QUALIFICATION</b>	<b>UNIVERSITY/BOARD</b>
B.TECH. (ELECTRICAL ENGINEERING)	G.B. PANT UNIVERSITY OF AGRICULTURE AND TECHNOLOGY PANTNAGAR
M.TECH. (ENERGY STUDIES)	IIT DELHI